

Scuola Internazionale Superiore Studi Avanzati (S.I.S.S.A.)

International School for Advanced Studies (I.S.A.S.)

Trieste, Italy



THERAPEUTIC APPROACHES FOR PRION DISEASES AND RELATED NEURODEGENERATIVE DISORDERS

Thesis submitted for the degree of Doctor of Philosophy (Ph.D.)

Academic Year 2010/2011

Candidate

Tran Hoang Ngoc Ai

Supervisor

Prof. Giuseppe Legname

**THERAPEUTIC APPROACHES
FOR PRION DISEASES AND RELATED
NEURODEGENERATIVE DISORDERS**

Candidate

Tran Hoang Ngoc Ai

Supervisor

Prof. Giuseppe Legname

Contents

List of abbreviations	1
1. Introduction	2
1.1 Protein misfolding	2
1.2 Protein aggregation and fibrillation	4
1.3 Prion proteins and diseases	6
1.4 Prion replication	11
1.5 Prion infectivity	16
1.6 Therapies for prion diseases	18
1.7 Therapies for other neurodegenerative disorders	29
1.8 Aim of the present work	34
2. Polyelectrolyte multilayer-coated gold nanoparticles as multi-target compounds for treatment of prion diseases and related neurodegenerative disorders	36
2.1 Introduction	36
2.2 Materials and methods	36
2.3 Results	45
2.4 Discussion	56
2.5 Conclusion	58
3. Discovery of a class of diketopiperazines as anti-prion compounds	60
3.1 Introduction	60
3.2 Materials and methods	61
3.3 Results and discussion	64
3.4 Conclusion	72
4. Anti-prion activity and preliminary structure-activity relationship of benzoquinones	73
4.1 Introduction	73
4.2 Synthesis and evaluation of a library of 2,5-bisdiamino-benzoquinone derivatives as probes to modulate protein–protein interactions in prions	75
4.3 Evaluation and preliminary structure-activity relationship of 2,5-diamino-1,4-benzoquinones as a novel class of bivalent anti-prion compound	79
5. Synthesis and biological evaluation of lipoic acid hybrids as novel compounds against prion diseases	92

<i>5.1 Introduction</i>	92
<i>5.2 Materials and methods</i>	93
<i>5.3 Results and discussion</i>	97
<i>5.4 Conclusion</i>	102
6. Concluding remarks	103
List of publications	105
Acknowledgements	106
References	107

To My Dad and Mom

To My Husband Ha M.Tuan

List of abbreviations

A β , β -amyloid;

α -syn, alpha-synuclein;

AuNP, gold nanoparticle;

BBB, blood-brain barrier;

BC, BiCappa;

BQ, 2,5-diamino-1,4-benzoquinones;

CoQ, coenzyme Q;

DKP, diketopiperazine;

GT1, mouse hypothalamus cells;

HOBt, N-hydroxybenzotriazole;

MTDL, multi-target directed ligand;

N2a, mouse neuroblastoma cells;

NQO1, NAD(P)H/quinone oxidoreductase 1;

OS, oxidative stress;

PK, proteinase K;

PPIs, protein-protein interactions;

PrP, prion protein;

PrP^C, normal cellular prion protein;

PrP^{Sc}, infectious conformational form of prion protein;

recMoPrP, recombinant mouse prion protein;

ROS, reactive oxygen species;

ScGT1, scrapie-infected mouse hypothalamus cells;

ScN2a, scrapie-infected mouse neuroblastoma cells;

TBARS, thiobarbituric acid-reactive substances;

TSE, transmissible spongiform encephalopathy.

1. Introduction

1.1 Protein misfolding

In protein folding, the three-dimensional (3D) structure of a protein is determined by its amino acid sequence and the biological function of a protein depends on its 3D structure. However, the conformational changes in the secondary and/or tertiary structure of a normal protein may promote diseases including several neurodegenerative diseases such as Alzheimer's disease (AD), transmissible spongiform encephalopathies (TSEs), Huntington's disease (HD), Parkinson's disease (PD), amyotrophic lateral sclerosis (ALS) and other amyloidoses such as diabetes type II, etc.¹

The protein misfolding may be associated to disease by either gain of a toxic activity by the misfolded protein or by the lack of biological function of the natively folded protein. The misfolded protein is rich in β -sheets which are formed of alternating peptide pleated strands linked by hydrogen bonding between the NH and CO groups of the peptide bond. In β -sheets the bonds are between one strand and another and formation of β -sheets is usually stabilized by protein oligomerization or aggregation since the second β -strand can come from a different region of the same protein or from a different molecule. In contrast to the misfolded protein, the natively folded protein is rich in α -helices with the hydrogen bonds are between groups within the same strand.¹⁻³ The role of protein misfolding in disease is provided by neuropathologic and genetic studies as well as the development of transgenic animal models that the end point of protein misfolding is aberrant protein aggregation and accumulation as amyloid-like deposits in diverse organs.^{2,4-6}

Three different hypotheses have been proposed to describe the relationship between conformational changes and aggregation (Fig. 1). The critical event in protein conformational disease is the formation of protein oligomers that act as seeds to induce protein misfolding. In this model, the polymerization hypothesis has been shown that misfolding occurs as a consequence of protein aggregation (Fig. 1A).⁷ An alternative conformational hypothesis is that the underlying protein is stable in both the folded and misfolded forms in solution (Fig. 1B). In this model, protein misfolding is independent of aggregation, which is a non-necessary end point of conformational changes, can be an accompanying consequence rather than a direct cause of the disease.^{3,8,9} Moreover, the conformation/oligomerization hypothesis

represents an intermediate view in which slight conformational changes trigger oligomerization that is essential for the stabilization of protein misfolding (Fig. 1C). In this model, an unstable amyloidogenic intermediate formed by slight conformational changes is stabilized by intermolecular interactions with other molecules forming small β -sheet oligomers, which by further produce amyloid fibrils.^{2,3,10,11} The conformation/oligomerization hypothesis is the most comprehensive and accepted model of protein misfolding and aggregation.

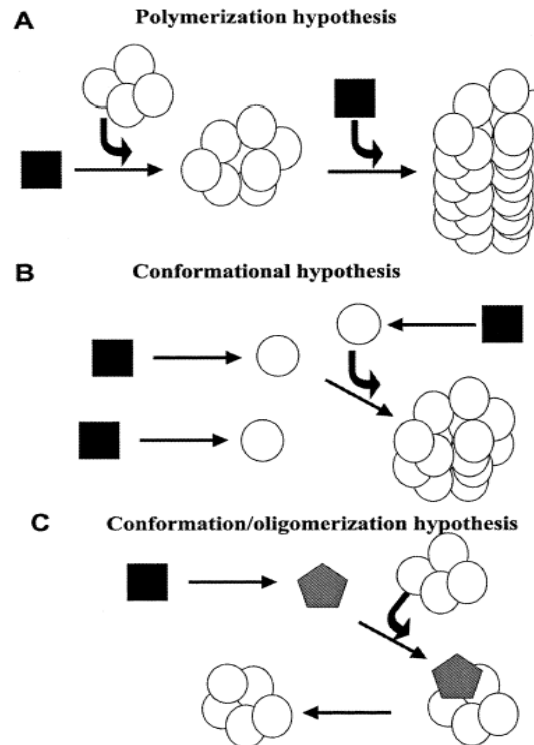


Figure 1. Models for the molecular mechanism of protein misfolding and aggregation. Three different hypotheses have been proposed to describe the relationship between conformational changes and aggregation. (A) The polymerization hypothesis, aggregation induces the protein conformational changes. (B) The conformational hypothesis, protein misfolding is independent of aggregation, which is a non-necessary end point of conformational changes. (C) The conformation/oligomerization model represents an intermediate view in which slight conformational changes trigger oligomerization that is essential for the stabilization of protein misfolding. Square represents the folded native conformation, circles represent the disease-associated conformer and pentagon corresponds to an unstable conformational intermediate. Adapted from Soto (2001).

Understanding molecular mechanism of protein misfolding and aggregation is useful to aim to inhibit or reverse the conformational changes as a therapy to protein conformational disease. Soto and co-workers designed peptides to prevent and to reverse β -sheet formation named by β -sheet breaker peptides for blocking the conformational changes and aggregation undergone by both A β and PrP.¹¹⁻¹³

1.2 Protein aggregation and fibrillation

The onset of aggregation may be triggered by any factor such as mutations, environmental changes or chemical modifications reducing the conformational stability of the protein. This results in a rise of the concentration of the amyloidogenic precursors such as a shift of the equilibrium between correctly folded and partially folded molecules. In Figure 2, under destabilizing conditions, the equilibrium (1) is shifted to the left thus increasing the population of partly folded molecules. Under normal conditions, these are refolded by the molecular chaperones or cleared by the ubiquitin-proteasome machinery. These machineries should be impaired or the population of misfolded molecules overwhelm their buffering possibility, disordered aggregates arise or the aggregation path is undertaken. Equilibrium (2) is intrinsically shifted to the right and the nucleation of ordered aggregates is kinetically favoured by mutations increasing the mean hydrophobicity or propensity to beta structure or reducing the net charge of the misfolded/unfolded molecules. In equilibrium (3), the formation of pre-fibrillar assemblies in the form of amyloid pores could be directly related to the cytotoxic effects of amyloids. Molecular chaperones (heat-shock proteins and others) may suppress the appearance of pre-fibrillar aggregates by reducing the population of misfolded protein molecules assisting their correct folding or favouring their complete misfolding for proteasome degradation. The chaperones may also clear amyloid assemblies by detaching monomers and favouring their clearance. Alternatively, specific mutations may enhance aggregation simply by favouring kinetically the assembly of the unfolded or partly folded monomers into the early oligomeric pre-fibrillar species.¹⁴

The general physicochemical features such as mean hydrophobicity, net charge and propensity to alpha and beta structure formation affect the tendency of an unfolded or partially folded polypeptide chain to aggregate.¹⁵ For instance, α -synuclein and tau carrying specific mutations enhancing their mean hydrophobicity or reducing their mean net charge. Intracellular aggregates of these proteins are the pathologic hallmark of the familial forms of synucleinopathies (Parkinson's disease and others) and tauopathies (Alzheimer's disease and others), respectively.¹⁴ In addition, the prion diseases (Creutzfeld-Jacob disease and others) where aggregates of the prion protein (PrP^{Sc}) recruit the natively folded PrP^C molecules and thus propagating the PrP^{Sc} aggregates, meet a suitable template favouring a specific conformational modification.⁹

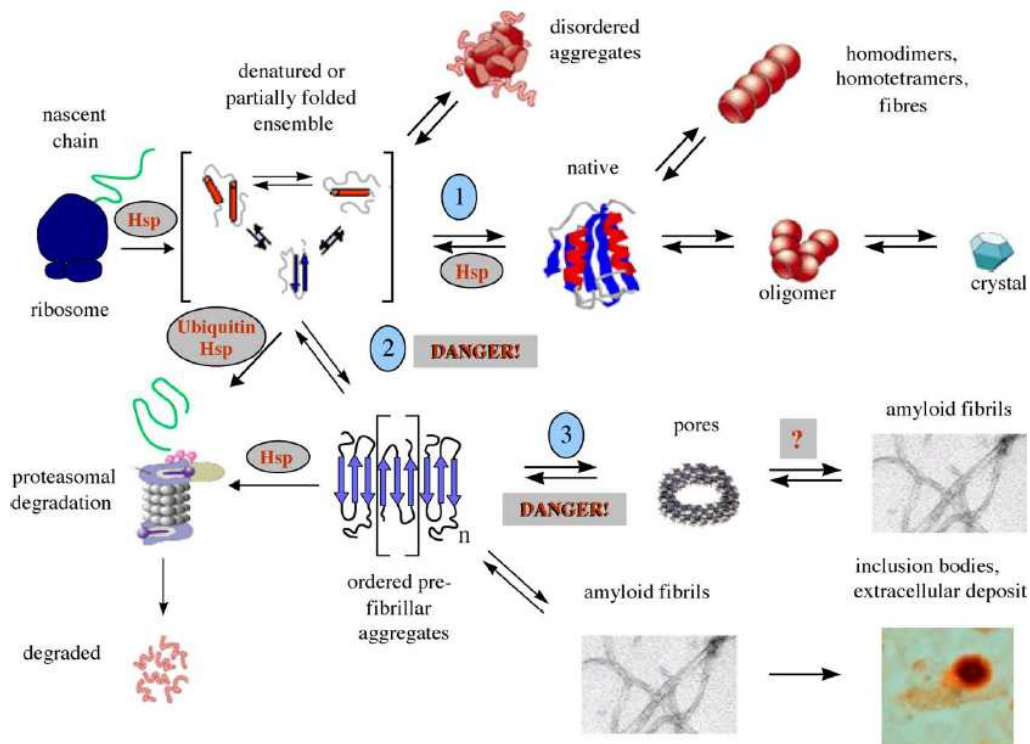


Figure 2. The possible fates of newly synthesized polypeptide chains. Modifications of protein structure or medium conditions may favour protein-protein interactions into fibers or into crystalline lattices. DANGER! indicates the processes generating the pre-fibrillar assemblies presently considered mostly associated with cell impairment. The question mark indicates that it is not known whether amyloid pores (when formed) are on path or dead end intermediates of fibril formation. Adapted from Stefani (2004).

Protein aggregation may be favoured under conditions resulting in the impairment or overwhelming of the molecular machineries. These molecular machineries comprise the molecular chaperones of the endoplasmic reticulum (ER) such as Bip, Grp94, calnexin and of the cytosol (heat-shock proteins, crystallins, prefoldin, Hsc70) and the ubiquitin-proteasome pathway in ensuring the quality control of protein folding.¹⁶⁻¹⁸

Under destabilized conditions, a protein or a peptide undergoes the path eventually leading to the appearance of mature amyloid fibrils which share basic structural features found in the differing amyloidoses. Typically, amyloid fibrils are straight, unbranched, 6-12 nm wide (but larger in some cases) formed by a variable number of elementary filaments (protofilaments) around 1.5-2.0 nm in diameter, twisted around each other in a rope-like structure (Fig. 3).^{19,20} These structural features have been studied by differing biophysical techniques such as transmission and cryoelectron microscopy, atomic force microscopy and solid-state NMR. By X-ray diffraction technique, the ordered core of the amyloid fibrils as a cross-beta structure, where each

protofilament results from a double row of beta-sheets provided by each monomer, has been described. The strands of the cross-beta structure of the core of amyloid aggregates run parallel to each other and perpendicular to the main fibril axis (Fig. 3).¹⁴

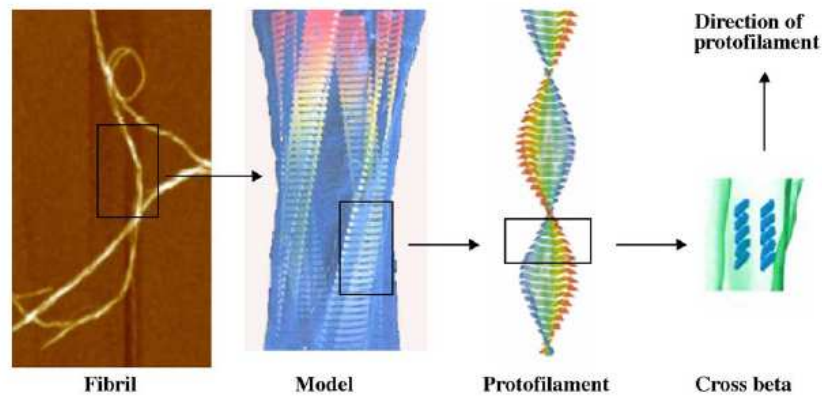


Figure 3. Close-up view of the structural organization of an amyloid fibril. The four protofilaments are wound around each other and their core structure is a row of β -sheets where each strand runs perpendicular to the fibril axis. Adapted from Stefani (2004).

The studies have been reported that the pathogenic protein aggregates are the destabilised monomeric, or the non-fibrillar oligomeric species of distinct morphology (protofibrils) preceding mature fibrils in the aggregation pathway. The earliest protofibrils typically appear as globular assemblies 2.5-5.0 nm in diameter spontaneously organizing into chains and variously sized rings comprising small doughnuts with a central pore, further organising into ribbons, protofilaments and mature fibrils.^{21,22}

1.3 Prion proteins and diseases

Prion diseases, also known as transmissible spongiform encephalopathies (TSEs) are fatal and incurable neurodegenerative disorders of animals and humans.⁹ They can manifest as genetic, infectious and sporadic illnesses and they include bovine spongiform encephalopathy (BSE) of cattle, scrapie of sheep, chronic wasting disease (CWD) of deer, moose and elk, Creutzfeldt-Jakob (CJD) and Gerstmann-Sträussler-Scheinker (GSS) diseases of humans.²³

The prion hypothesis

In 1967, Alper and co-workers demonstrated that the infectious materials was not destroyed under very high doses of ionizing radiation and ultraviolet (UV) which

obliterate nucleic acids.²⁴ And also in this year, Griffith demonstrated that a protein can act as the infectious agent causing scrapie.²⁵ However, until 1982, Prusiner first proposed the prion (proteinaceous infectious particles) hypothesis.²⁶ Over decades of research, there have been crucial evidences for this hypothesis by starting with the initial indication that prion diseases can be transmissible, owing to the accidental transmission of scrapie in sheep and ending with the demonstration that infectious materials can be generated in vitro using pure recombinant prion protein (Fig. 4).²⁷

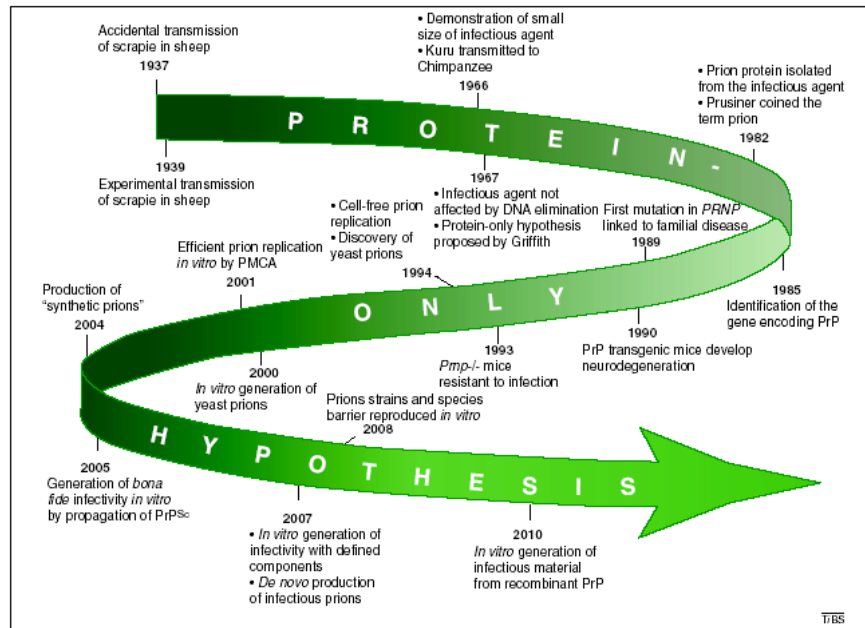


Figure 4. A timeline representation of the major milestones in the prion hypothesis. Adapted from Soto (2010).

Cellular prion protein and its biological functions

The cellular prion protein (PrP^C) is highly conserved protein in mammals and paralogues, present in turtle,²⁸ amphibians²⁹ and fish.³⁰ PrP^C expression is broad and diverse in heart, kidney, pancreas, skeletal muscle, central nervous system (CNS) and peripheral nervous system (PNS).^{31,32}

PrP^C is expressed in synaptic membranes of neurons, oligodendrocytes, Schwann cells and astrocytes in CNS and PNS.³³ In addition, PrP^C presents in lymphocytes and a stromal cell of the immune system as the follicular dendritic cell.³⁴

PrP^C, a detergent-soluble and protease-sensitive ubiquitous protein, is located mainly in lipid rafts of extracellular membrane and is a glycosyl phosphatidyl inositol (GPI)-linked glycoprotein which can be in three glycosylated patterns of either un-, mono- or di- forms (Fig. 5B).³⁴ There are common features in the 3D structure of mouse,

Syrian hamster, cattle and human mature PrP^C including a long, flexible N-terminal (residue 23-121), three α -helices and a two-stranded anti-parallel β -sheet that flanks the first α -helix.³⁵ The C-terminal is stabilized by a disulfide bond linking α -helices two and three (Fig. 5A,B).³⁶

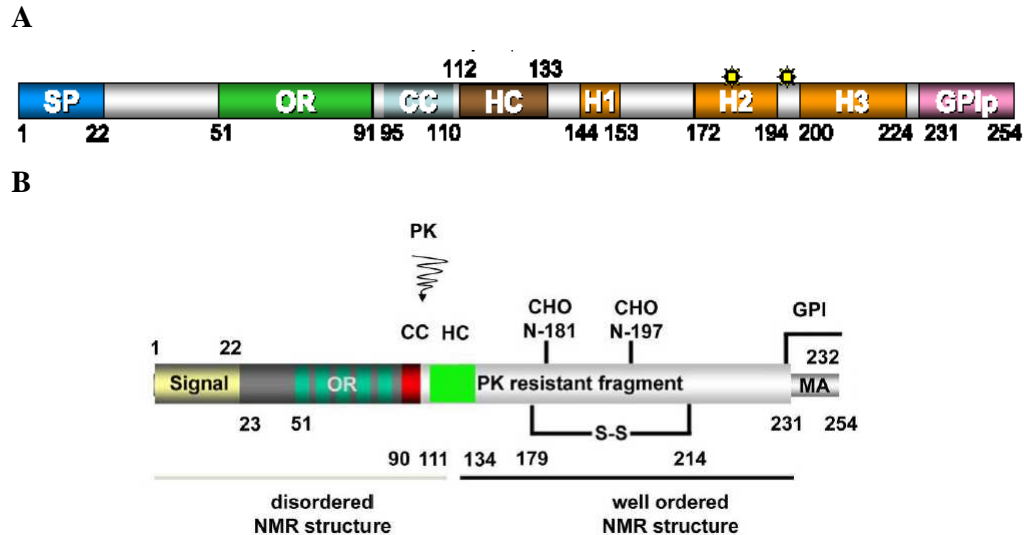


Figure 5. Structural features of cellular prion protein. (A) The human PrP^C protein contains 208 amino acid residues. A secretory signal peptide resides at the extreme N-terminus. CC, charged cluster; HC, hydrophobic core; GPI, glycosyl phosphatidyl inositol anchor; OR, octa-repeats; H1- H3: three α -helices. The numbers describe the position of the respective amino acids. (B) Scheme of the primary structure of PrP^C and its posttranslational modifications. S-S, single disulfide bridge; MA, membrane anchor region; the proteinase K (PK) resistant core of PrP^{Sc} is depicted in grey; the approximate cutting site within PrP^{Sc} is indicated by the arrow. The size of the PK resistant fragment is variable, being cut at various positions between amino acids 78-102. Adapted from Liden et al. (2008) and Heikenwalder et al. (2007).

PrP^C has many different functions such as neuroprotection, synaptic transmission, regulation of immune system, inducing apoptosis or being anti-apoptotic, etc.³⁷ Cerebellar granule cell apoptosis was observed in mice expressing toxic N-terminal deletion mutants of PrP. PrP^C has often been reported to promote neuronal survival, in particular following apoptotic or oxidative stress. Neurite outgrowth, including growth of axons and dendrites, was observed to be reduced in neurons lacking PrP^C.³⁸ In addition, functions of PrP^C have also been found in transmembrane signaling, cell adhesion and trafficking of metal ions, e.g. copper binding.³⁹ A role in myelination and involvement in synaptic activity which is often affected in the first stage of prion diseases and whose formation was found to be reduced in neuronal cultures devoid of PrP^C have been attributed to PrP^C. The transgenic mice show an impaired maintenance of myelinated axons in the white matter. Furthermore,

electrophysiological studies indicate a role of PrP^C in synapse function, especially in neurotransmitter release.³⁸

The central role of PrP^{Sc} and characteristics of prion diseases

Prion protein (PrP) is normally present in its native conformation (PrP^C), but in all prion diseases the protein is in an abnormal conformation (PrP^{Sc}). PrP^{Sc} can be distinguished from PrP^C by its insolubility in detergent and partial resistance to protease digestion. PrP^{Sc} accumulates and forms deposits around neurons. Prion diseases are infectious, sporadic and genetic. Differing from other neurodegenerative diseases and amyloidoses such as Alzheimer's disease and Parkinson's disease, prion diseases have a unique feature is that they are transmissible among humans and across species. Remarkably, the infectious agent in all prion diseases is composed exclusively of PrP^{Sc} aggregates although other cellular factors may be required in the conversion process from PrP^C to PrP^{Sc}.⁴⁰ The structure of PrP^C corresponds to the experimentally determined 3D conformation of the protein by nuclear magnetic resonance (NMR)³⁵ and the structure of PrP^{Sc} corresponds to a model based on low resolution techniques.⁴¹ Characteristics of PrP^{Sc} compared with PrP^C are displayed in Table 1.

Typical neuropathological changes for prion diseases include vacuolation of the neuropil in the gray matter, synaptic alterations, prominent neuronal loss, exuberant reactive astrogliosis and cerebral accumulation of prion protein aggregates.⁴² The loss of a critical biological function of PrP^C is one possible mechanism by which PrP^{Sc} formation might result in neurodegeneration.³⁹ Another possible mechanism by which PrP^{Sc} formation might be linked to the disease is by direct toxicity of the misfolded protein. Moreover, synaptic damage and dendritic atrophy, spongiform degeneration, brain inflammation and neuronal death have been proposed for prion diseases (Fig. 6).⁴³

Table 1. Comparison of PrP^C with PrP^{Sc}

Properties	PrP ^C	PrP ^{Sc}
Isoform	Normal	Pathogenic
Protease resistance	No	Stable core containing residue 90-231
Location in or on cells	Plasma membrane	Cytoplasmic vesicles
Solubility	Soluble	Insoluble
PK-sensitivity	Sensitive	Partially resistant
Structure	Extended	Globular
α -Helices	45%	30%
β -Sheets	3%	45%
Glycoforms	Mixture of un-, mono and di-glycosylated forms	Mixture of un-, mono and di-glycosylated forms
Infectivity	No	Yes
Turnover	Hours	Days
Sedimentation properties	Consistent with monomeric species	Multimeric aggregated species

*PrP denotes prion protein and PrP^{Sc} the scrapie isoform of PrP^C

Adapted from Pandeya et al. (2010).

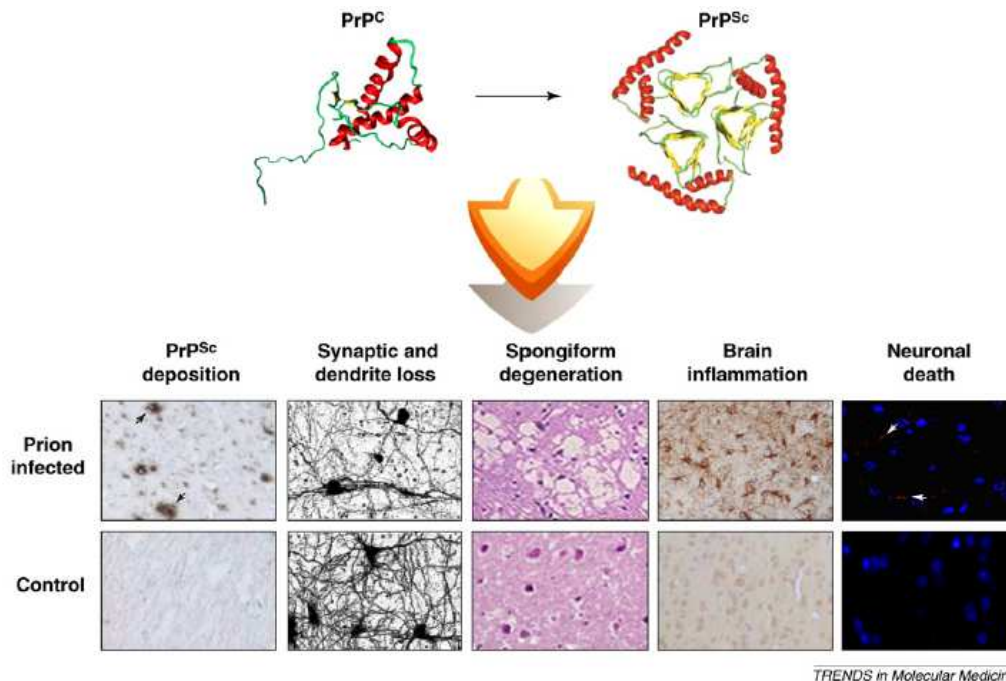


Figure 6. Multiple neurodegenerative pathways are implicated in TSEs. The conversion of the natively folded PrP^C to PrP^{Sc} triggers disease. PrP^{Sc} deposition was determined after immunohistochemical staining with anti-PrP antibodies (black arrowheads). Dendrites were labeled by Golgi-silver staining to illustrate the substantial decrease on dendrites and synaptic connections in prion-infected animals. Spongiform degeneration was evaluated after hematoxylin and eosin staining. Astrogliosis (brain inflammation) was detected by immunohistochemical staining of reactive astrocytes with an anti-GFAP (glial fibrillary acidic protein) antibody. Apoptosis was detected by staining with caspase-3 antibody (red indicated by white arrowheads) and DAPI (40,6-diamidino-2-phenylindole, blue) staining of nucleus. Adapted from Soto et al. (2011).

In addition, the mechanisms for neurodegeneration of prion diseases include microglial activation, ER stress and oxidative stress (Fig. 7). It is possible that multiple mechanisms contribute to the pathology of prion diseases. However, the absolute mechanism still remains obscure.⁴³

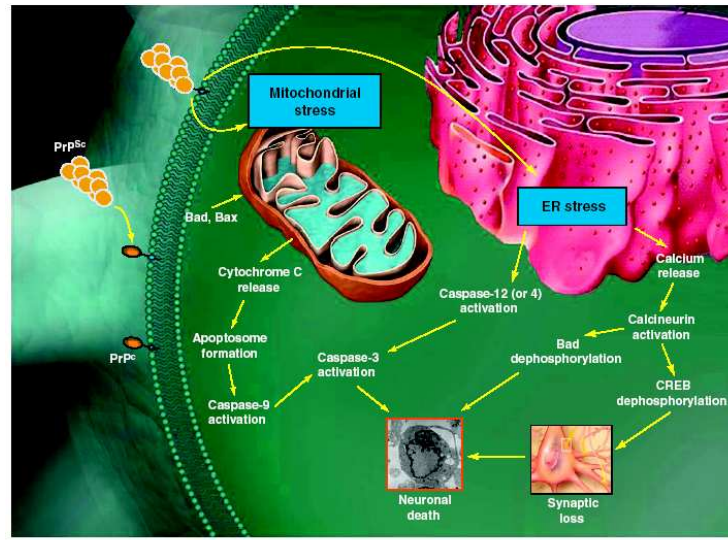


Figure 7. Putative signaling pathways for PrP^{Sc}-induced neurodegeneration in prion diseases. Several mechanisms have been proposed by which PrP^C to PrP^{Sc} conversion results in neurodegeneration. PrP^{Sc} might produce mitochondrial stress, leading to apoptosis. An alternative model implicates sustained ER stress. Adapted from Soto et al. (2011).

Recently, Soto and Satani proposed a model in which the primary abnormality is PrP^{Sc} formation and accumulation, from in peripheral tissues to in the brain. The disease process starts with the formation of PrP^{Sc}, beginning a long and clinically silent presymptomatic phase, in which PrP^{Sc} slowly but gradually accumulates in the brain. PrP^{Sc} accumulation triggers ER stress and activation of the unfolded protein response, which represents the first line of defense against protein misfolding. Other early consequences of PrP^{Sc} accumulation are brain inflammation (in the form of astrocytosis and microglial activation) and autophagy. Both inflammation and autophagy might initially be defensive mechanisms, but later could also contribute to neuronal death and perhaps brain vacuolation. The first damage leading to noticeable clinical consequences is probably synaptic disruption, ending the presymptomatic phase and beginning the early clinical phase of the disease. Synaptic dysfunction produces loss of dendrites and finally neuronal death. The end and irreversible stages of the disease are characterized by massive spongiform degeneration and neuronal death, which are probably triggered by a variety of interconnecting cellular pathways.⁴³

1.4 Prion replication

Prion replication involves the direct interaction between the PrP^{Sc} template and the endogenous cellular PrP^C driving the formation of nascent infectious prions.⁴⁴

The central feature of prion pathogenesis is the conversion of PrP^{C} to PrP^{Sc} which is thought to proceed via formation of a complex between PrP isoforms and an unknown molecular chaperone "X" (Fig. 8).⁴⁵ This conversion occurs post-translationally and thought to involve conformational change rather than covalent modification. The mechanism by which the conversion of PrP^{C} to PrP^{Sc} takes place and results in the distinct pathogenesis of prion diseases remains unknown.

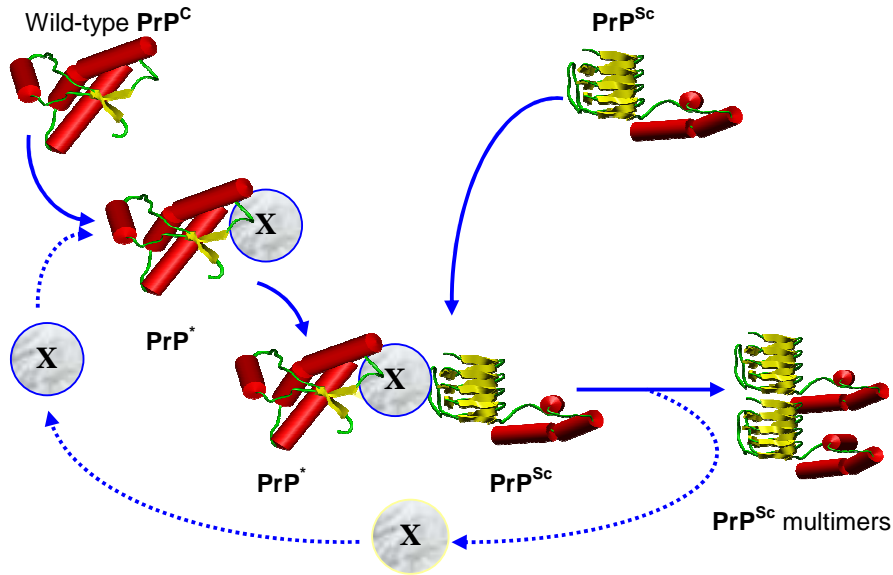


Figure 8. The conformational conversion of the PrP^{C} to PrP^{Sc} , which is thought to involve an unknown molecular chaperone "X". Adapted from Telling et al. (1995).

Models for the conformational conversion of PrP^{C} to PrP^{Sc}

There are two models to explain the conversion of PrP^{C} to PrP^{Sc} as the "refolding" and the "seeding" models. In the first model, there is an interaction between exogenously introduced PrP^{Sc} and endogenous PrP^{C} , which is induced to transform itself into further PrP^{Sc} . A high energy barrier may prevent spontaneous conversion of PrP^{C} to PrP^{Sc} (Fig. 9A). In the latter, by nucleation-polymerization, PrP^{C} and PrP^{Sc} are in a reversible thermodynamic equilibrium. The seed formation begins very slowly, then monomeric PrP^{Sc} can be recruited and eventually aggregate to amyloid. Fragmentation of PrP^{Sc} aggregates increases the number of nuclei, which can recruit further PrP^{Sc} and thus results in apparent replication of the agent (Fig. 9B).⁴⁶

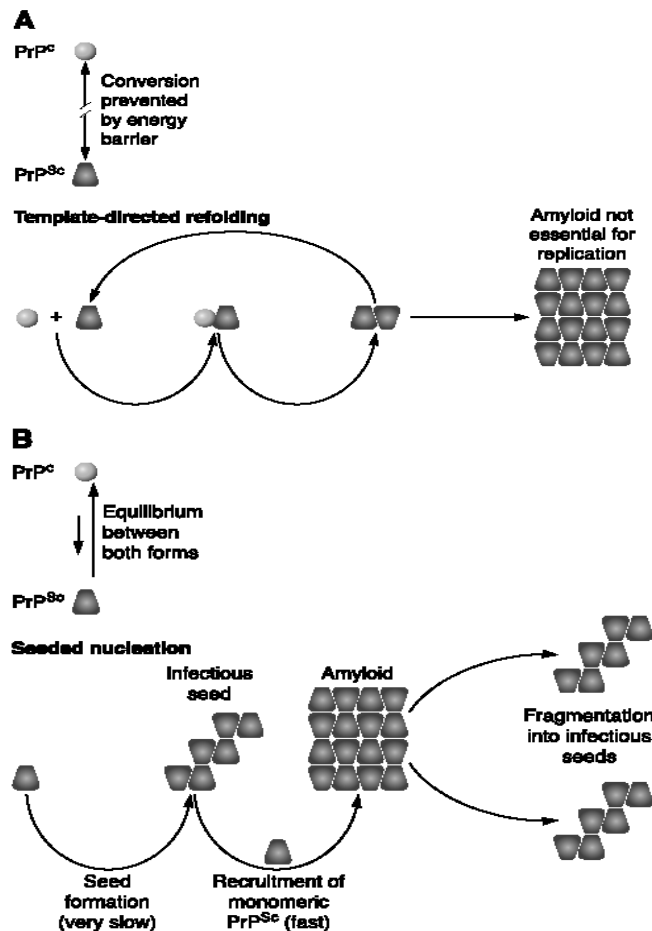


Figure 9. Models for the conformational conversion of PrP^C to PrP^{Sc}. (A) the “refolding” or template assistance model. (B) the “seeding” or nucleation-polymerization model. Adapted from Aguzzi et al. (2009).

Recently, the protein misfolding cyclic amplification (PMCA) technique which is designed to mimic PrP^{Sc} autocatalytic replication has been developed.⁴⁷⁻⁴⁹ In the PMCA, PrP^{Sc} is amplified in a cyclic manner by incubating small amounts of PrP^{Sc}-containing brain homogenate with PrP^C-containing brain homogenate. Hence, PrP^C is recruited into growing aggregates of PrP^{Sc} and it undergoes conformational conversion and becomes PrP^{Sc}. The growing PrP^{Sc} species are disrupted by repeated sonication in the presence of detergents to generate multiple smaller units functioning as a seed for the continued formation of new PrP^{Sc} aggregates. The whole procedure is repeated several times (Fig. 10).⁴⁶

In addition, an important mechanism of prion replication process is the propagation of prions through fragmentation of existing fibrils verified for yeast prions,⁵⁰ mammalian prion⁵¹ and non-prion related amyloid fibrils.⁵²

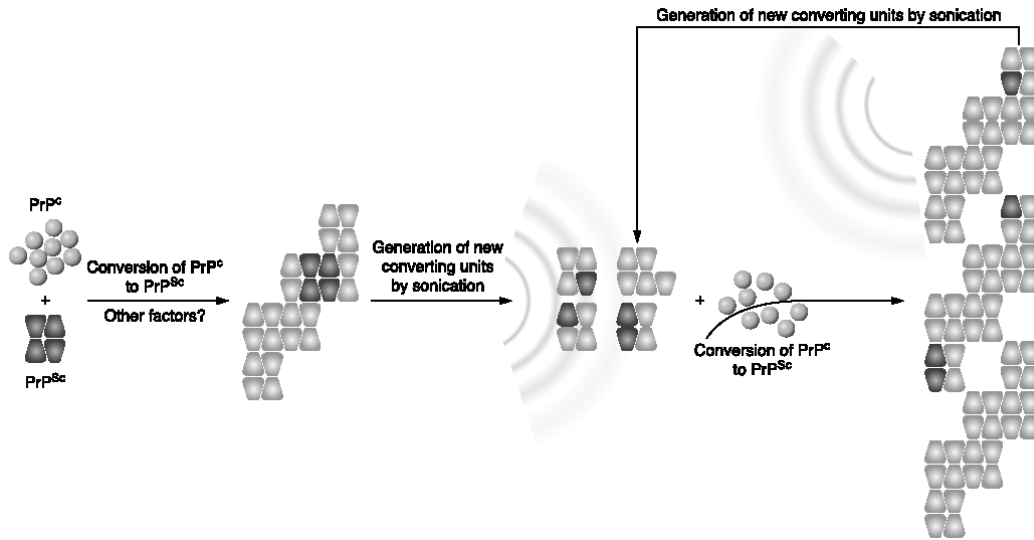


Figure 10. Schematic representation of the protein misfolding cyclic amplification (PMCA) reaction. PrP^C is shown as light gray spheres. PrP^{Sc} is shown as trapezium. The original seed is in dark gray, and the newly formed PrP^{Sc} is in light gray. Adapted from Aguzzi et al. (2009).

Cell biology of PrP^C and PrP^{Sc} with potential sites of conversion

PrP^C is usually associated with detergent-resistant membrane domains known as rafts. The scrapie-associated conversion site for membrane-anchored wild-type PrP^C seems to be on the cell surface and/or in endosomes. However, PrP^C released from the cell due to lack of a GPI anchor may be converted to extracellular deposits such as amyloid fibrils and plaques.³⁷ In N2a cells, PrP^{Sc} mainly accumulates in late endosomes and lysosomes^{53,54} and only very small amounts of PrP^{Sc} are located at plasma membrane.⁵⁵ In addition, some PrP^{Sc} was also found in the Golgi apparatus detected in N2a cells persistently infected with RML/Chandler scrapie, but not in hamster cells infected with a hamster scrapie strain by immuno-EM study.⁵⁶ Also in this cell line infected with RML or 22L scrapie strain, increased PrP^{Sc} levels are along with increased retrograde transport to Golgi and ER.⁵⁷ Furthermore, misfolded PrP^C can be subject to the ER-associated degradation pathway (ERAD). Under conditions of proteasome inhibition, cytoplasmic forms of PrP aggregates are associated with neurotoxicity such as aggresomes.⁵⁸ Excessive levels of misfolded proteins in the cytosol might impair proteasome function, either directly or after incorporation into aggresomes.³⁷

Regarding the presence of co-factors in conformational conversion of PrP, the laminin receptor or its precursor as crucial co-factors is important for PrP^{Sc} formation in GT1 cells infected with Chandler scrapie strain. Although it is

unclear how glycosaminoglycans (GAGs) contribute to PrP^{Sc} biogenesis, cell surface GAGs might bind to both PrP^C and PrP^{Sc} to generate conversion of PrP^C to PrP^{Sc} (Fig. 11).^{59,60}

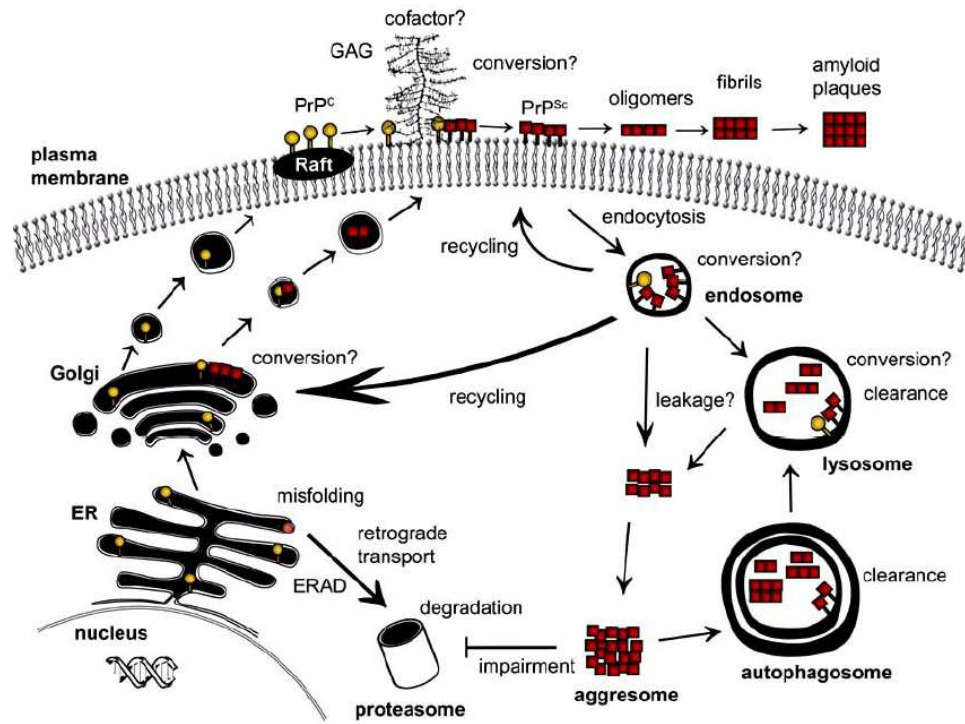


Figure 11. Cell biology of PrP^C and PrP^{Sc} with potential sites of conversion. The conformational refolding of PrP^C to PrP^{Sc} is thought to take place at the cell surface and/or along the endocytic pathway, probably involving co-factors, e.g. glycosaminoglycans (GAGs). Adapted from Krammer et al. (2009).

Involvement of cellular co-factors in prion replication

Conversion factor activity is not present in the lower organisms such as yeast, bacteria and flies, but is only present in mammals. Several evidences indicate that co-factors might participate in prion replication. Although “protein X” refers to this factor coined by Prusiner as mentioned above, there is no formal proof that the accessory molecule is indeed a protein.²⁷ Further evidence is from PMCA studies in which purified hamster PrP^C is converted when added brain homogenate to the sample but not converted when mixed with highly purified PrP^{Sc}.^{61,62} These results suggest that unknown factors in brain homogenate are essential for prion replication. Also there are evidences for nucleic acids such as RNA involved in prion replication.⁶³⁻⁶⁵ Supattapone’s group has shown that natural or synthetic RNA can act as conversion factors and catalyze prion replication in hamsters but not in mice and the negative charge of RNA is responsible for the interaction with

PrP.⁶⁶ In addition, synthetic anionic phospholipids are required for PrP^{Sc} replication⁶⁷ and higher infectivity was reported with lipid membrane-associated PrP^{Sc}.⁶⁸ Surprisingly, treatments that eliminate nucleic acids, lipids, or proteins do not prevent prion replication *in vitro*. Indeed, the addition of various classes of molecules (synthetic nucleic acids, heparin, albumin or fatty acids) produces a small but detectable effect on enhancing prion replication *in vitro*. These findings suggest that various different compounds might act as a conversion factor *in vitro*, that elimination of only some of them does not prevent prion replication.^{27,62}

At least five different scenarios can be proposed for the involvement of cellular co-factors in prion propagation. (i) The co-factor might integrate into the infectious agent, alter PrP^{Sc} folding, and provide biological information to the infectivity process, perhaps by determining strain characteristics. (ii) The co-factor might act as an essential catalyst for prion replication, perhaps by interacting with PrP^C, altering its folding, and permitting its interaction with PrP^{Sc}. (iii) Through binding and integration into the PrP^{Sc} polymer, the co-factor might help to stabilize the conformation of PrP^{Sc}. (iv) The co-factor might participate in the key process of fragmenting PrP^{Sc} polymers to produce smaller structures, and multiplying the number of seeds to allow the continuation of prion replication. (v) The co-factor might bind to PrP^{Sc}, thus increasing its biological stability, reducing its clearance *in vivo*, and increasing its chances to reach target organs. It is important to highlight that these possibilities are not mutually exclusive, and indeed, it is likely that a co-factor could be involved in several of these processes simultaneously.²⁷

Therefore, in prion therapy, the molecules binding to either PrP^C or PrP^{Sc} conformers at the binding interface may inhibit the interaction of PrP^C with PrP^{Sc}, thus interrupting prion production. Additionally, the compounds that bind to the molecules supporting and participating in prion replication, such as chaperones or other ligands, may also be good candidates for blocking prion replication.

1.5 Prion infectivity

In peripheral infection, prions silently accumulate and replicate in peripheral organs or reservoirs and transit through at least one PrP-positive (PrP⁺) tissue before reaching the CNS.⁶⁹ Prions replicate in lymphoid organs during the early stages of infection.⁷⁰ Within the lymphoreticular system, follicular dendritic cells (FDCs) are a prominent

site of PrP^{Sc} deposition.⁷¹ In rodent scrapie models, prion replication is typically detected first in the spleen and reaches plateau levels before detectable neuroinvasion after peripheral inoculation was performed. Then brain levels rise exponentially to 100-fold or more above splenic levels before clinical disease occurs. Infectivity can be recovered from the spleen very early during the incubation period (Fig. 12a).⁷² Infectivity is detectable on hamster and mouse bioassay following inoculation of wild-type CD-1 mice with 263K hamster prions. On hamster bioassay, infectivity can be recovered early in incubation period and at low level of the original 263K inoculum or new infectivity can be accumulated slowly. On mouse bioassay, infectivity appears after a lengthy period and the animal dies of natural causes following a normal lifespan. At this stage, on both hamster and mouse bioassay, infectivity can be recovered at high levels from these clinically normal animals (Fig. 12b).⁷²

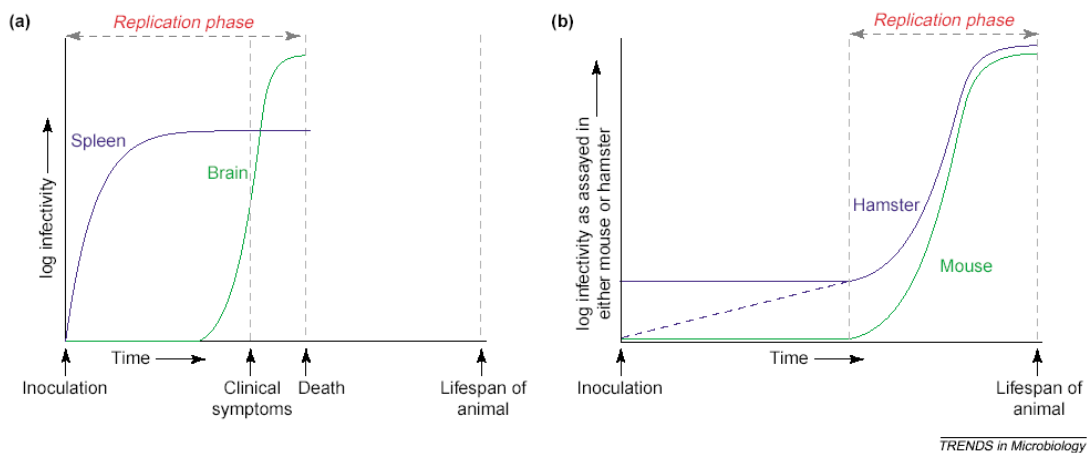


Figure 12. Prion infection *in vivo*. Adapted from Hill et al. (2003).

Thus, neuroinvasion typically begins upon ingestion of the TSE agent. The pathogen must first cross the intestinal epithelium in a process that still remains elusive. Migratory dendritic cells are known to directly capture antigens within the intestinal lumen and could also be responsible for initial uptake of the TSE agent. After absorption through the intestinal epithelium, PrP^{Sc} appears to be phagocytosed by antigen-displaying cells such as macrophages and dendritic cells. While macrophages appear to serve a more protective role,⁷³ dendritic cells deliver the TSE agent to FDCs located in the germinal centers of B cell-rich follicles present in Payer's patches and other gut-associated lymphoid tissue (GALT) underlying the

intestinal epithelium. After incubation in lymphoid tissue such as the GALT and spleen, the TSE agent spreads to CNS via the enteric nervous system (Fig. 13).⁶⁹ Routes for neuroinvasion including tunneling nanotubes, exosomes and blood have been studied. Tunneling nanotubes are important for intracellular transfer of prion during neuroinvasion.⁷⁴ Prions gain access into and between neurons by hijacking tunneling nanotubes (for 12 hours of co-culture) which is more effective than transportation by exosomes (for 5 days of co-culture).⁷⁵ Recently, for removing TSE infectivity from whole blood, the removal of all white cells reduced infectivity by only 42%, suggesting that other blood components, cells or plasma, could be infectious.^{69,76}

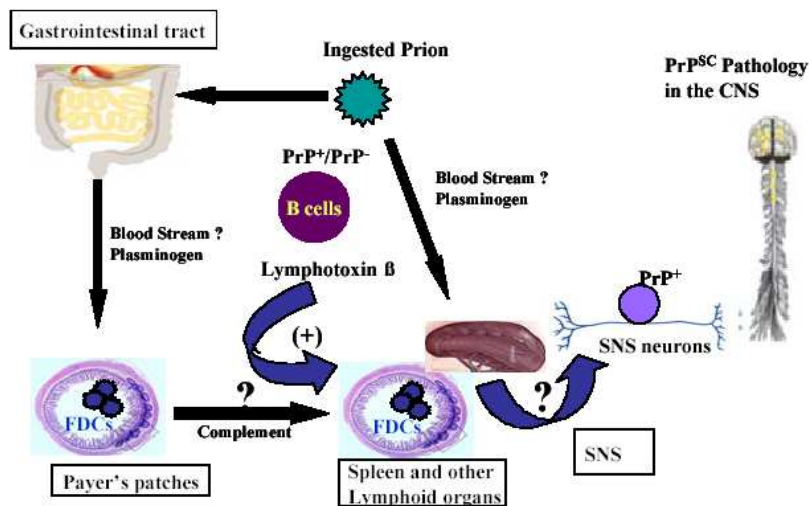


Figure 13. The route of prion neuroinvasion. After absorption through the intestinal epithelium, prion reach the peyer's patches, via blood constituents (Plasminogen that bind to PrP^{Sc}). FDCs are infected in the patches and in other lymphoid organs, including the spleen. The prions reach the spleen by a B-cell independent route involving complement factors. Other factors that are required for spreading infection to the CNS are lymphotoxin (stimulus for FDCs), and at least one interposed PrP⁺ tissue. Adapted from Pandeya et al. (2010).

1.6 Therapies for prion diseases

Early treatment regimes, including various prophylactic compounds and immunotherapies, have sought efficacy through neutralization of infectious sources, blockade of infection via the most common peripheral routes, and/or blockade of neuroinvasion. Effective therapies targeting later disease, which are initiated after the appearance of clinical signs, will most likely involve some combination of inhibiting pathogenic PrP formation, destabilizing or enhancing clearance of existing pathogenic

PrP, blocking neurotoxic effects of the infection, and/or promoting the recovery of lost functions in the CNS.⁷⁷

1.6.1 Chemotherapy for prion diseases

Many compounds have been proposed for the treatment of prion diseases, including polysulfated anions, dextrans, and cyclic tetrapyrroles.⁷⁸⁻⁸¹ Recently, some success has been achieved using pentosan polysulfate⁸² although this compound seems to be unsuccessful in the treatment of human prion diseases.⁸³ In addition, molecules targeting the different molecular steps involved in pathological prion replication have also been investigated.⁸⁴⁻⁹⁰ However, to date, the use of these compounds in clinical applications is limited, due to their high toxicity and poor crossing of the blood-brain barrier (BBB). Thus, there is an urgent need to develop systematic pharmacological and mechanistic studies for the identification of a new class of compounds as therapeutic agents capable of inhibiting several pathways in prion conversion and replication.

Strategies for developing new drugs

Three strategies are usually developed to identify new drugs against a well-characterized disease. (i) A rational approach will specifically target the key molecules responsible for the disease. The limiting factor here is to possess the structure of one or more proteins implicated in the pathogenesis of the disease. (ii) A blind screening on a large panel of drug already synthesized and commercially available. The idea is to identify new molecules with a chemical structure different from those already existing and which can serve as lead molecule for the pharmaceutical chemistry. (iii) Synthesis of chemical derivatives of recently identified lead molecules that showed promising therapeutic properties. The idea here is to modify some chemical characteristics of the drug in order to make it more potent or to facilitate its delivery, especially in the brain for instance. Various combinations between these three strategies are possible in the drug development field.⁹¹

A common task in pharmaceutical research is the search for new lead compounds against diseases that show a greater specificity and/or fewer side effects than already-known agents. Therefore, a widely used search method as high throughput screening (HTS) of large compound collections was established. However, since this approach is expensive and time consuming and further on only can be used once a suitable test

assay is developed, the *silico* design and proposal of new lead structures becomes more important.⁹² Moreover, the nature of the prion agent as well as its replication cycle which are not yet completely understood, does not facilitate HTS.⁹¹ A central origin of the strategy of *in silico* screening of drug database is the experience that similarities in structures are indicative of similarities in activities of drugs. Thus, a structural search of large compound databases is of great interest. Today, about two million chemical compounds are available commercially.⁹³ The use of SuperDrug⁹⁴ (<http://bioinf.charite.de/superdrug>), a new data base of essential WHO approved drugs (2003), for 2D and 3D search for new lead structures starting from compounds against prion diseases was performed by Lorenzen and co-workers.⁹² In this method, the authors started with known lead compounds, a data base is searched to create a pool of putative drugs. These compounds are compared to known inhibitors and non-inhibitors, and drugs with similarities to inactive structures are removed from the list of proposed inhibitors. Combining structural features of ineffective substances with property filtering rules allows the exclusion of further candidates. Drugs surpassing this sieve are proposed as new TSE inhibitors. Furthermore, the first PrP(90-231) NMR structure solved in 1996 provided some structural information to monomeric structure of the PrP protein and opened a new area of drug research since PrP constitutes an attractive therapeutic target within the replication cycle of prions. However, the surface of the PrP(90-231) NMR structure presented no crevasses, so the classical docking program used for the structure-based drug design was not adapted in this case.⁹¹ For the rational approach, Perrier and co-workers (2000) found two drugs Cp60 and Cp62 that could mimic a small region at the PrP surface to inhibit prion replication.⁹⁰

In addition, Korth and co-workers (2001) have performed a blind screening on drugs known to cross the BBB. They found that quinacrine and chlorpromazine, both tricyclic compounds with an aliphatic side chain in their middle ring, exhibited an anti-prion activity with EC_{50} of 0.3 and 3 μ M respectively. Hence, Korth and co-workers synthesized nine derivatives of quinacrine in order to establish a structure-activity relationship study.⁹⁵ Their results have revealed the importance of the aliphatic side chain for the inhibition of PrP^{Sc} formation.⁹¹

Models for studying chemotherapeutic candidates

In vivo tests provide the most rigorous evaluations of anti-TSE treatments, but are slow, costly, and impractical for screening purposes. A variety of relatively high throughput, low cost, cell culture models,^{96,97} and some yeast models,⁹⁸ have enabled the identification of a number of different classes of anti-prion compounds which then have shown efficacy in animal models. Also, *in vitro* assays have allowed investigation of the mechanisms of prion inhibition. In many cases, anti-prion compounds which bind to PrP^C cause it to cluster and internalize, thus rendering PrP^C inaccessible or incompatible for conversion to protease-resistant prion protein (PrP^{res}).^{37,97,99} Non-cellular *in vitro* assays have also been developed to assess a wide range of potentially effective compounds. These methods generally assess the competitive binding of PrP^C and PrP^{res} or the prevention of PrP amyloid fibril formation. Recent techniques include surface plasmon resonance,¹⁰⁰ fluorescence correlation spectroscopy,¹⁰¹ semiautomated cell-free conversion,¹⁰² and a fluorescence polarization-based competitive binding assay.¹⁰³ Computer “*in silico*” modeling is also being used to predict binding molecules.^{90,104}

Ultimately, promising treatments discovered *in vitro* require testing in animals and humans. Of the many compounds studied in rodent models, few have made their way into human trials or case reports, and the effectiveness of treatment administered at the onset of clinical symptoms, or when there is significant neuropathology, is low. However, many compounds show some prophylactic or early treatment effect in TSE-infected animals, and are therefore relevant to decontamination and early therapy efforts. These drugs need not be permeable to the BBB since they can target the peripheral replication of the agent, before neuroinvasion that arise following oral or other peripheral exposures. The option for early treatment has been hindered by a lack of early diagnosis, but with the recent development of new sensitive detection assays,^{66,105-108} there is hope for early preclinical TSE diagnostics, and more effective screening and testing of at risk individuals. This, coupled with the rising concern of blood transmission of variant Creutzfeldt Jakob disease (vCJD), the occurrence of BSE in livestock, and the spread of CWD, lends tremendous relevance to such chemoprophylaxis compounds and potential decontaminants in the management of prion diseases.⁷⁷

Identification of prion drug targets

A major focus of drug screening efforts has been the PrP conversion reaction. Many inhibitors prevent conversion by directly binding and blocking interactions between PrP^C and PrP^{Sc}. Others affect conversion by interfering with important accessory molecules, or by altering PrP^C expression and distribution.³⁷ Many different chemical classes of compounds have been screened and tested *in vitro*, and additional *in vivo* data are available for some (Table 2), including early or prophylactic treatments and later stage therapies.⁷⁷

Targeting PrP conversion of the compounds include binding PrP^C and/or PrP^{res}, redistribution or sequestration of PrP^C (e.g. cholesterol-depleting agents such as the statin drug simvastatin¹⁰⁹ and polyene antibiotics such as amphotericin B¹¹⁰), suppressing PrP^C expression by using small interfering RNA (siRNA) to the PrP gene,¹¹¹ targeting accessory molecules and pathways to conversion with Laminin receptor precursor protein (LRP/LR) antibodies¹¹² or tyrosine kinase inhibitor STI571 (known as imatinib mesylate),^{113,114} enhanced PrP^{res} clearance with polycations¹¹⁵⁻¹¹⁷ and other unknown mechanisms by using copper chelators^{118,119} or dimethylsulfoxide (DMSO)¹²⁰ or antivirals such as vidarabine (adenine arabinoside).¹²¹

For binding PrP^C and/or PrP^{res}, the compounds include polyanions (RNA,^{63,122,123} sulfated glycosaminoglycans (GAGs),^{124,125} pentosan polysulfate (PSS),⁸² fucoidan,¹²⁶ phosphorothioate oligonucleotides,¹²⁷ copaxone¹²⁸), sulphonated dyes and similar compounds (Congo red,^{84,129} suramin,^{130,131} curcumin¹³²⁻¹³⁴), cyclic tetrapyrroles (porphyrins, phthalocyanines),^{81,135,136} lysosomotropic factors (quinacrine, quinoline, acridines, phenothiazines),^{95,137-140} tetracyclic compounds (tetracycline, doxycycline),¹⁴¹⁻¹⁴³ other amyloidophilic compounds,¹⁴⁴ pyridine dicarnitride compounds,¹⁴⁵ peptide aptamers and β -sheet breaker.^{13,89,146}

In addition, compounds without direct effects on PrP^C, PrP^{res} or conversion may have therapeutic potential as neuroprotective agents or symptomatic treatment including analgesics such as flupirtine maleate,¹⁴⁷ cannabidiol (a nonpsychoactive constituent of cannabis)¹⁴⁸ and antioxidants such as pyrazolone derivatives¹⁴⁹ (Table 2).

Table 2. Chemical-based therapeutic and prophylactic agents

+ Effect demonstrated
 - Effect not present
 # Induces conversion *in vitro*

Compound	<i>In vitro</i>	<i>In vivo</i> (early)	<i>In vivo</i> (late)	Comments
POLYANIONS				
Heteropolyanion-23	+	+	-	
Dextran sulphate	+	+	-	Prolongs incubation after ic inoculation if given within 2 hours (hamsters).
Pentosan polysulphate (PPS)	+	+	+	Intraventricular infusion prolongs incubation (tg7 mice). Used in humans. Inhibits PrP ^{Sc} formation in cell culture but can stimulate cell-free conversion. PPS + Fe-TSP has more than additive effects <i>in vivo</i> .
Heparan sulphate	+	+	-	Inhibits PrP ^{Sc} formation in cell culture but can stimulate cell-free conversion.
Heparan sulphate mimetics, e.g. HM2606, CR36	+	+	-	
Fucoidan	+	+		Non-toxic. Oral administration. Strain dependent.
Phosphorothioate oligonucleotides	+	+		
RNA aptamers	+	-	-	
Copaxone	+	+	-	
SULPHONATED DYES AND RELATED COMPOUNDS				
Congo red	+	+	-	Only modest prophylactic effects <i>in vivo</i> . Subinhibitory concentrations stimulate PrP ^{Sc} in cell-free conversion. Possible teratogen and/or carcinogen.
Suramin	+	+		Only modest prophylactic effects <i>in vivo</i> .
Curcumin	+	+	+	Low dose effective 100 dpi in intracerebrally inoculated mice.
CYCLIC TETRAPYRROLES				
PcTS, DPG ₂ -Fe ³⁺ , TMPP-Fe ³⁺	+	+	-	
In-TSP	+			
Fe-TAP, Fe-TSP	+	+	+	Fe-TSP & PPS have more than additive effects <i>in vivo</i> .
QUINACRINE, QUINOLINE, ACRIDINES, PHENATHIAZINES				
Quinacrine	+	-	-	Quinacrine + desipramine or simvastatin better than quinacrine alone in cells. Quinacrine + rPrP-Q218K enhances inhibition in cells. No human benefit seen to date; trial ongoing. Increases amount of PrP ^{Sc} in the spleen. Crosses blood-brain barrier.
Chlorpromazine	+	+		
Quinine and biquinoline	+	+	-	
Mefloquine	+	-	-	

Compound	<i>In vitro</i>	<i>In vivo</i> (early)	<i>In vivo</i> (late)	Comments
OTHER AMYLOIDOPHILIC COMPOUNDS	+	+		Oral administration.
PYRIDINE DICARBONITRILES	+			
PEPTIDE APTAMERS AND B-SHEET BREAKERS				
Peptide aptamers	+			
β-sheet breaker peptides	+	+		Tested by mixing with inoculum only. May be strain or cell model specific.
CHOLESTEROL DEPLETING AGENTS				
Lovastatin, squalastatin	+			
Simvastatin	+	+	+	Effect may be unrelated to cholesterol lowering; brain cholesterol levels do not drop.
Amiodarone, progesterone	+			
Mevinolin				Causes sequestration of PrP ^{Sc} in Golgi apparatus. No infectivity experiments.
7-dehydrocholesterol reductase and 24-dehydrocholesterol reductase inhibitors	+	-	-	No effect even if given prior to inoculation.
POLYENE ANTIBIOTICS				
Amphotericin B, MS-8209	+	+	+	Human treatments ineffective.
Mepartricin	+	+	-	
Filipin	+			
COPPER/CHELATORS				
D(-)penicillamine	+	+		
Clioquinol		+		Structurally similar to quinacrine.
Copper	#	+	-	Can promote or inhibit PrP conformational conversions.
Chrysoidine	+			Mechanism of action may not relate to chelating properties.
DMSO	+	-		Conflicting treatment outcomes.
ANTIVIRALS				
Adenine arabinoside		+	+	2 out of 3 CJD patients had moderate temporary improvement if treated early in course. Mouse studies failed to show effect.

Compound	<i>In vitro</i>	<i>In vivo</i> (early)	<i>In vivo</i> (late)	Comments
INTRACELLULAR MECHANISMS				
MEK½ inhibitors (SL327)	+			
Cysteine-protease inhibitors (E64d)	+			
Phospholipase inhibitors	+			
P53 inhibitors (Pifitriin-alpha)	+	-	-	
Tyrosine kinase inhibitors (ST1571, imatinib mesylate)	+	+	-	
POLYCATIONS				
Polypropyleneimine gen. 4.0, polyethyleneimine, polyamidoamide gen. 4.0	+			
Phosphorus dendrimers generation 4	+	+		
Spermine, spermidine	+			
DOSPA	+			
NEUROPROTECTION				
Flupirtine maleate	+		+	Tested in human trials; some improvement in cognition. May be neuroprotective via up-regulation of bcl-2 and normalization of glutathione levels.
Cannabidiol	+	+	-	No apparent interaction with PrP ^C or PrP ^{res} . May be protective via inhibition of PrP ^{res} -induced microglial cell migration, or antagonism of the NMDA receptor.
Antioxidant pyrazolone derivatives	+			Properties other than antioxidant ones may be responsible for effect.

Adapted from Sim et al. (2009)

From given the partial efficacies of treatments targeting PrP conversion, PrP^{res} clearance, PrP^C expression, and neuroprotection, we could try combining therapies and look for cooperative or synergistic effects.⁷⁷ For instance, quinacrine enhanced PrP^{res} inhibition in cell culture when used in combination with the conversion-resistant mutant rPrP-Q218K.^{150,151} Quinacrine also produced more than additive inhibition when cells were co-treated with simvastatin or desipramine. This latter observation led to the creation of a more potent cell culture inhibitor of PrP^{res}, called quipramine, by covalently linking the acridine scaffold of quinacrine with the iminodibenzyl scaffold of desipramine.¹⁵²

1.6.2 Immunotherapy for prion diseases

Rational drug design strategies which are the basis of most modern drug discoveries are difficult to set up for prion diseases, due to the absence of a well-defined tertiary and/or quaternary structure of both PrP isoforms and lack of knowledge of the replication cycle of the prion agent. Only antibodies directed against the prion protein can set free from these barriers as they specifically recognized PrP isoforms and bind to their target with a high affinity.¹⁵³ Treatment of cells with Fab fragments D18 and D13, which recognized epitope 132-156 and 97-106 of PrP protein respectively, has been proven effective in clearing pre-existing PrP^{Sc} in ScN2a cells.⁸⁸ Monoclonal anti-PrP antibody 6H4 which recognized epitope 144-152 of PrP protein, also prevents infection of susceptible N2a.¹⁵⁴ Moreover, transgenic mice expressing anti-PrP antibody 6H4 in their spleen, prevent scrapie pathogenesis *in vivo*, sustaining the development of vaccination strategy.¹⁵⁵

For the roles of the lymphoid system and immune cells in prion pathogenesis, immunotherapeutic approaches to prion diseases have been studied. At least four strategies including removal of functional FDCs and therefore ablation of lymphoid prion replication sites; stimulation of the innate immune system; enhancement of elimination of PrP^{Sc} using PrP-specific antibodies; or binding of available PrP^C or PrP^{Sc} so that they are unavailable for conversion have been studied (Fig. 14). All of these approaches, which include both suppression and stimulation of the immune system, are now being tested in suitable *in vivo* systems using mice experimentally infected with mouse-adapted scrapie. However, because the lymphoid system has been found to be involved in almost all forms of TSE, it is reasonable to presume that mouse-adapted scrapie provides a realistic generic model for TSE therapy.⁴⁶

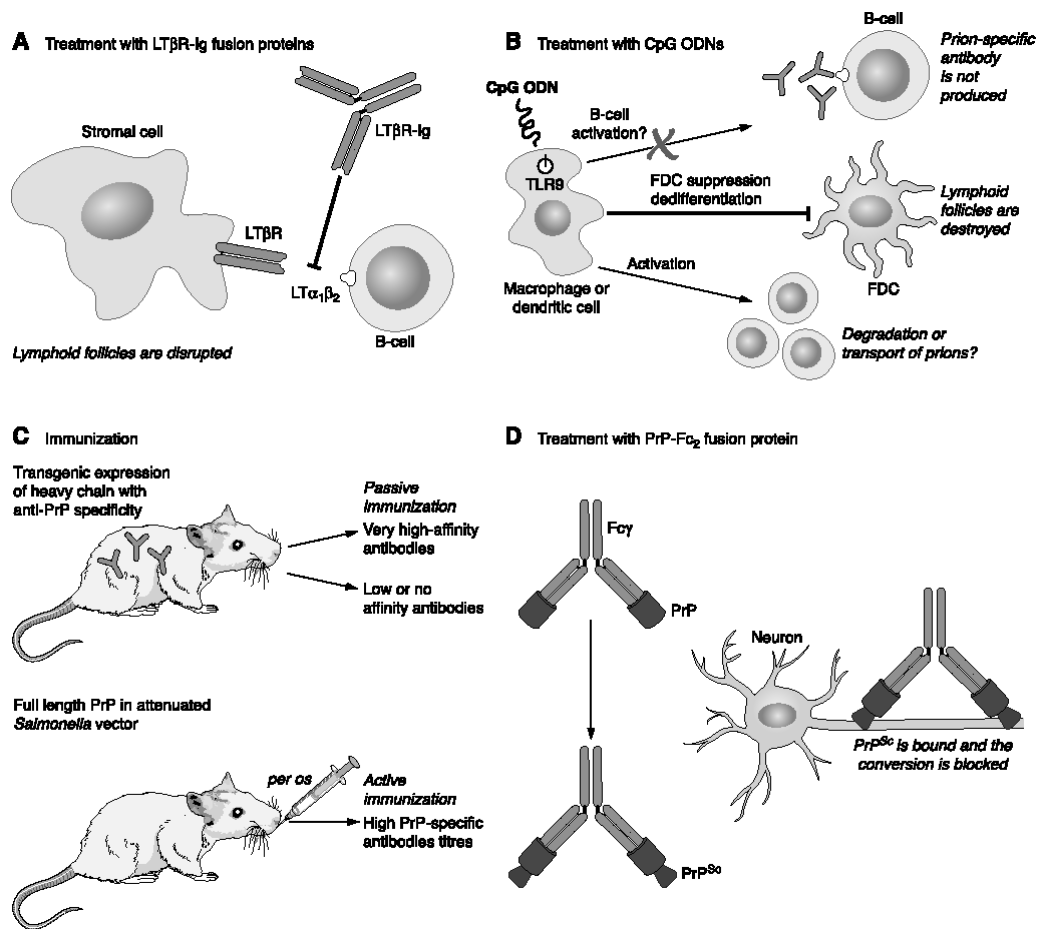


Figure 14. Immunotherapeutic strategies for prion disease. (A) treatment with the lymphotoxin-β receptor fusion protein (LTβR)-Ig breaks up the FDC networks and disrupts lymphoid follicles. The best protection is achieved when the fusion protein is administered immediately after exposure to prions. (B) ablation of mature follicular dendritic cells (FDCs) delays the development of prion disease in mice. However, treatment with multiple doses of CpG-containing oligodeoxynucleotides (CpG ODNs) produces severe unwanted side effects, including immunosuppression, liver necrosis, and thrombocytopenia. (C) vaccination against a self-protein is difficult because of immune tolerance, and it has the potential to induce autoimmune disease. Transgenic expression of an immunoglobulin μ chain containing the epitope-interacting region of 6H4, a high-affinity anti-PrP monoclonal antibody, associated with endogenous κ and λ chains, leads to high anti-PrP^C titers in *Prnp*^{0/0} and *Prnp*^{+/+} mice. It suffices to block prion pathogenesis upon intraperitoneal prion inoculation. After active immunization with full-length PrP in attenuated *Salmonella* vector, the mice develop high PrP specific antibody titers. (D) treatment with dimeric full-length PrP fused to the Fc portion of human IgG1 (PrP-Fc₂) delays the development of prion disease in mice, most probably owing to its interaction with the disease-associated PrP (PrP^{Sc}). LT-α1β2, LT heterotrimer; TLR, Toll-like receptor. Adapted from Aguzzi et al. (2009).

1.6.3 Cell and gene therapies for prion diseases

Therapeutic use of RNA interference (RNAi) in prion diseases

RNA interference (RNAi) is a highly conserved, sequence-specific posttranscriptional gene-silencing mechanism, whereby small interfering RNA (siRNA) targets homologous mRNA for degradation. siRNAs are generated from endogenous or exogenous double-stranded RNAs (dsRNAs) by the dsRNA

endonuclease Dicer; subsequently, siRNA activates the RNA-induced silencing complex (RISC) to degrade the target mRNAs (Fig. 15).¹⁵⁶ Rapid advancement in the understanding of RNAi in general, and mammalian RNAi in particular¹⁵⁷, makes it feasible to use RNAi to develop therapeutics for a variety of human diseases.¹⁵⁸

The first therapeutic use of lentivirally mediated RNAi against prion protein was demonstrated in scrapie-infected mice.¹⁵⁹ Knockdown of PrP by RNAi and resultant inhibition of PrP^{Sc} replication in cell culture have been described.^{111,160} Virally expressed RNAi has been used to reduce the levels of PrP^C in goats, cattle¹⁶¹ and mice.¹⁶² Pfeifer and co-workers have shown that anti-PrP^C short hairpin RNA (shRNA) carried on a lentivector is transfected into neuronal or embryonic stem cells, integrated into chromosomal DNA, and transcribed; anti-PrP^C shRNA is released into the cytoplasm, where it is processed by Dicer into siRNA. This in turn activates the RISC to degrade PrP mRNAs, leading to reduced expression of PrP^C and consequently diminished PrP^{Sc} accumulation and significantly improved survival time after prion infection (Fig. 15).¹⁶² These data indicate that RNAi has therapeutic potential for prion disease, providing a novel venue for the search of an effective prion disease treatment.¹⁵⁸

In contrast to many previous candidate treatments for prion diseases, which have suffered from inconsistent results dependant upon the prion strain involved, the RNAi therapeutic approach has a significant advantage of its applicability to all known strains of prion disease. Within any species the primary sequence of PrP^C and PrP^{Sc} is the same for all strains, thus RNAi should be an effective treatment for all variants. This should also apply to familial prion diseases that arise from a coding mutation in gene encoding PrP^C, *PRNP*. Genetic testing can identify these patients during the preclinical phase, so successful treatment of this category may be possible through preventative silencing of the mutant *PRNP* allele expression prior to development of pathology.¹⁶³

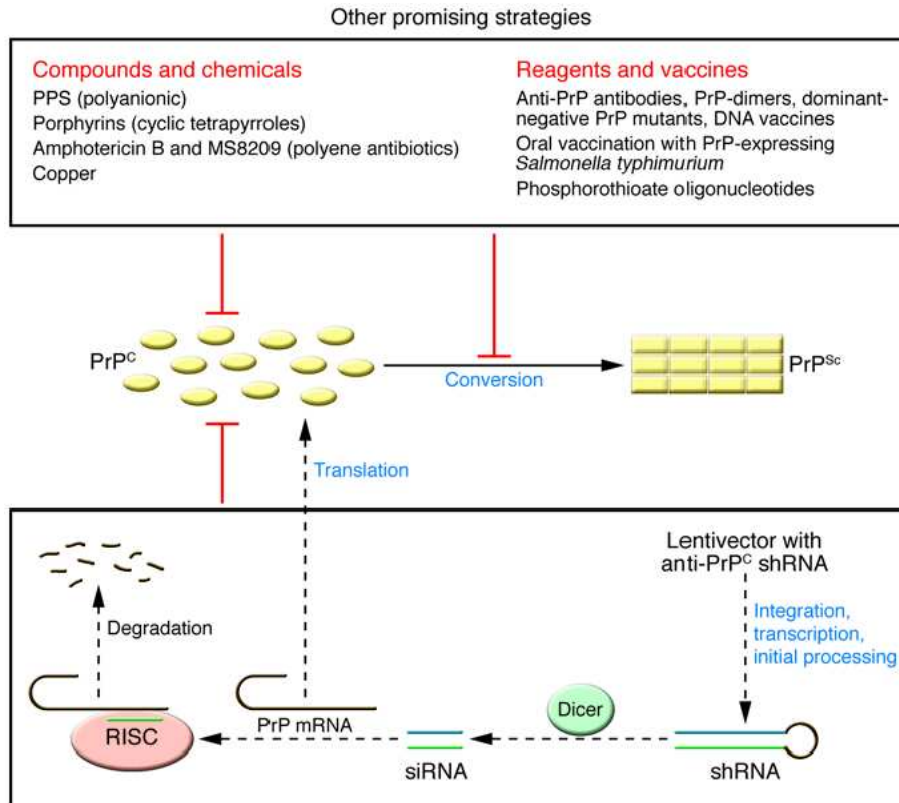


Figure 15. RNAi and other strategies for prion disease treatment. Monomeric PrP^C (yellow ovals) converts into multimeric PrP^{Sc} (yellow rectangles) in the process of prion replication and prion pathogenesis. Reagents or strategies that effectively reduce the PrP^C level or interfere with the PrP^C-to-PrP^{Sc} conversion process have shown therapeutic potential for prion disease. Adapted from Kong (2006).

Cell grafting therapy for prion diseases

The transplantation of embryonic cells or tissue to protect against neuronal loss could be a promising strategy for late stage treatment of prion diseases. Since PrP is essential for prion replication, grafting of PrP knock-out cells would prevent prion replication in the transplanted cells. Therefore, Brown and co-workers have used the fetal cells from PrP knock-out mice (PrP^{0/0}) to inject in hippocampal area 150 days after scrapie infection in C57bl/6//VM mice and observed a neuron survival of 54% greater than the control group despite no delay in the incubation time of the disease.^{91,164}

1.7 Therapies for other neurodegenerative diseases

1.7.1 Therapies for Alzheimer's disease

Alzheimer's disease (AD), the most common neurodegenerative disorder, is currently the focus of some of the most exciting and rapidly progressing research on

amyloid therapeutics. AD is a progressive neurodegenerative disorder and the leading cause of dementia in the elderly. As the incidence and prevalence of AD rise steadily with increasing longevity, AD threatens to become a catastrophic burden on health care, particularly in developed countries. AD patients typically present with symptoms of global cognitive decline and loss of memory.¹⁶⁵ AD pathology is characterized by the formation of two types of protein aggregates in the brain: amyloid plaques (Fig. 16a), which form an extracellular lesion composed of the A β peptide; and intracellular neurofibrillary tangles (Fig. 16b), which are composed of abnormal, hyperphosphorylated filaments of the microtubule-associated protein tau.⁴⁰ Genetic evidence implicates deregulated A β homeostasis as an early event in AD pathology.¹⁶⁶ Indeed as all familial AD mutations lead to increased production of this peptide or preferential production of a more fibrillogenic A β isoform (A β ₄₂).¹⁶⁷ For this reason, most AD therapeutics have targeted the A β peptide although tau-targeted therapies are also being pursued.^{168,169}

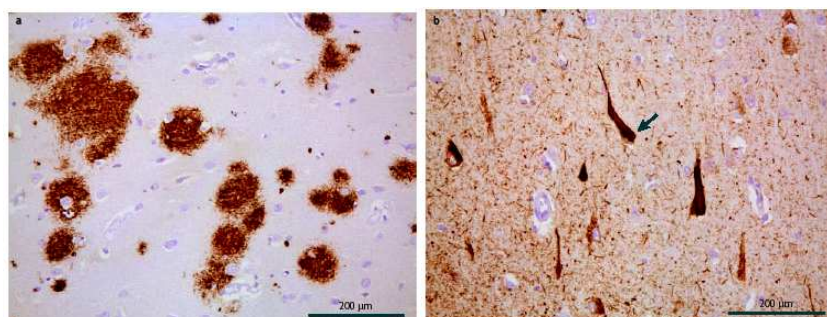


Figure 16. Characteristics of Alzheimer's disease (AD). (a) A human cortical section from a patient affected by AD, stained with an amyloid- β (A β)-specific antibody. One of the classical hallmarks of AD histopathology is the appearance of extracellular lesions known as senile or amyloid plaques. (b) A human cortical section from a patient affected by AD, stained with a phospho-tau-specific antibody. The second histopathological hallmark of AD is the presence of intraneuronal lesions known as neurofibrillary tangles (indicated by an arrow). Adapted from Aguzzi et al. (2010).

Pharmacological inhibition of the enzymes responsible for A β formation (γ -secretase and β -secretase) is a prime strategy for blocking A β production. The γ -secretase complex is responsible for the carboxy-terminal cleavage of amyloid precursor protein (APP) to produce A β ₄₀ or A β ₄₂. Potent small-molecule inhibitors of γ -secretase can dramatically reduce A β ₄₀ and A β ₄₂ production.^{170,171} These compounds either selectively inhibit γ -secretase cleavage of APP, leaving Notch cleavage unaffected, or alter γ -secretase cleavage of APP to favour A β ₄₀ production rather than A β ₄₂ which seems to be more closely associated with the development of

amyloid pathology than A β ₄₀.⁴⁰ Drugs that modulate γ -secretase activity in this manner include non-steroidal anti-inflammatory drugs (NSAIDs). The NSAID (*R*)-flurbiprofen (also known as tarenflurbil), effectively reduced amyloid plaque formation¹⁷² and rescued memory deficits¹⁷³ in APP-transgenic mice. It also yielded encouraging results in early human trials.^{174,175}

The amino-terminal cleavage of APP to form both A β ₄₀ and A β ₄₂ results from β -secretase activity. After the discovery that β -secretase cleavage of APP seemed to be due to the activity of a single aspartic protease, β -secretase 1 (BACE1; also known as memapsin 2 and ASP2), there was much interest in the possibility of targeting β -secretase for the treatment of AD.¹⁷⁶⁻¹⁸⁰ Inhibition of BACE1 activity can block the production of A β , prevent the development of amyloid pathology in the brain and rescue AD-related memory deficits in mice.¹⁸¹⁻¹⁸⁴ The large BACE1 active site requires the identification of large compounds for potent BACE1 inhibition that also readily penetrate the BBB¹⁸⁵ and are reasonably stable. Unfortunately, the slow progress of the BACE1 inhibitor field is a testament to the fact that such molecules are relatively rare.⁴⁰ Nevertheless, some BACE1 inhibitors have progressed to early clinical trials.¹⁸⁶

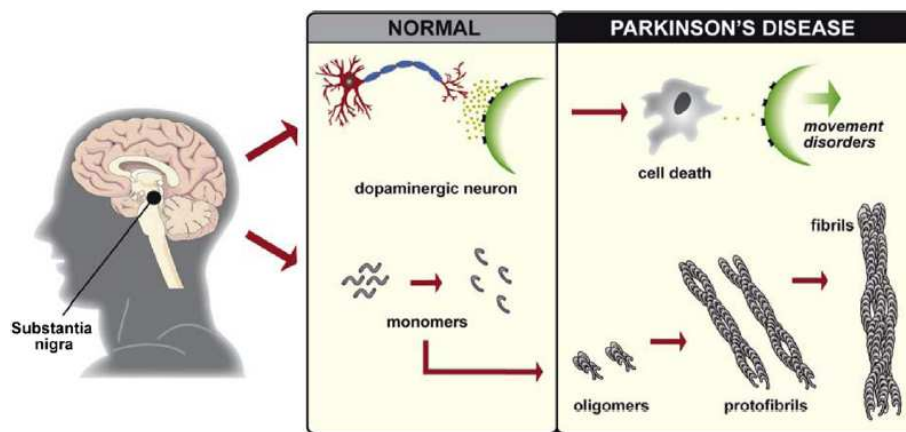
An alternative approach to protein aggregation therapeutics is to enhance the degradation of the aggregating protein or the aggregates themselves. Manipulating the immune system for the purpose of enhancing A β clearance has been pursued as a therapeutic approach for AD.⁴⁰ Several studies reported dramatically reduced A β levels and plaque pathology and/or cognitive improvements upon active immunization of APP-transgenic mice with full-length A β peptide,^{187,188} A β peptide fragments¹⁸⁹ and passive transfer of A β -specific antibodies.¹⁹⁰⁻¹⁹² Based on these studies and encouraging results from Phase I trials, active A β immunotherapy in humans subsequently progressed to a widely publicized Phase II clinical trial in 2001. Unfortunately, this trial was halted in January 2002 owing to the development of sterile meningoencephalitis in some patients.^{40,193}

In addition, several compounds, such as Congo red,¹⁹⁴ anthracycline,¹⁹⁵ rifampicin,¹⁹⁶ anionic sulphonates¹⁹⁷ or melatonin,¹⁹⁸ can interact with A β and prevent its aggregation into fibrils *in vitro*, thereby reducing toxicity. Moreover, certain non-fibrillogenic, A β homologous peptides can bind to A β and break the formation of β -sheet structure.^{12,199}

1.7.2 Therapies for Parkinson's disease

Parkinson's disease (PD) is the second most common progressive neurodegenerative brain disorder of humans, after Alzheimer's disease. The pathogenesis of the movement disorder PD and dementia with Lewy bodies (DLB) is associated with loss of dopaminergic neurons and the accumulation of aggregated forms of the alpha-synuclein (α -syn) protein (Fig. 17A,B).^{200,201} An early event in the neuropathology of PD and DLB is the loss of synapses and a corresponding reduction in the level of synaptic proteins. Loss of substantia nigra neurons and the presence of Lewy bodies and Lewy neurites in some remaining neurons are the hallmark of pathology seen in the final stages of the disease.²⁰²

A



B

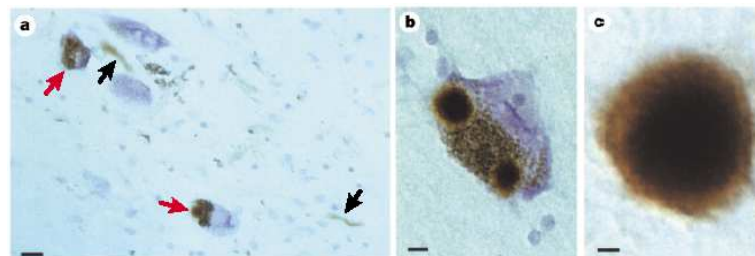


Figure 17. The alpha-synuclein (α -syn) pathology of Parkinson's disease (PD). (A) Formation of α -syn fibrils and the loss of dopaminergic neurons in the substantia nigra are observed in patients with PD. α -Syn (in grey) is normally a monomeric unstructured protein which undergoes conformational changes upon interaction with lipids and also upon fibrillation. (B) Lewy bodies and Lewy neurites in the substantia nigra and several other brain regions define PD at a neuropathological level. Here, these entities are labelled by α -syn antibodies. (a) Two pigmented nerve cells, each containing an α -syn-positive Lewy body (red arrows). Lewy neurites (black arrows) are also immunopositive. Scale bar, 20 μ m. (b) Pigmented nerve cell with two α -syn-positive Lewy bodies. Scale bar, 8 μ m. (c) α -Syn-positive extracellular Lewy body. Scale bar, 4 μ m. Adapted from Ruiperez et al.(2010) and Goedert (2001).

Alpha-synuclein, the main constituent of Lewy bodies, is a small soluble protein expressed primarily at presynaptic terminals in the CNS. The function of α -syn remains unclear although several evidences suggest that α -syn is involved in synaptic vesicle trafficking probably via lipid binding.^{200,202} Moreover, interactions with cholesterol and lipids have been shown to be involved in α -syn aggregation.²⁰³ Not only is α -syn found in Lewy bodies characteristic of PD, but also mutations in the gene for α -syn can cause an inherited form of PD and expression of normal α -syn can increase the risk of developing PD in sporadic or non-familial cases. Although the exact pathogenic mechanisms leading to cell death in the PD are not fully understood, various pathways including aggregation of natively unfolded α -syn, oxidative stress, or mitochondrial impairment can lead to cause cell death (Fig. 18).²⁰⁴

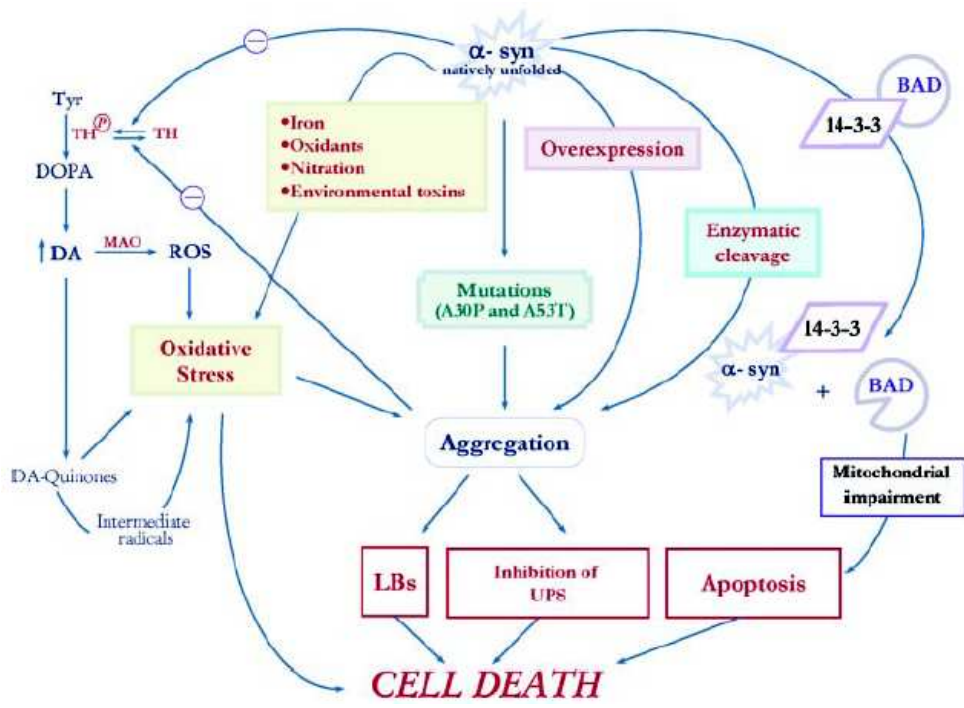


Figure 18. α -Syn aggregation and toxic effects in dopaminergic neurons. A hypothetical scheme depicts various pathways that leading to aggregation of natively unfolded α -syn, oxidative stress, or mitochondrial impairment, cause cell death. DA, dopamine; DOPA, dihydroxyphenylalanine; LBs, Lewy bodies; MAO, monoamine oxidase; ROS, reactive oxygen species; TH, tyrosine hydroxylase; TH^P, phosphorylated tyrosine hydroxylase; Tyr, tyrosine; UPS, ubiquitin proteasome system. Adapted from Recchia et al. (2004).

There have been therapeutic approaches for PD such as dopaminergic therapy, gene therapy, stem cell therapy, drug therapy. Current treatment of PD is symptomatic and the primary pharmacological therapies include dopamine replacement with levodopa,

synthetic dopamine agonists, and drugs which increase dopamine supply by inhibiting its metabolism (catechol-O-methyltransferase inhibitors and monoamine oxidase B inhibitors).²⁰⁵ Though pharmacological treatment and brain stimulation have been shown to reduce symptoms of PD, they are not cures. The controlled production of dopaminergic cells in large amounts for cell replacement (neurotransplantation) in PD is technically possible. Embryonic stem cells might have a great potential for cell replacement strategies in PD, either concerning their proliferative or their differentiative capacity. The use of fetal tissue-specific neural stem cells seems to be the safest and most likely the fastest way to establish a transplantation protocol in PD.²⁰⁶

To determine if statins, cholesterol synthesis inhibitors, might interfere with α -syn accumulation in cellular models, Bar-on and co-workers studied the effects of lovastatin, simvastatin, and pravastatin on the accumulation of α -syn in a stably transfected neuronal cell line (B103 neuroblastoma cells) and in primary fetal human neurons. Their results revealed that statins reduced the levels of α -syn accumulation in the detergent insoluble fraction of the transfected cells and enhanced neurite outgrowth while the contrastive results were obtained if the media supplemented with cholesterol. These results suggest that regulation of cholesterol levels with cholesterol inhibitors might be a novel approach for the treatment of PD.²⁰³

In addition, several compounds, such as dopamine analogs^{207,208} can interact with α -syn and prevent its aggregation into fibrils *in vitro*.

1.8 Aim of the present work

One of the causes for neurodegenerative diseases including Alzheimer's disease, Parkinson's disease and prion diseases is protein misfolding and aggregation. The protein misfolding may be associated to the diseases by either gain of a toxic activity by the misfolded protein or by the lack of biological function of the natively folded protein. Therefore, designed drugs aim to inhibit or reverse the conformational changes as a therapy to protein conformational diseases. However, the effective pharmacological tools for the diseases are not yet available. Moreover, the recently established interplay between prion and Alzheimer's diseases have led to an urgent demand to develop systematic pharmacological and mechanistic studies for the identification of new classes of compounds as therapeutic agents capable of inhibiting several pathways in prion conversion and replication. Thereby, the molecules binding

to either PrP^C or PrP^{Sc} conformers at the binding interface may interrupt prion production by inhibiting the interaction between the PrP^{Sc} template and the endogenous cellular PrP^C. Additionally, the compounds that bind molecules supporting and participating in prion replication, such as chaperones or other ligands, may also be good candidates for blocking prion replication. Most of the lead compounds identified so far are derived from screening approaches in established cellular models.

Based on these considerations, it emerges that rational design of anti-prion compounds is still a big challenge for medicinal chemists. However, a favorable point that could further motivate rational drug discovery in prion diseases, is that the lessons we can learn from their investigation with small molecules might have an impact on other conformational diseases, characterized by a similar pathological aggregation and accumulation of misfolded proteins.²⁰⁹ In this connection, it is relevant to note the recent discovery that PrP^C is a mediator of A β oligomer-induced synaptic dysfunction, and hence PrP^C-specific compounds may have therapeutic potential for Alzheimer's disease.^{210,211}

In the thesis, we discuss about therapeutic approaches for prion diseases and other neurodegenerative diseases from biological evaluation of four new libraries of the compounds designed and synthesized on nanotechnology, computational study and chemistry as well as study their mechanism of action in inhibiting prion replication. The most active anti-prion compounds may be therapeutic agents for the diseases.

2. Polyelectrolyte multilayer-coated gold nanoparticles as multi-target compounds for treatment of prion diseases and related neurodegenerative disorders

2.1 Introduction

The field of nanoparticle technology is rapidly expanding and promises revolutionary advances in the diagnosis and treatment of many devastating human diseases. Nanoparticles have been developed to allow targeted delivery and sustained release of therapeutics. Such nanoparticle-based drug formulations interact with biological systems both at molecular and supra-molecular levels. Nanoparticles can be tailored to respond to specific cell environments, and even to induce desired physiological responses in cells, whilst minimizing unwanted side effects. Compared to conventional drugs, nanoparticles-bearing therapeutics possess higher intrinsic pharmacological activity and their main advantage is their small dosage that would not require the administration of large amounts of potentially toxic therapeutics.²¹²

Here, we report the preparation of coated gold nanoparticles (AuNP) exposing, on their surface, functional groups that can selectively bind, inhibit or prevent the formation of misfolded protein aggregates such as prions. The build-up of nanoparticles was carried out with gold nanoparticles as core and a layer-wise deposition of oppositely charged polyelectrolytes, such as polycation polyallylamine hydrochloride (PAH) and polyanion polystyrenesulfonate (PSS). To examine the structure-activity relationship, we tested different numbers of layers, as well as the nanoparticles' outermost layer surface charge, for their possible role in inhibiting scrapie prion formation *in vitro* and *in vivo*. Our findings represent the first report of functionalized nanoparticles as novel potent anti-prion drugs.

2.2 Materials and methods

2.2.1 Synthesis of gold nanoparticles

Monodisperse AuNPs were prepared as described by Turkevich and co-workers.²¹³ For particles with a size of 15 ± 1 nm, 5.3 mg of $\text{NaAuCl}_4 \cdot 2 \text{H}_2\text{O}$ in 25 mL of Milli-Q grade water were boiled under reflux. One milliliter of a 1% trisodium citrate solution was rapidly added to the boiling pale yellow solution,

which resulted in a color change to deep red. After boiling for additional 20 min, the solution was cooled down to room temperature and stored protected from light at room temperature. All experiments described here were performed with the above colloidal gold nanoparticle stock solution.

The 46 nm gold particles were prepared using the same procedure but with 10.6 mg of NaAuCl_4 in 25 mL water and the fast addition of 750 μL 1% trisodium citrate solution.

2.2.2 Polyelectrolyte coating

The polyelectrolyte coating was applied in accordance to the method previously described with a few modifications.²¹⁴⁻²¹⁶ Briefly, 1 mL colloidal AuNPs were added drop-wise under constant stirring to 200 μL of PSS solution (10 mg/mL) or 500 μL PAH solution (3 mg/mL). Both solutions are supersaturated to allow for an immediate coverage of the particles with polyelectrolytes. After incubation for 20 min in the dark, this solution was centrifuged for 20 min at $20,000 \times g$. The supernatant was removed and the particles were washed twice by centrifugation/resuspension in Milli-Q water. Prior to the next layer deposition the coated AuNPs were stored in the dark for 1 hour. The coated particles were then incubated with the oppositely charged polyelectrolyte (Fig. 19).

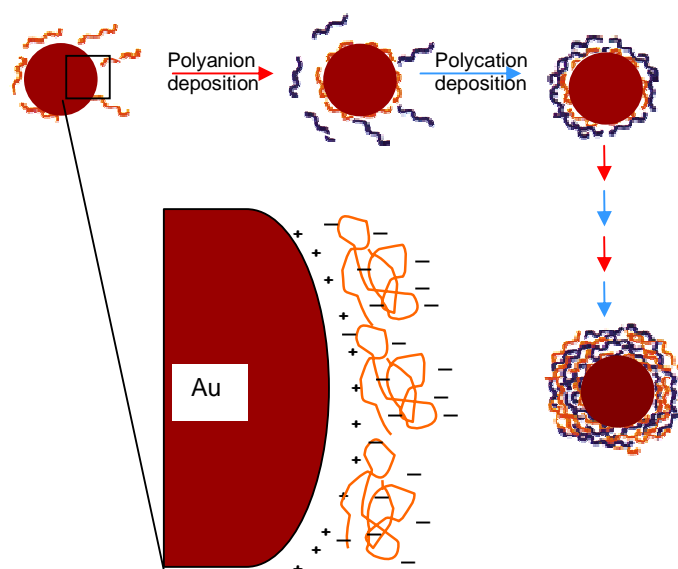


Figure 19. Layer-by-Layer technique for oppositely charged polyelectrolyte coating. Polystyrenesulfonate (PSS) and polyallylamine hydrochloride (PAH) are used as polyanion and polycation, respectively.

Each coating step was proved on a NS Zetasizer (Malvern, Milan, Italy) with dynamic light scattering (DLS) for size and polydispersity index (PDI) and zeta-potential measurements for changes in the surface charge. The concentration of the AuNPs was determined at 580 nm in a UV/Vis spectrometer applying the Beer-Lambert law ($\lambda_{\text{abs}} = 518 \text{ nm}$, $\epsilon = 5.14 \times 10^7 \text{ M}^{-1} \text{ cm}^{-1}$).²¹⁷

2.2.3 Transmission electron microscopy of coated gold nanoparticles

High-resolution transmission electron microscopy (HRTEM) measurements were performed by diluting the coated AuNP solution with Milli-Q water to a ratio of 1:100. Then the solution was deposited on a carbon-covered 200-mesh copper grid and dried in air at room temperature. The images were acquired with acceleration voltage ranging from 18.5 to 150 kV. The non-digital images were digitized and the data analyses of the images were performed using ImageJ software.

2.2.4 Cell culture, drug treatment and cell viability

Cell culture, drug treatment and cell viability were performed in accordance to protocols described previously.²¹⁸

Cell culture

ScGT1 cells were seeded in 10-cm plates containing 10 mL of Dulbecco's modified Eagle's medium (DMEM) culture media, supplemented with 10% fetal bovine serum (FBS) and 1% penicillin-streptomycin. ScN2a cells were cultivated in 10-cm plates, containing 10 mL of minimal essential medium with Earle's salt (EMEM) culture media, supplemented with 10% FBS, 1% non-essential amino acids, 1% L-glutamax, 1% penicillin-streptomycin. The cells were grown at 37°C in 5% CO₂ to 95% confluence for 1 week before splitting at 1:10 for further cultivation.

Drug treatment

Quinacrine was dissolved in PBS at 1 mM. Imipramine was dissolved in 100% dimethyl sulfoxide (DMSO) to a solution with a concentration of 100 mM. This solution was then further diluted into the final stock solution of 10 mM with 10% (v/v) DMSO/PBS. The final concentration of DMSO in the cell medium was never above 0.1%. The nanoparticles were diluted in PBS. The media were refreshed and drugs were added to the cultures 2 days after splitting of the cells and incubated for 5 days. Each experiment was performed using triplicate cultures.

Cell viability

ScGT1 and ScN2a cells were maintained in DMEM and EMEM, respectively, and supplemented with 10% FBS. After 1 day of incubation, media were aspirated from a confluent 10-cm plate of cells, and cells were detached by addition of 1 mL of 1X trypsin-EDTA solution. Media were added, and cell density determined by cell counting using a haemocytometer. The cell density was adjusted to 2.5×10^5 cells/mL with DMEM for ScGT1 cells and 3.0×10^5 cells/mL with EMEM for ScN2a cells. A 96-well, tissue culture-treated, clear bottom, black plate (Costar) wetted with 90 μ L of DMEM or EMEM, was incubated at 37°C, prior to use. One hundred μ L of the cell suspension were added to each well and the cells were allowed to settle for 2 hours, prior to the addition of the test compound. Compound library stocks were prepared as described above and diluted 1/20 with sterile PBS prior to use at the required concentrations in 96-well plates. Ten μ L of the compounds were added to each well, and the plates were incubated at 37°C in 5% CO₂. Final DMSO concentration was never above 0.1% (v/v). Media were aspirated after incubation of 5 days and cells were washed twice with 200 μ L of PBS. One hundred μ L of 2.5 μ M calcein-AM were added, and the plates were incubated at 37°C for 30 min. Fluorescence emission intensity was quantified using a SpectraMax Gemini EM or SpectraMax M5 fluorescence plate reader, excitation/emission ratio equal to 492/525 nm.

2.2.5 PrP^{Sc} detection in cell lysates by Western blot

After 5 days of drug treatment, the accumulation of PrP^{Sc} was detected by proteinase K (PK) digestion followed by immunoblotting of lysed cells as described previously.⁸⁸ One mL of lysis buffer (10 mM Tris-HCl pH 8.0, 150 mM NaCl, 0.5 % nonidet P-40, 0.5 % deoxycholic acid sodium salt) was added to cell plates and the cell lysates were collected after centrifugation at 2,000 rpm for 5 min in a bench microfuge (Eppendorf). The total protein amount of the samples was measured by the bicinchoninic acid assay (BCA) (Pierce). Five hundred μ L of 1 mg/mL ScGT1 or 100 μ L of 1 mg/mL ScN2a cell lysates were digested by 20 μ g/mL of PK for 1 hour at 37°C. The reaction was stopped with 2 mM phenylmethylsulphonylfluoride (PMSF) and the PK-digested cell lysates centrifuged at 48,000 rpm for 1 hour at 4°C in an ultracentrifuge (Beckman Coulter). The pellets were resuspended in 1X sample loading buffer. For the non-PK digested sample, 50 μ g of cell lysates for ScGT1 or 25 μ g of cell lysates for

ScN2a were used and 2X loading buffer (125 mM Tris HCl, pH 6.8, 10% 2-mercapethanol, 4 % SDS, 0.2 % bromophenol blue, 20 % glycerol) was added in a 1:1 ratio. The samples were boiled for 5 min at 100°C, loaded onto either a 12% or a 15% Tris-Glycine SDS- PAGE gel, and transferred overnight onto Immobilon P PVDF membranes (Millipore). Membranes were blocked by 5% nonfat milk, incubated with 1 µg/mL anti-PrP Fab D18 followed by incubation with goat anti-human IgG F(ab)2 fragment conjugated with horseradish peroxidase. Blots were developed with the enhanced chemiluminescent system (ECL, Amersham Biosciences) and visualized on Hyperfilm (Amersham Biosciences).

2.2.6 PrP^{Sc} quantification by ELISA

The quantification of PrP^{Sc} by ELISA followed a protocol described previously.¹³⁷ Briefly, PK digestion of cell lysates was as described above. PK-digested PrP^{Sc} was selectively precipitated by the addition of 0.5% aqueous phosphotungstic acid (PTA, Sigma-Aldrich) solution with continuous shaking at 37°C, 350 rpm for 1 hour, and centrifuged at room temperature, 14,000 x g for 30 min. Pellets were dissolved and denatured in 50 µL of 8M guanidine hydrochloride (GdnHCl) in coating buffer (0.1 M sodium bicarbonate, pH 8.2) for 1 hour and diluted into 500 µL of coating buffer. Twenty µL of the suspension were transferred to 96-well MaxiSorp ELISA plates (Nunc), with each well containing 180 µL coating buffer and the plates were sealed and incubated overnight at 4°C. To increase the immunoreactivity of PrP^{Sc}, coated proteins were denatured *in situ*. Fifty µL of 8M GdnHCl were added to each well and incubated for 10 min at room temperature. The ELISA plates were washed three times with TBST (20 mM Tris-HCl, 137 mM NaCl, 0.05% Tween-20, pH 7.5) and blocked with 200 µL of 3% BSA, made up in TBS (20 mM Tris-HCl, 137 mM NaCl, pH 7.5) sealed and incubated at 37°C. After 1 hour, the plates were washed three times with TBST, and incubated with 100 µL of anti-PrP antibody D18 (2 µg/mL) in 1% BSA/TBS, at 37°C for 2 hours. They were then washed seven times with TBST. One hundred µL of goat anti-human IgG Fab conjugated to HRP and diluted 1:1000 with 1% BSA/TBS were added to the plates and incubated at 37°C for 1 hour. Again, plates were washed seven times with TBST, and then developed with 100 µL of 1-step TMB (3,3',5,5'- tetramethylbenzidine) Turbo ELISA HRP substrate (Pierce). The reaction was stopped by the addition of 100 µL of 2 M sulfuric acid to the plates. Absorbance at 450 nm was measured using a microplate

reader (VersaMax, Molecular Devices). Dose-response curves and EC₅₀ values were computed using GraphPad Prism (version 4.0).

2.2.7 Coated nanogold uptake studies

GT1 and N2a neuronal cell lines (1.0×10^5 cells) were seeded on 24 x 24 mm cover slips in 35 mm-plates with 2 mL of DMEM supplemented with 10% FBS, 1% penicillin-streptomycin and EMEM with 10% FBS, 1% non-essential amino acids, 1% L-glutamax, 1% penicillin-streptomycin, respectively, and were cultured for 24 hours at 37°C in 5% CO₂. For the uptake 50 µL of a solution containing either nanogold particles coated with (PSS/FITC-PAH) tagged as 2A, or coated with (PSS/FITC-PAH)₂/PSS called 5S were added, along with 30 µM of DiA [4-di-16-ASP, (4-(4-dihexadecylamino)styryl)-N-methylpyridinium iodide, Molecular Probes] (labeling intracellular membranes) and incubated for 2, 6, 12, 24 or 48 hours at 37°C in 5% CO₂. After incubation, the culture media were aspirated and the adherent cells were washed 2 times with 2 mL of respective media, without antibiotics and sera. Then, the cells were studied by confocal fluorescence microscopy. The experiments were repeated at least 3 times for each cell line and time.

Imaging acquisition was performed with Nikon C1 laser scanning confocal unit (Nikon D-eclipse C1, Japan) attached to an inverse fluorescence microscope (Nikon D-eclipse C1Si, Japan) with 100 X/1.49 oil Apo TIRF objective (Nikon, Japan). Excitation was performed with an air-cooled Argon laser emitting at 488 nm for FITC ($\lambda_{ex} = 488$ nm, $\lambda_{em} = 520$ nm) and a diode laser at 561nm exciting DiA ($\lambda_{ex} = 570$ nm, $\lambda_{em} = 630$ nm), with appropriate filter sets to collect the fluorescence emission. Images were acquired and processed using the operation software EZ-C1.

2.2.8 Detection of *in vitro* effect of the nanoparticles on prion fibril formation and amyloid seeding assay (ASA)

Fibril formation was performed in accordance to the method previously described with a few modifications.²¹⁹ Briefly, 500 µL of 2 mg/mL ScN2a or ScGT1 cell lysates was used for PTA precipitation by adding 500 µL of PBS/4% Sarkosyl/protease inhibitor and 0.5% PTA with continuous shaking at 37°C, 350 rpm for 1 hour, and centrifuged at room temperature, 14,000 x g for 30 min. The pellets were washed with 500 µL of PBS/2% Sarkosyl/protease inhibitor, centrifuged and resuspended in 150 µL of water and then stored at -80°C until use.

In ASA, 4 μL of resuspended PTA pellets was diluted into 400 μL of water and 20 μL of the diluted sample was added to each well containing 180 μL of reaction solution (50 $\mu\text{g}/\text{mL}$ MoPrP(23-230), 0.4 M GdnHCl, 10 μM ThT in PBS 1X buffer) in a 96-well black plate (BD Falcon). The nanoparticles added in different concentrations to each well. Each sample was performed in four replicates. Each well contained one 3-mm glass bead (Sigma). The plate was covered with sealing tape (Fisher Scientific), incubated at 37°C with continuous shaking and read on SpectraMax M5 or Gemini EM fluorescence plate reader (Molecular Devices) by top fluorescence reading every 5 min at excitation of 444 nm and emission of 485 nm.

2.2.9 Detection of *in vitro* effect of the nanoparticles on β -amyloid and α -synuclein fibril formation

Twenty μL of the nanoparticles added in different concentrations to each well containing 180 μL of reaction solution (10 $\mu\text{g}/\text{mL}$ A β_{1-40} wild-type, 10 μM ThT in 50 mM Tris-HCl pH 7.4 for β -amyloid fibril formation; or 1 mg/mL recombinant human α -synuclein, 100 mM NaCl, 10 μM ThT in 20 mM Tris-HCl pH 7.4 for α -synuclein fibril formation) in a 96-well black plate (BD Falcon). Each sample was performed in four replicates. Each well contained one 3-mm glass bead (Sigma). The plate was covered with sealing tape (Fisher Scientific), incubated at 37°C with continuous shaking and read on SpectraMax M5 fluorescence plate reader (Molecular Devices) by top fluorescence reading every 5 min at excitation of 444 nm and emission of 485 nm.

2.2.10 Binding activity of the nanoparticles to prion proteins in cultured cells

N2a, GT1, ScN2a, ScGT1 were cultured for 5 days, refreshed media and added 100 pM of nanogold particles coated with (PSS/FITC-PAH) tagged as 2A, or coated with (PSS/FITC-PAH)₂/PSS called 5S, and then incubated for 2 more days. The cells were washed by media without antibiotics and sera and the cell proteins were extracted. Five hundred μg protein was used with or without 20 $\mu\text{g}/\text{mL}$ of PK, PTA-precipitated and pellets dissolved in 200 μL lysis buffer. The samples were added in each well of 96-well black plate and relative fluorescence unit (RFU) values were measured by Gemini EM fluorescence plate reader (Molecular Devices) at 488/525 nm.

2.2.11 Preparation of the nanoparticles pre-treated brain homogenates

Ten % RML (Rocky Mountain Laboratories) infected brain homogenate (wt/vol) was prepared from pools of brains of terminally RML-sick CD-1® IGS mice (Charles River Laboratories), while 10% mock homogenate (wt/vol) was obtained from pools of brains of healthy CD-1 mice. 2A and 5S coated AuNPs were separately pre-incubated with both RML and mock brain homogenates at 4°C for 24 hours. Even RML and mock brain homogenates untreated with nanoparticles were subjected at the same pre-treatment. The final 2A coated AuNPs concentration in both RML and mock homogenates was 25.35 nM while that of AuNPs 5S was 26.65 nM.

2.2.12 Analysis of the homogenates by transmission electron microscopy

Mouse brain homogenates (both RML and mock) treated with 2A or 5S particles were dissolved in distilled water (1:2) then 5 µL of the final suspension were applied to Formvar-carbon-200-mesh nickel grids for 6 min, negatively stained with uranyl acetate and observed with an electron microscope (EM109 Zeiss, Oberkoken, Germany) operated at 80 kV at a standard magnification (X 30,000), calibrated with an appropriate grid. The samples were evaluated for the presence and amount of AuNP aggregates.

2.2.13 Animal inoculation

All mice were divided in six different groups, housed in ventilated cages and identified by ear-tags. Each group was intracerebrally inoculated with 30 µL of a precise solution: i.e. (i) RML or (ii) mock brain homogenate pre-incubated with AuNPs 2A; (iii) RML or (iv) mock brain homogenate pre-incubated with AuNPs 5S; (v) RML and (vi) mock brain homogenates untreated. 10-15 mice for each group were anesthetized with sevoflurane and inoculated into the right caudatus nucleus by using Hamilton syringes with 26G needle. Both preparations of the inocula and their injection were carried out using sterile instrumentation and disposable equipment for each animal and each inoculum. Groups of mock-inoculated and untreated mice were included as controls.

2.2.14 Behavioral monitoring

Behavioral monitoring was carried out weekly, beginning at 16 weeks post-inoculation, and included spontaneous locomotor activity in the open field, nest

construction test, reactivity to external stimuli and inverted screen test.^{220,221} The incubation time was calculated as the period between the day of inoculation and the appearance of clinical signs of disease, confirmed by a subsequent assessment at 3 days interval. At the terminal stage of disease (characterized by ataxia, hunched dorsal kyphosis, and suppressed righting reflex) clinically affected mice were sacrificed, while the other mice were monitored for the entire predicted life span and then culled and subjected to necropsy.

2.2.15 Histological examinations

All mouse tissues were collected for the study. Regarding CNS, the left hemisphere of each mouse brain was fixed in Carnoy solution at 4°C for 24 hours,²²² while the right hemisphere was frozen at -80°C for Western blot analysis. The same procedure was followed for the other organs (i.e. brain stem, muscle, spleen, liver, kidney, Peyer's patch, etc.). Fixed brain samples were cut in four standard coronal levels,²²³ dehydrated, and embedded in paraplast. 7 µm thick serial sections from paraffin embedded tissues were stained with hematoxylin-eosin (HE) or probed with different antibodies (i.e. 6H4, GFAP, Caspase-3, etc.). Spongiform profiles were determined on HE-stained sections, by scoring the vacuolar changes in nine standard grey matter area as described.²²³

2.2.16 Immunohistochemical staining

Sections were immunostained with monoclonal antibody to PrP (6H4 1:1000, Prionics), monoclonal antibody to myelin protein (CNPase 1:500, Sigma-Aldrich), polyclonal antibody to glial fibrillary acidic protein (GFAP 1:1000, Dako), monoclonal antibody to T-lymphocyte (CD3ε 1:500, Millipore) and a polyclonal antibody to apoptotic cells (Caspase-3 1:100, Millipore). Before PrP immunostaining, the sections were sequentially subjected to PK digestion (10 µg/mL, room temperature, 5 min) and guanidine isothiocyanate treatment (3M, room temperature, 20 min), and non-specific binding was prevented using Animal Research Kit Peroxidase (Dako). Immunoreactions were visualized using 3-3'-diaminobenzidine (DAB, Dako) chromogen.

2.2.17 PK immunoblot analysis of mouse brain homogenates

Ten % (wt/vol) brain homogenates from frozen tissues were prepared in lysis buffer (100 mM sodium chloride, 10 mM EDTA, 0.5% Nonidet P40, 0.5% sodium

deoxycholate in 10 mM Tris-HCl, pH 7.4). Aliquots of cleared lysate equivalent to 100 µg were digested with 50 µg/mL of PK for 1 hour at 37°C. Reactions were terminated by the addition of phenylmethanesulfonyl fluoride (PMSF, 5mM). Treated homogenates were loaded on 12,5% polyacrylamide gels, transferred to polyvinylidene fluoride membranes and probed with anti-PrP antibody 6H4 (1:10000, Prionics), anti-CNPase antibody (1:1000, Sigma-Aldrich) and anti-Caspase-3 antibody (1:100, Millipore). The immunoreactions were visualized by enhanced chemiluminescence system (Amersham).

2.2.18 Magnetic resonance imaging (MRI)

MRI was performed in clinically symptomatic CD-1 mice challenged with RML and in non-infected control mice on a Bruker BioSpec 70/30 USR Tesla scanner. Mice were anesthetized with isoflurane at a dose approximately of 2.5 L/min, modulated according to the breathing frequency. The animals were positioned on opposite bed inside the magnet and were monitored throughout the procedure for breathing frequency and body temperature with specific probes. Twenty-six axial slices were acquired for each mouse with T2 High Resolution Turbo Spin Echo sequences. The following parameters were employed: thickness 0.60 mm without gap, TR 3000 ms, TE 27.1 ms, FOV 2.20/2.20 cm, and 256 matrix.

2.2.19 Statistical analysis

Statistical analyses were performed using the GraphPad-Prism 4.0 software. Kaplan-Meier survival curves were plotted, and differences in survival between groups of mice inoculated with RML (positive control) and RML pre-incubated with AuNPs 2A or AuNPs 5S were compared using the log-rank test.

2.3 Results

2.3.1 Physical characteristics of polyelectrolyte multilayer-coated gold nanoparticles

The physical characteristics of the coated nanoparticles are given in Table 3. For the experiments to inhibit PrP^{Sc} replication *in vitro*, particles from 1 to 5 layers were prepared, finishing with either a positive (PAH) or negative (PSS) charged layer. All particle preparations finishing with PSS were tagged as nS (n = 1-5) and each one with PAH was labeled mA (m = 1-5). The layers were deposited onto

AuNPs with a hydrodynamic diameter (D_h) of 19.9 ± 0.2 nm via an electrostatic driven self-assembly process and their size was measured by dynamic light scattering (DLS). DLS usually gives a larger diameter than electron microscopy, because it also measures the ionic shell (citrate) around the hard core (gold). As an example, in Figure 20 we show a high-resolution transmission electron microscopy (HRTEM) image of a coated (2A) AuNP. As can be noted, the particle is around 15 nm in diameter and, in the dehydrated form in ultra-high vacuum, the 2 layers of the coating measures less than 1 nm. The thickness is not perfectly homogenous, but the coating is covering the particle surface completely.

The concentration was determined via UV-VIS absorption spectrometry. It has to be noted that with UV-VIS it was only possible to quantify the AuNPs concentration but not the concentration of the active compounds which are the polyelectrolyte. Experiments are under development to quantify directly the polycation and polyanion concentration on the surface. Table 3 shows that the particle diameter increases with every deposited layer. In addition, the successful deposition of the polyelectrolyte layers was confirmed by the change in surface charge (ζ -potential measurements).

Finally, experiments were performed to investigate if the curvature of the AuNPs had an effect on functionality. To this purpose, AuNPs with a bigger diameter (45.7 ± 0.3 nm) were prepared and tested.

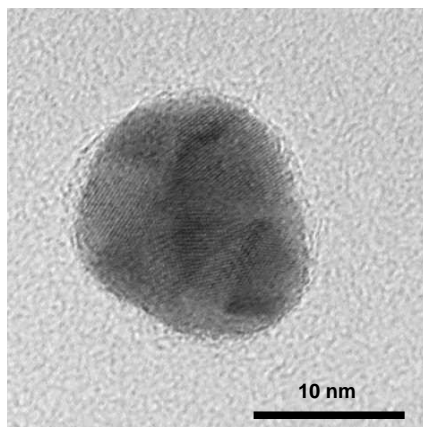


Figure 20. HRTEM image of a 2A coated nanogold particle. It was acquired with an acceleration voltage of 200 kV.

Table 3. Physical characteristics of the nanoparticles

Nanoparticles	(D_h) (nm)	ζ -potential (mV)	Concentration (nM)	Number of particles/mL
	Mean \pm SD	Mean \pm SD		
NG-15nm	19.9 \pm 0.2	-40.0 \pm 0.4	33.0	1.99 $\times 10^{+13}$
1A*	105.1 \pm 2.9	52.8 \pm 0.9	18.7	1.12 $\times 10^{+13}$
2A	128.9 \pm 9.9	63.0 \pm 0.9	30.3	1.83 $\times 10^{+13}$
3A	112.8 \pm 6.3	58.8 \pm 0.9	32.7	1.97 $\times 10^{+13}$
4A	110.9 \pm 3.2	65.4 \pm 5.4	14.2	8.55 $\times 10^{+13}$
5A	110.1 \pm 1.4	56.4 \pm 3.2	14.2	8.55 $\times 10^{+13}$
1S*	59.0 \pm 1.7	-50.7 \pm 1.3	37.9	2.28 $\times 10^{+13}$
2S	88.7 \pm 5.4	-48.1 \pm 3.8	29.2	1.76 $\times 10^{+13}$
3S	103.8 \pm 0.6	-56.0 \pm 3.3	24.5	1.48 $\times 10^{+13}$
4S	98.6 \pm 5.0	-49.8 \pm 6.1	16.1	9.72 $\times 10^{+13}$
5S	94.0 \pm 0.7	-53.6 \pm 0.5	14.2	8.55 $\times 10^{+13}$
NG-46nm	45.7 \pm 0.3	-32.4 \pm 3.2	82.9	4.99 $\times 10^{+13}$
2A	86.9 \pm 1.8	50.8 \pm 0.8	61.3	7.38 $\times 10^{+12}$
5S	155.4 \pm 8.3	-39.6 \pm 0.83	34.0	4.10 $\times 10^{+12}$

*A - outermost layer PAH and S - outermost layer PSS

The mean particle size (D_h) and zeta-potential (ζ -potential) were obtained from cumulative measurements (SD, n = 6).

2.3.2 Anti-prion potency and cytotoxicity of nanoparticles in cell lines

Potency of known drugs such as quinacrine and imipramine was used as a control for anti-prion activity in our cellular models, two different types of immortalized neuronal cells, GT1 and N2a. The potency of quinacrine and imipramine was similar to previous publications,⁹⁵ as indicated in Table 4; namely EC_{50} of quinacrine was 0.4 ± 0.1 and 0.3 ± 0.1 μ M for ScGT1 and ScN2a, respectively; whereas for imipramine EC_{50} was 6.2 ± 0.4 and 5.5 ± 0.5 μ M for ScGT1 and ScN2a, respectively. In comparison, citrate stabilized AuNPs without polyelectrolyte layers did not show any detectable prion inhibitory activity. The number of layers and the surface charge of the nanoparticles influenced survival of the neuronal cells, ScGT1 and ScN2a. Cytotoxicity was determined by measuring the number of cells surviving after incubation in the drug-doped medium for five days, assayed with calcein-AM in a fluorescence plate reader. With positively charged particles (1-5 A) a 92-100% cell viability was obtained and with negatively charged particles (1-5 S) the 74-100% of the cells survived (Table 4).

Table 4. PrP^{Sc} inhibition and cellular toxicity of quinacrine, imipramine and the nanoparticles in ScGT1 and ScN2a cells

Compounds	PrP ^{Sc} inhibition*		% cell viability ± SE [†]	
	ScGT1 (EC ₅₀ ± SE, μM)	ScN2a (EC ₅₀ ± SE, μM)	ScGT1	ScN2a
Small molecules				
Quinacrine	0.4 ± 0.1	0.3 ± 0.1	100 ± 4	100 ± 2
Imipramine	6.2 ± 0.4	5.5 ± 0.5	100 ± 7	100 ± 5
Nanoparticles	ScGT1 (EC ₅₀ ± SE, pM)	ScN2a (EC ₅₀ ± SE, pM)	ScGT1	ScN2a
Positive surface charge -PAH (NG-15nm)				
1A	8.3 ± 0.5	8.4 ± 0.6	100 ± 6	100 ± 3
2A	8.8 ± 0.2	24.5 ± 1.0	100 ± 1	97 ± 1
3A	10.1 ± 0.2	20.4 ± 0.5	100 ± 7	96 ± 3
4A	25.4 ± 1.3	25.1 ± 1.2	100 ± 6	100 ± 5
5A	20.1 ± 1.1	30.0 ± 1.4	100 ± 3	92 ± 1
Negative surface charge -PSS (NG-15nm)				
1S	121.4 ± 6.5	248.7 ± 12.9	95 ± 2	92 ± 5
2S	99.8 ± 4.7	220.3 ± 11.8	97 ± 1	87 ± 3
3S	70.1 ± 3.2	149.5 ± 6.1	74 ± 7	90 ± 3
4S	50.3 ± 2.0	130.1 ± 5.4	100 ± 2	90 ± 7
5S	35.0 ± 1.4	129.9 ± 7.1	84 ± 8	93 ± 4
NG-46nm				
2A	10.3 ± 0.3	30.2 ± 1.7	100 ± 4	94 ± 2
5S	89.7 ± 3.5	329.5 ± 10.7	90 ± 1	91 ± 6

*EC₅₀ - Compound concentration required to reduce PrP^{Sc} level 50% versus untreated cells.

†Cell viability at EC₅₀ values was determined by calcein-AM cytotoxicity assay and expressed as an average percent of viable cells versus control untreated cells (SE, n = 3).

Moreover, the concentration at which complete inhibition of PrP^{Sc} formation in ScGT1 and ScN2a cells is achieved was determined by immunoblotting. Particle preparations were added at different concentrations to scrapie-infected cells, and the inhibitory activity was measured over five days. PrP^{Sc} levels were quantified by ELISA. The resulting EC₅₀ of the particles with a positive outermost layer (mA) was in the range of 8.3 ± 0.5 - 25.4 ± 1.3 pM in ScGT1 and 8.4 ± 0.6 - 30.0 ± 1.4 pM in ScN2a cells (Table 4). In both cases, the influence of size and number of layers on efficacy was limited. However, prion inhibition by particles with a negative outermost layer (nS) showed an increase in efficacy with a higher number of layers. In particular, EC₅₀ of 1S was 121.4 ± 6.5 pM and 5S was 35.0 ± 1.4 pM in ScGT1 while EC₅₀ of 1S was 248.7 ± 12.9 pM and 5S was 129.9 ± 7.1 pM in ScN2a cells (Table 4).

To investigate the influence of particle curvature on prion inhibition, bigger

AuNPs were used. Regarding the AuNPs with a diameter of 46 nm, efficacy and cytotoxicity were only tested for 2A and 5S coatings. Both tested cell types showed cell viability in the range of 90-100% (Table 4). Prion inhibition of 2A-46 nm was similar to 2A, and 5S-46 nm was three times less effective than 5S (Fig. 21 and Table 4).

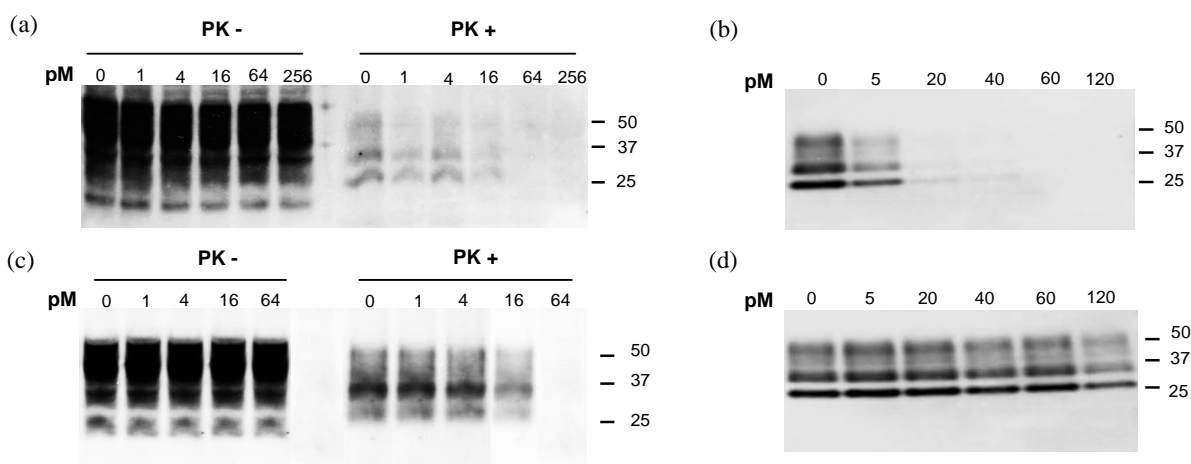


Figure 21. Western blot of cell lysate from ScGT1 cells treated with nanoparticles. (a) 2A, (b) 2A-46 nm, (c) 5S, (d) 5S-46 nm. After a two-day cell culture, the media were refreshed, the nanoparticles added at the indicated concentrations and the cells were incubated for five more days. Proteins from the cell lysate were quantified, treated with or without PK and immunoblotted using anti-PrP Fab D18.

2.3.3 Coated gold nanoparticles uptake studies

The uptake mechanism of AuNPs coated with 2A or 5S was monitored in the two different types of immortalized neuronal cells used in this study, GT1 and N2a. Figure 22 shows the uptake of 5S nanoparticles by GT1 (Fig. 22a,b) and N2a cells (Fig. 22c) at 2 and 24 hours. This was deduced by co-localization of two fluorescent dyes evident from the yellow signal due the overlap of the red fluorescence emitted by lipid dye DiA, incorporated in the membrane encircling the nanoparticles, and the green fluorescence from FITC-PAH bound to AuNP (Fig. 22a, arrow in 7th image). In contrast if the particles are only attached to the plasma membrane the fluorescence is green (Fig. 22a, ring in 3rd image). Images were acquired 2 hours after incubation of GT1 cells with the coated AuNPs. After 24 hours GT1 cells still show the yellow signal of nanoparticles in vesicles (Fig. 22b). The same uptake mechanism was observed for N2a cells (Fig. 22c) imaged 2 hours after incubation with particles.

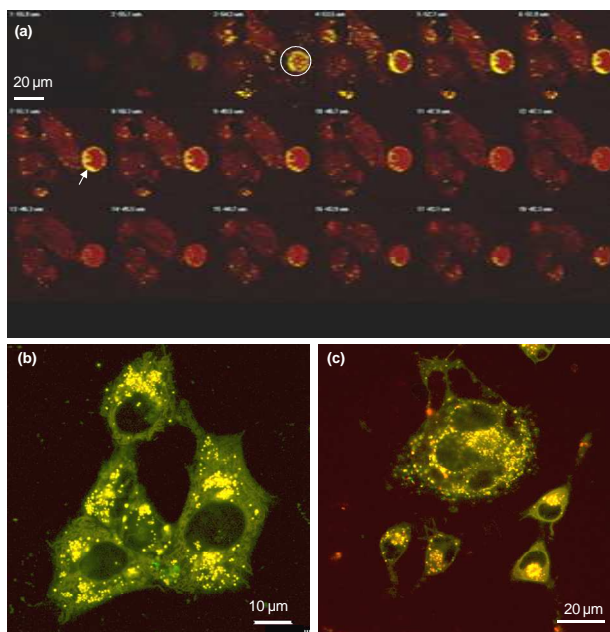


Figure 22. Uptake of coated nanoparticles into immortalized neuronal cells. The particles were labeled with FITC (green) and cell membranes were stained with DiA (red). Co-localization of particles in vesicles gave a yellow signal. **(a)** 3D optical sectioning of GT1 cells incubated for 2 hours with 5S coated nanogold. The white circles in section 3 indicate coated gold nanoparticles attached to the cell surface and therefore showing only green fluorescence. The arrow in section 7 indicates membrane encircled structures filled with nanoparticles (yellow). **(b)** 5S nanoparticles in GT1 cells after 24 hours of incubation. **(c)** 5S nanoparticles in N2a cells after 2 hours of incubation.

2.3.4 *In vitro* effect of the nanoparticles on prion fibril formation

Given 2A and 5S potent anti-prion activity in scrapie-infected cells, these two particles were chosen to test their ability of inhibiting recombinant PrP fibril formation in an amyloid seeding assay (ASA).²¹⁹ Using full-length recombinant mouse (Mo) PrP(23-230) as template and ScN2a- and ScGT1-PTA precipitated prions as seeds in a standard ASA assay, 2A and 5S, at concentrations of 50 pM and 200 pM respectively, extended the lag phase by 5-15 hours, hence showing a much slower kinetics than the control (Fig. 23). The potency of 2A and 5S in delaying PrP fibril formation suggests that these nanoparticles may directly interact with PrP and prevent its conversion into the pathogenic PrP^{Sc}-like form. In light of these results, ASA could also be utilized to study the mechanistic steps involved in the inhibitory effects of drugs screened for prion diseases, and of AuNPs in particular.

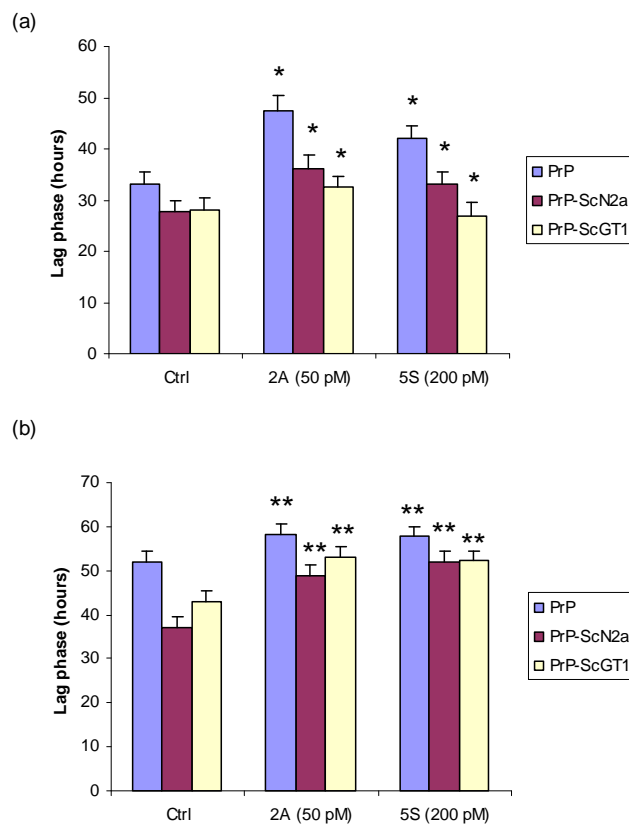


Figure 23. Effect of the nanoparticles on prion fibril formation and ASA. Lag phase of amyloid formation kinetics are compared between (a) SpectraMax M5 and (b) Gemini EM instruments (Molecular Devices) in the assays, using full-length MoPrP(23-230) and amyloid seeding with ScN2a and ScGT1-PTA precipitated protein in presence of coated gold nanoparticles. Fifty pM of 2A nanoparticles or 200 pM of 5S nanoparticles were added to each well; Ctrl = control. The Student's t-test (two-tailed) was used to determine significant differences among measurements (n=4). *P<0.05, **P<0.01.

2.3.5 *In vitro* effect of the nanoparticles on β -amyloid and α -synuclein fibril formation

To demonstrate if the nanoparticles may directly interact with $A\beta$ and α -synuclein to prevent the fibril formation of the proteins, 2A and 5S were chosen to add to the reaction of $A\beta_{1-40}$ and α -synuclein fibril formation. In fact, 2A, at concentrations of 100-1000 pM, extended the lag phase by 1-3 hours in a 24 hour-running assay of β -amyloid fibril formation; and at 500-1000 pM, 2A nanoparticles also extended the lag phase by 8 hours in a 96 hour-running assay of α -synuclein fibril formation when compared to the controls (Fig. 24a,b). Although 5S did not show any delay of β -amyloid fibril formation, 5S extended the lag phase by 5-10 hours at 200-1000 pM in α -synuclein fibril formation (Fig. 24a,b). These results suggest that these nanoparticles may directly interact with $A\beta$ and/or

α -synuclein, hence slowing amyloid formation kinetics of the proteins.

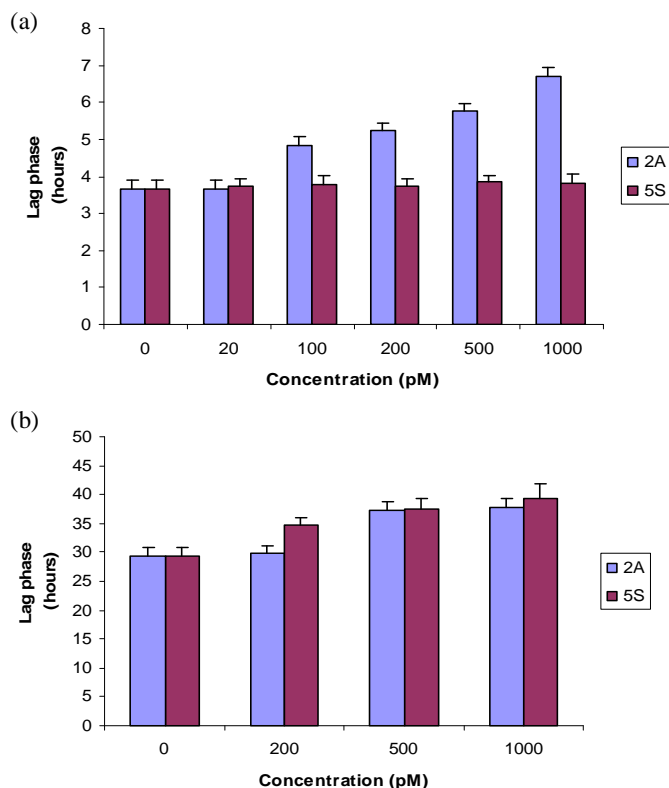


Figure 24. Effect of the nanoparticles on fibril formation of A β and α -synuclein. (a) Lag phase of A β amyloid formation kinetics; (b) Lag phase of α -synuclein amyloid formation kinetics in the assays, using A β ₁₋₄₀ peptide and recombinant human α -synuclein protein in presence of coated gold nanoparticles. Concentrations of 20-1000 pM of 2A and 5S nanoparticles were added to each well. Values are means \pm SD (n = 4).

2.3.6 Binding activity of the nanoparticles to prion proteins in cultured cells

Labeling FITC green fluorescent marker for 2A and 5S nanoparticles tagged as 2A-F and 5S-F respectively is to be able to measure binding activity of the nanoparticles to prion proteins from the samples of cell lysate proteins treated with or without PK by a fluorescence microplate reader. Figure 25 shows that 2A and 5S might bind to both PrP^C and PrP^{Sc} and binding activity of 2A is stronger than 5S in both cell lines of cultured N2a, ScN2a cells (Fig. 25a) and GT1, ScGT1 cells (Fig. 25b). These results suggest that the nanoparticles bound to prion proteins, hence inhibiting prion replication in cellular model.

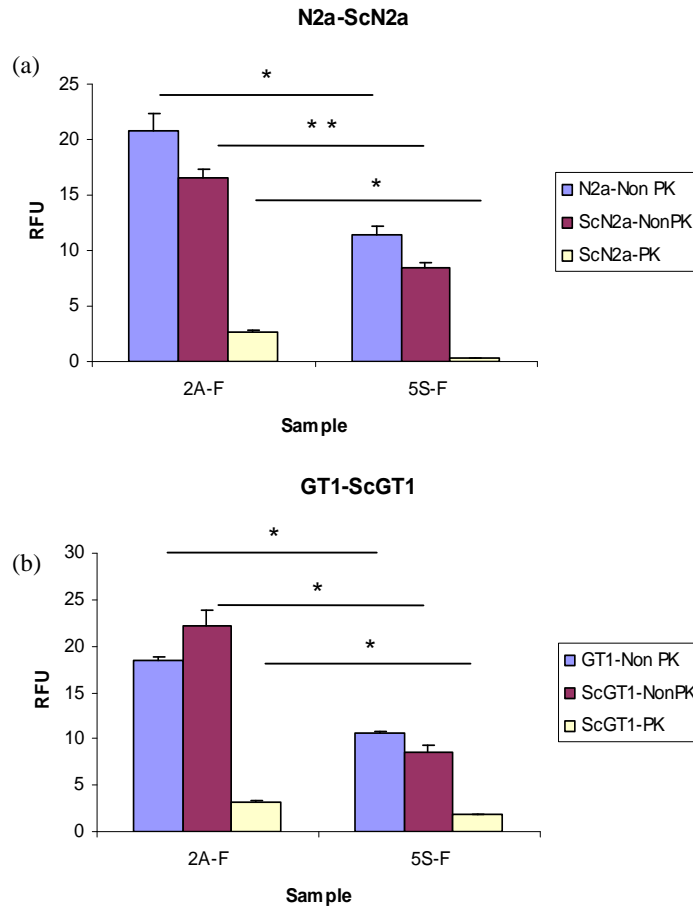


Figure 25. Binding activity of the nanoparticles to prion proteins. The particles 2A and 5S were labeled with FITC (green) as 2A-F and 5S-F respectively. 100 pM of 2A-F and 5S-F were added to (a) N2a, ScN2a cells and (b) GT1, ScGT1 cells cultured for 5 days, and then the nanoparticles-treated cells were incubated for 2 more days. Proteins from the cell lysate were quantified, treated with or without proteinase K (PK) and PTA-precipitated. Relative fluorescence unit (RFU) values were measured at 488/525 nm. The Student's t-test (two-tailed) was used to determine significant differences among measurements (n=3). *P<0.05, **P<0.01.

2.3.7 *In vivo* application of the nanoparticles

Outbred CD-1 mice were intracerebrally inoculated with 30 μ L of 10% RML brain homogenates, pre-incubated with a nanomolar concentration of gold nanoparticles 2A or 5S. Before the inoculation, TEM analysis of nanoparticles-treated homogenates confirmed the presence of sparsely distributed particles. The incubation period of mice treated with both 2A (mean \pm standard error of the mean SEM: 139 \pm 3 days) and 5S (mean \pm SEM: 135 \pm 2 days) were significantly longer (respectively $p = 0.0021$ and $p = 0.023$, log-rank test) than that of control animals infected with pure RML homogenate (mean \pm SEM: 128 \pm 2 days) (Fig. 26a).

Only 2A-treated animals showed a modest, but statistically significant, increase of survival time compared with controls (163 ± 3 vs 152 ± 3 days, $p = 0.025$ log-rank test), whereas treatment with nanoparticles 5S was not effective (151 ± 1 vs 152 ± 3 days, $p = 0.075$ log-rank test) (Fig. 26b). Histopathological assessment of haematoxylin and eosin (H&E)-stained sections was carried out on all mice brains (Fig. 26c). Neuropathological results showed similar moderate spongiform alterations in each group of mice, with a major involvement of the hippocampus (Fig. 26d-f), thalamus (Fig. 26g-i) and somatosensory cortex.

For PrP^{res} immuno-histochemical and biochemical analysis (Fig. 27) brain homogenates were treated with proteinase K (PK), analyzed by SDS-PAGE and Western blotting, using anti-PrP monoclonal antibody 6H4. Immunohistochemistry showed similar PrP^{res} immunoreactivity in the form of synaptic and diffuse deposits in the cerebral cortex, basal ganglia, hypothalamus, hippocampus, brainstem, cerebellum, and thalamus (Fig. 27b-d), which was often affected by coarse PrP^{res} deposition (Fig. 27e-g). Glial immunoreaction (GFAP) was mainly detected in the hippocampus, thalamus, mesencephalic nuclei, brainstem and the granular layer of the cerebellar cortex. To summarize, all immunohistochemical analysis (6H4, GFAP, CNPase) did not underline any difference between groups of mice challenged with different inocula. Kidneys, spleens and livers of mice inoculated with both RML and mock nanoparticles-treated homogenates were analyzed, and indicated the lack of acute systemic toxicity following the injection of the particles. Even the brains of mice inoculated with mock pre-incubated with nanoparticles 2A or 5S did not reveal specific alterations correlated to a potential toxic effect of the particles on the CNS. These results were also confirmed by periodical MRI analysis (data not shown). Immunoblot analysis of brain homogenates revealed the same PrP^{Sc} profile for all groups of mice (Fig. 27a).

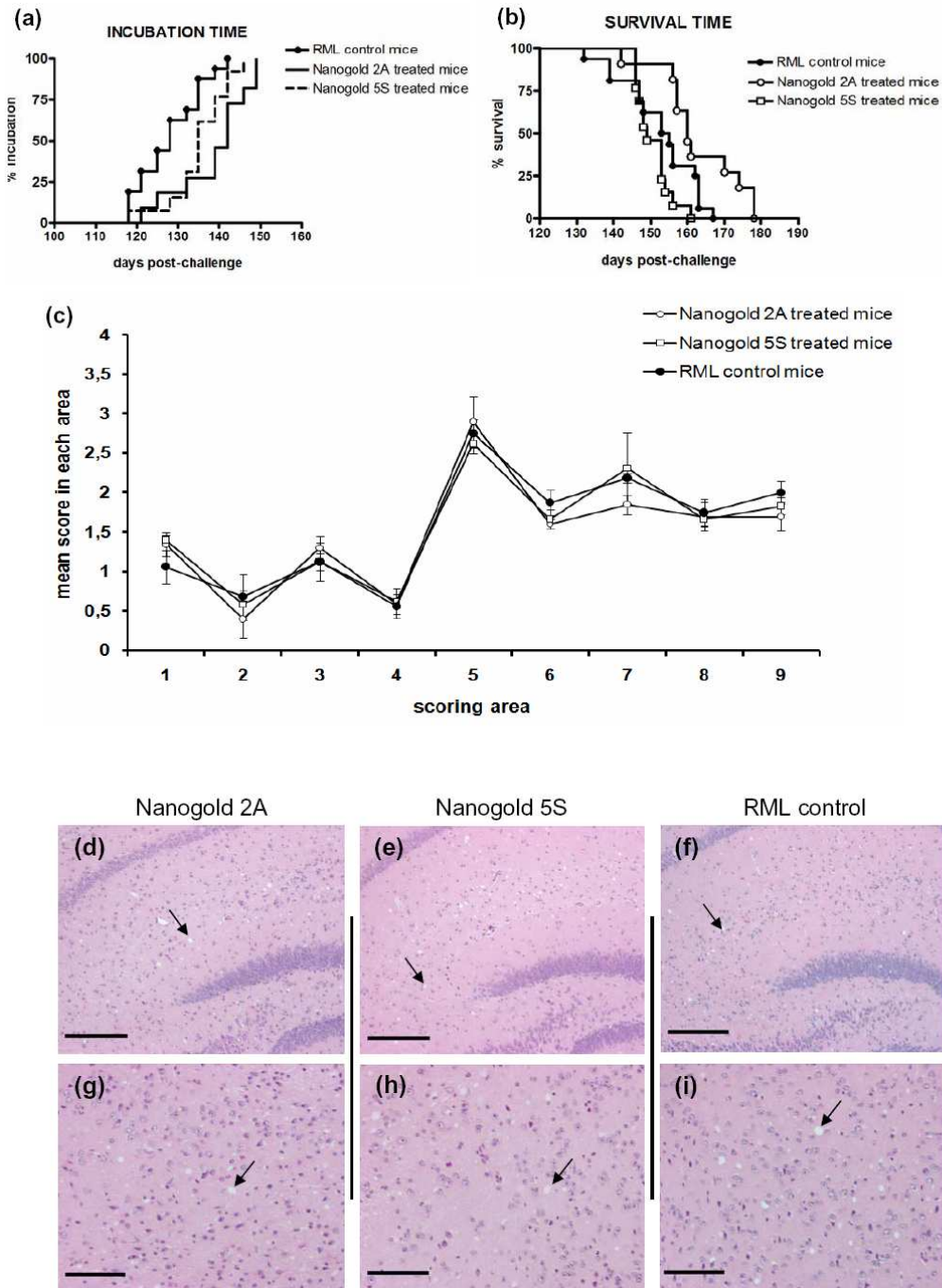


Figure 26. Incubation time, survival curves and vacuolation profile. Coated 2A and 5S gold nanoparticles were able to delay the incubation period of RML infected mice if compared with untreated controls (a), while only nanoparticles 2A treated animals showed a moderate but statistically significant increase in survival time compared with controls, whereas treatment with nanoparticles 5S was not effective (b). Vacuolation profile (c) was scored on a scale of 0-5 in the following brain areas: (1) dorsal medulla, (2) cerebellar cortex, (3) superior culliculus, (4) hypothalamus, (5) thalamus, (6) hippocampus, (7) septum, (8) retrosplenial and adjacent motor cortex, and (9) cingulated and adjacent motor cortex. Data are mean \pm SEM. Micrographs were obtained from areas of hippocampal and thalamic regions (most affected by vacuolation) stained with haematoxylin-eosin (d-i). Spongiosis in mice inoculated with RML brain homogenates pre-incubated with nanogold 2A (d and g) or 5S (e and h), and untreated (f and i) are shown. Scale bar: 200 μ m (d-f) and 100 μ m (g-i).

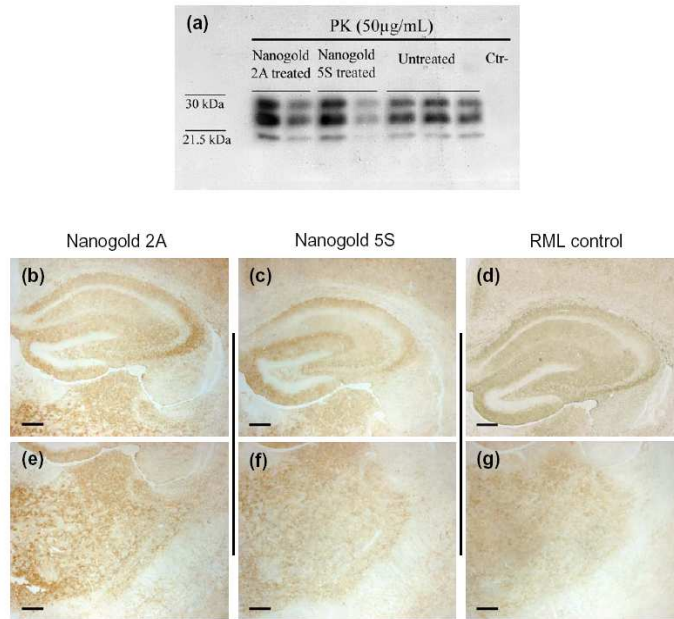


Figure 27. PrP^{res} immunohistochemical and biochemical analysis. Western blot analysis of PK-resistant mouse PrP^{res}. Immunoblot data revealed the same PrP^{Sc} profile in all groups of mice (a), while immunohistochemical results showed the same synaptic-diffuse pattern of PrP^{Sc} deposition for each group of mice (b-g). Micrographs were obtained from areas of hippocampus (b-d) and thalamus (e-g). Pyramidal cells layer and dentate gyrus of the hippocampus were spared from PrP^{res} accumulation. Synaptic and coarse PrP^{res} immunostaining was detected into the thalamus of every group of mice. Scale bar: 200 μ m.

2.4 Discussion

Due to their intrinsic properties as being non-toxic, inert to most chemical reactions, coupled with easy and fast preparation, pure AuNPs are excellent candidates for use in both therapeutic²¹⁴ and diagnostic approaches. Citrate-stabilized AuNPs maintain good long-term stability in solution. Gold nanoparticles can be functionalized using Layer-by-Layer (LbL) deposition.^{215,216} Polyelectrolyte assembling on AuNPs is induced by electrostatic interactions between the oppositely charged polyelectrolytes. A supersaturated concentration of the polyelectrolytes was chosen for the LbL, in order to guarantee fast and complete surface coverage and good stability.²¹⁴

The range for the number of deposited layers was chosen to present the precursor region described by Decher as model for the deposition of a strong and weak polyelectrolyte.²²⁴ The first five to eight layers of deposited polyelectrolytes differ from the following set of layers in terms of composition and thickness, and are called precursor layers. The attractive and repulsive forces of the underlying layers as well as that of the core contribute to the self-assembly of the

polyelectrolyte. If the core is negatively charged, the first positively charged polyelectrolyte layer will be self-assembled exclusively by attractive forces, and by binding they will overcompensate the charge of the core. For the next layer, the opposite charge of the first polyelectrolyte layer is present, but due to the vicinity to the core also the repulsive forces by the like-wise charged core. This leads to a less tight binding and a decreased amount of bound polyelectrolytes. Moreover, the polyelectrolyte layers penetrate each other in the precursor layer, and are thinner than the following set of layers, which are more distant from the core.²²⁴ We used the intercalation of polycations and polyanions, containing either sulfonate or primary amine groups, to selectively bind and inhibit prion formation, creating a surface exposing both moieties randomly and in varying ratios. There is some reported evidence that polyamines can have an effect on PrP^{Sc}. Indeed, Supattapone and co-workers²²⁵ found that branched polyamines are able to disintegrate aggregates of PrP^{Sc} to undetectable levels. For polysulfates, the influence of their chemical structure on selective binding to either PrP^C or PrP^{Sc} leading to prion inhibitory activity was also demonstrated.²²⁶ In our work, both functional groups were combined on the surface of the AuNPs in varying ratios, to obtain a platform of possible interactive sites for the misfolded PrP.

Two studies on the bio-distribution of citrate stabilized AuNPs should also be considered, though the results were somehow contradictory: De Jong and co-workers²²⁷ found that only 10 nm particles were crossing the BBB, while Sonavane and co-workers²²⁸ found 50 nm particles in the brain. Our particles were found to have a hydrodynamic diameter 90 to 130 nm, and in electron microscopy the fully dehydrated polyelectrolyte matrix was condensed until it was only 1-2 nm thick. We assume that the polyelectrolyte shell loses some of its water molecules while crossing the BBB.

From previous experiments on cells of the BBB, it is known that AuNPs coated with different numbers of polyelectrolyte layers are cytotoxic (for example, porcine brain capillary endothelial cells).²¹⁵ Moreover, a strong dependency on the number of layers and surface charge was observed. Polycations were more cytotoxic than polyanions and with lower number of layers were more cytotoxic than a higher number of layers. An additional binding of albumin to the final polyelectrolyte layer should diminish the toxicity, and animal experiments confirmed that after intracranial inoculation no toxicity leading to morphological

changes in the brain was present.²²⁹

Preliminary *in vitro* experiments showed the efficacy of both nanoparticles (2A and 5S) to interfere with prion propagation. Because of the limited information available about the toxic effects of these particles when injected in animals, we started our experiments by using a dosage of compound lower than those generally reported in the literature for other therapeutic approaches.²²⁷ Whereas 5S nanoparticles significantly increased only the incubation time of treated mice, 2A nanoparticles showed higher anti-prion activity. Indeed, even when 2A were used at nanomolar concentrations (25.35 nM), a moderate but statistically significant increase in both incubation and survival time was observed, thus indicating a possible interaction between PrP^{Sc} and the nanoparticles. Even though the animals were treated with just a single dose of nanoparticles the increase of incubation and survival time was statistically significant. Several studies are currently underway to determine the best 2A concentration, able to inhibit or perhaps completely block disease progression. To this end, several mice were intracerebrally infected with RML brain homogenate pre-incubated with higher dosages of 2A particles (53 nM vs 25.35 nM). Groups of control mice were also included to monitor the onset of general toxic effects. Since the gold 2A, modified with the addition of albumin in the outermost layer, were able to cross the BBB,²²⁹ new therapeutic approaches based on their injection into the tail vein of mice have already been scheduled. Coated nanogold is not only a potential drug delivery shuttle through the BBB but by itself it can be used as a drug for the treatment of prion disease and perhaps other neurodegenerative diseases. With different microscopic techniques like near infrared time domain (NIR-TD) imaging, X-ray tomography, confocal fluorescence microscopy and standard cell stains visualized by wide field light microscopy combined with fluorescence staining, it was possible to show that the particles accumulate in regions of the brain close to possible target cells of prion, Alzheimer's and Parkinson's diseases.²²⁹

2.5 Conclusion

The polyelectrolyte multilayer-coated gold nanoparticles are a novel class of potential anti-prion drugs. While they showed *in vitro* very high efficacy at very low concentration, their potential *in vivo* to inhibit completely prion aggregation needs further improvement. A slight increase in incubation time and survival time

was observed for the 2A coated particles and at the tested concentration. Further concentrations as well as other coatings need to be studied *in vivo* as the correlation between the *in vitro* experiments and the *in vivo* inoculation is not so striking. Especially the extremely low concentration required to suppress complete the prion aggregation raise the expectations that this small amount of particles will pass the blood-brain barrier and will enter the brain parenchyma.

3. Discovery of a class of diketopiperazines as anti-prion compounds

3.1 Introduction

Prion diseases, also known as transmissible spongiform encephalopathies (TSEs), are neurodegenerative and infectious disorders that affect both humans and animals, and are not curable with drugs. Although reliable proof of principle was demonstrated in a variety of experimental models, and several small molecules have been identified as active against TSE, the mode of action and targets for most of these molecules remain largely unexplored. As a result, drugs effective against this process are still years away from approval.²³⁰ There are two main reasons why drug discovery for the treatment of prion diseases has not progressed as rapidly as in other pharmaceutical fields. First, human prion diseases are very rare. Each year, only approximately 300 people in the USA and approximately 100 people in the UK succumb to various forms of prion disease.²³¹ Nevertheless, these disorders have come to public and scientific attention due to the fact that they can be transmissible among humans and, in particular conditions, from animals to humans. The emergence of a CJD variant in the 1990s demonstrated the transmissibility of BSE to humans and set the scene for a hypothetical epidemic scenario.²³¹ Second, TSE is a conformational disease,²³² where the cellular form of the prion protein (PrP^C) is converted to a misfolded variant (PrP^{Sc}) through a nucleated polymerization process.³⁷ From a medicinal chemistry perspective, all conformational diseases are 'black boxes' because the knowledge of the 3D structure and mechanistic properties of the target, fundamental prerequisites in modern drug discovery, are mostly unknown. In general, high-resolution structural information on amyloid fibrils is very scarce and is currently almost exclusively restricted to amyloid fibrils formed by small peptides. This is mostly due to the inability of X-ray crystallography and NMR spectroscopy to address insoluble, filamentous specimens.²³³ In the case of PrP, the partial structure of PrP has been solved to high resolution,²³⁴ whereas for PrP^{Sc} only models have been proposed, including the β -helix fold⁴¹ and the spiral model.²³⁵ As a consequence, if we exclude the discovery of aptamers²³⁶ and RNA interference,¹⁶³ most of the lead compounds identified so far are derived from screening approaches in established cellular models. Based on these considerations, it

emerges that rational design of anti-prion compounds is still a big challenge for medicinal chemists.

3.2 Materials and methods

3.2.1 Design rationale

In an effort to identify anti-prion lead compounds with unprecedented molecular frameworks, we started from the following basic assumption. We noticed that most of the anti-prion molecules possessed a symmetrical bifunctional structure consisting of two moieties joined via an appropriate spacer. This is the case for the dye Congo red⁸⁴ and its analogues,²³⁷ the polysulfonated aromatic urea derivative suramin,¹³¹ the natural product curcumin,¹³² the bis-acridine²¹⁸ and bis-quinoline analogues,²³⁸ and the diphenylmethane derivative GN8²³⁹ (see Fig. 28 for structures). Notably, among them, planar molecules with aromatic end groups share common anti-aggregating properties.²⁴⁰ For all of these compounds, and for bivalent compounds in general, the role of the spacer has been demonstrated to be very critical.²⁴¹

Therefore, in our search of novel bifunctional molecules, we looked for a spacer that might have an active role in the molecular recognition process. In inhibiting protein-protein interactions (PPIs), peptides mimicking the interacting zone have been considered as relevant starting points in the rational design of effective molecules.²⁴² Similarly, peptidomimetics have become effective modulators of a range of biologically significant PPIs²⁴³ by orienting their side-chain substituents in a spatially defined manner. Furthermore, these compounds are stable to proteolysis and consequently possess better drug-like properties than peptides.

Among possible peptidomimetic fragments, we focused on the 2,5-diketopiperazine (DKP) scaffold for several reasons: (i) it is synthetically readily accessible and amenable to compound library generation; (ii) DKP derivatives have been shown to modulate PPIs,²⁴⁴ to possess neuroprotective activities,²⁴⁵ and also to cross the blood-brain barrier (BBB);²⁴⁶ (iii) it has been extensively explored in medicinal chemistry.²⁴⁷ Therefore, it seemed conceivable that DKPs carrying (*Z*)-alkene units of general structure **I** (Fig. 28) could serve as a template for a diverse array of pharmacophores towards the identification of novel bifunctional structures for the treatment of prion diseases. Building on this, a compound library was generated by appending several aromatic and heteroaromatic rings in positions 3 and 6 of the 3,6-dimethylenepiperazine-2,5-dione scaffold. The role of aromatic residues in molecular recognition and self-assembly processes leading to various fibrillar aggregates has

been recognized as critical.²⁴⁸ Consequently, targeting these aromatic residues has been proposed as an important strategy to inhibit amyloid formation.²⁴⁸

In the case of our DKPs **1a-c** (see Table 5 for structures), we selected various polymethoxylated benzenes as aromatic appending groups, in view of their structural similarity with those of curcumin.¹³² The choice of pyridine^{90,104} and quinoline^{140,238} rings present in **1d-i** was dictated by the fact that these ring systems are frequently observed in anti-prion compounds. Indole, furan, thiophene and benzene derivatives **1j-n** were then also synthesized to enlarge the chemical diversity of the library. Heteroaromatic β -carboline derivatives **1o** and **1p** were purposely designed with the aim to obtain potential fluorescent probes, owing to the excellent native fluorescence found in carboline systems²⁴⁹ that has led to their use as probes for biomolecules.²⁵⁰ To study the importance, if any, of an appropriate planar conformation of **1a-p**, some singly reduced (**2a-d**, **2j-k**, **2q**) and a saturated derivative (**3d**) were also synthesized (structures given in Table 6).

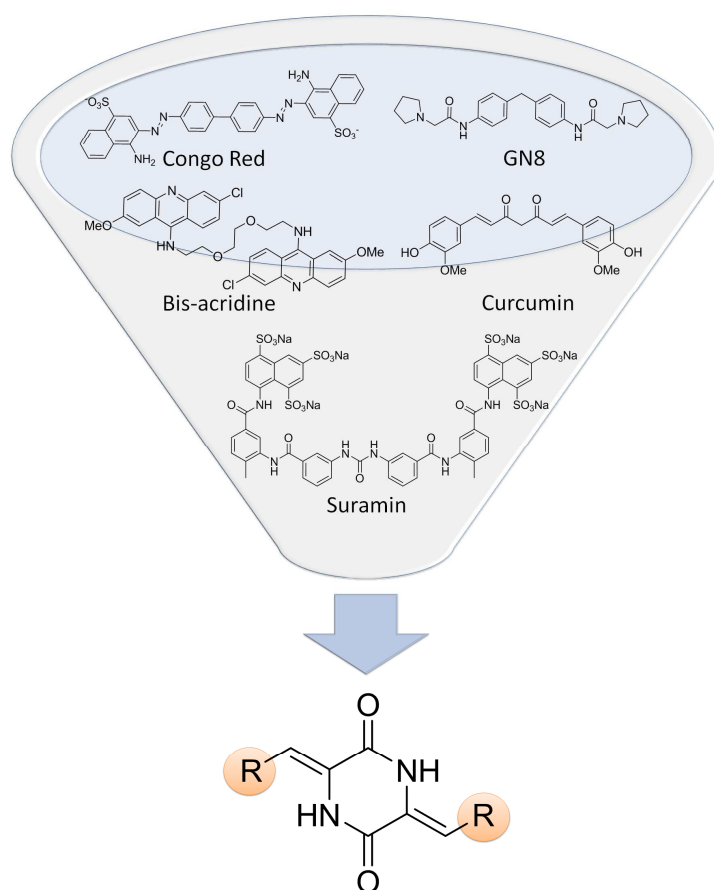
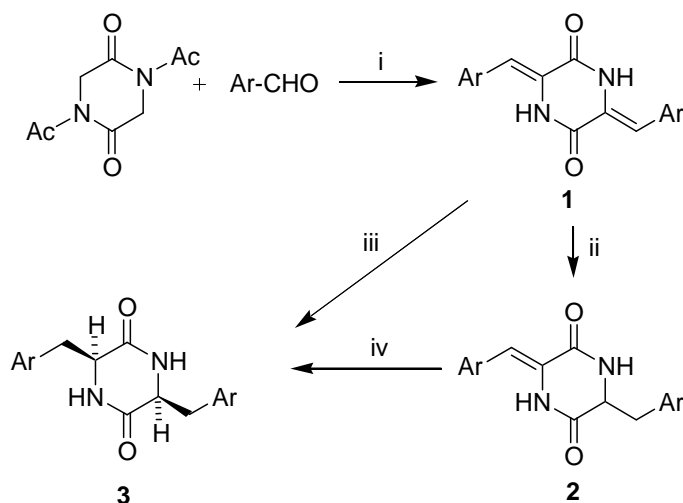


Figure 28. Design strategy leading to novel DKP derivatives of general structure **I**.

3.2.2 Library synthesis

The preparation of 3,6-bis(arylmethylene)-2,5-piperazinedione compounds **1a-p** was achieved in a single step by means of an AB₂-type three-component reaction²⁵¹ involving treatment of commercially available 1,4-diacetyl-2,5-piperazinedione with two equivalents of the suitable aromatic aldehydes in the presence of a base (triethylamine). As expected based on literature precedent,²⁵² the double aldol condensations were accompanied by nitrogen deacetylation and were completely diastereoselective, affording exclusively the *Z,Z*-isomers. Selective reduction of one of the double bonds in a selection of these compounds (**1a-d**, **1j-k**, **1q**) was achieved by treatment with zinc in refluxing acetic acid.²⁵³ These conditions left all other groups present in the starting materials unaffected, with the exception of formyl groups, which were reduced to the hydroxymethyl units found in **2q**. The preparation of the doubly saturated compound **3d** was achieved either by catalytic hydrogenation of **1d** or by prolonged treatment of **2d** with zinc in acetic acid (Scheme 1, Tables 5 and 6).



Scheme 1. Library synthesis. Reagents and conditions: (i) Et₃N, DMF, room temperature (RT), 14 h or Et₃N, DMF, 150°C, 12-48 h; (ii) Zn, AcOH, reflux, 1-48 h; (iii) H₂ (30 psi), 30% Pd-C, CH₃OH, RT, 24 h; (iv) Zn, AcOH, reflux, 24 h.

3.2.3 Screening methodology

A cell-screening assay was used to test anti-prion activity across the synthesized compounds. Their ability to reduce PrP^{Sc} concentrations in scrapie-infected mouse hypothalamus (ScGT1) cells was determined by Western blotting followed by densitometry of the PK-resistant PrP^{Sc}, and PrP^{Sc} levels were quantified by ELISA. Library compounds were initially screened at 10 μM, and their ability to reduce PrP^{Sc}

levels for five days was evaluated by comparison with the untreated control. For entries **1d** and **1o** the EC₅₀ values, which represent the effective concentrations for half-maximal inhibition, were also calculated (Table 7). Two well-documented anti-prion agents were investigated as positive controls; EC₅₀ values of 6.2 ± 0.4 and 0.4 ± 0.1 μM were obtained for imipramine and quinacrine, respectively.

All assays for cell culture, drug treatment, cell viability, PrP^{Sc} detection and quantification were performed in accordance to the protocols described in parts **2.2.4**, **2.2.5** and **2.2.6**.

3.2.4 *In vitro* effect of test compounds on prion fibril formation

Fibril formation of PrP was performed using a previously described method with minor modifications.²¹⁹ Briefly, 20 μL of test compound at the indicated concentrations were added to each well containing 180 μL of reaction solution, including 50 μg/mL recMoPrP (23-230) or recMoPrP(89-230), 0.4 M GdnHCl and 10 μM ThT in PBS buffer (1X) in a 96-well black plate (BD Falcon). Each sample was performed in four replicates. Each well contained one 3 mm glass bead (Sigma). The plate was covered with sealing tape (Fisher Scientific), incubated at 37°C with continuous shaking and read on SpectraMax Gemini EM fluorescence plate reader (Molecular Devices) by top fluorescence reading every 5 min (excitation, 444 nm; emission, 485 nm).

3.3 Results and discussion

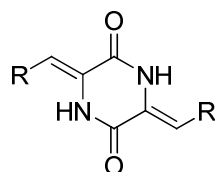
3.3.1 Biological activity

Firstly, the cytotoxic effects of series **1**, **2**, and **3** compounds were determined by calcein-AM assay in ScGT1 cell line. As reported in Tables 5 and 6, the treatment of ScGT1 cells with most test compounds (10 μM) did not lead to any significant change in cell viability, with the exception of **1a**, **1c**, **1p**, **2a** and **2j**, where the cell viability was lower than 50%. Therefore, the latter were not screened for prion replication, whereas the other library members were assayed at a concentration of 10 μM. From an analysis of the results, it is possible to derive that, at this concentration, not all of the tested DKPs displayed activity. The DKP fragment may be a scaffold for anti-prion activity; however, the appended substituents have a crucial effect on biological activity. In fact, among the selected aromatic rings, derivatives bearing a benzene (**1n**), furan (**1l**), thiophene (**1m**) or quinoline (**1g-h**) moiety had very low or no activity. The most striking result of this investigation was the remarkable activity

displayed by the 2-pyridyl derivative **1d**, which completely inhibits prion replication at 10 μM (100.8 ± 2.5 % inhibition). Intriguingly, when the pyridine nitrogen was moved to positions 3 (**1e**) or 4 (**1f**), the activity decreased to 12.4% and 11.5%, respectively. Similarly, the potent activity of **1d** was reduced by fusing additional aromatic rings, as in the 2-quinolinyl **1g** and β -carbolin-2-yl **1o**.

Significant preliminary structure-activity relationships can be gathered from this first set of tested compounds. DKP bearing a 2-pyridine substituent was revealed as a strict requirement for potency in the cellular assay. Intriguingly, this result is in line with that obtained in a recently reported series of anti-prion compounds, where a 2-substituted pyridine conferred optimal activity.²⁵⁴ The only exception to this trend was the 4-quinolyl derivative **1i**, which was the only compound lacking the key molecular feature and displaying an activity higher than 20%. Notably, several 4-substituted quinolines have shown anti-prion activity.^{140,238} As a general comment, it should be mentioned that in cellular assays changes in activity also correlate to physicochemical parameters, such as solubility and permeability. However, the results obtained could imply that a planar conformation, as in **1d**, is as a basic requirement for activity. Starting from this assumption, we were keen to examine the effects of reduction on the double bonds at positions 3 and 6 of the DKP system. To this end, a second library was synthesized (**2a-d**, **2j-k**, **2q**), generated from the singly reduced DKP scaffold in combination with a subset of the aromatic substituents reported in Table 5 (Scheme 1, Table 6). As expected, even in this series the most active compound was the 2-pyridyl derivative **2d**. Again, this can be rationalized by assumption that at least one half of the molecule is able to assume the planar conformation critical for activity. In line with this speculation, the doubly saturated compound **3d** showed lower potency. In this second library, an interesting profile was shown by 1-tosylindole **2k**, which exhibited 37.7% inhibition.

Given the high inhibitory activity of **1d** and the possible use of **1o** as a fluorescent probe, their anti-prion potential was studied in more detail by calculating their EC_{50} values. For **1d**, a remarkable single-digit micromolar EC_{50} value (4.1 ± 0.2 μM ; Table 7) was observed, comparable to that of imipramine (6.2 ± 0.4 μM), a reference anti-prion compound. Notably, **1o** ($\text{EC}_{50} = 15.8 \pm 0.9$ μM) was only fourfold less active than **1d**, emerging as a promising fluorescent probe.

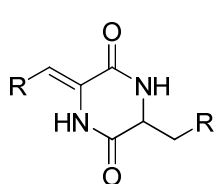
Table 5. Reaction conditions, yields and screening results for the DKP Series 1**1a-p**

Cpd	R	Conditions	Yield [%]	Viable cells [%] ^b	PrP ^{Sc} inhibition [%] ^c
1a		RT, 16 h	97	32.2 ± 1.0 ^a	ND ^d
1b		RT, 16 h	99	72.7 ± 3.3	1.4 ± 0.1 ^a
1c		RT, 16 h	74	20.6 ± 1.7	ND
1d		reflux, 48 h	64	50.9 ± 2.1	100.8 ± 2.5
1e		reflux, 16 h	41	102.7 ± 3.7	12.4 ± 0.5
1f		reflux, 24 h	68	108.5 ± 4.2	11.5 ± 0.5
1g		reflux, 20 h	80	71.7 ± 3.1	5.1 ± 0.1
1h		reflux, 16 h	65	63.7 ± 2.8	3.5 ± 0.1
1i		reflux, 16 h	84	94.8 ± 4.1	20.6 ± 0.8
1j		reflux, 16 h	94	81.3 ± 2.5	7.4 ± 0.5

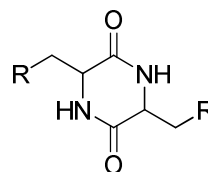
1k		RT, 16 h	80	98.4 ± 3.3	9.4 ± 0.4
1l		reflux, 16 h	68	83.0 ± 2.9	0.14 ± 0.02
1m		reflux, 16 h	61	73.6 ± 3.5	1.8 ± 0.1
1n		reflux, 16 h	60	85.6 ± 3.1	0.11 ± 0.01
1o		reflux, 16 h	52	77.0 ± 3.2	10.4 ± 1.2
1p		reflux, 16 h	58	37.3 ± 2.6	ND

^a Values are mean ± the standard deviation of three experiments. ^b ScGT1 cells were cultured in DMEM with 10% FBS and plated into 96-well plates (25000 cells per each well). The compounds were dissolved in DMSO (100%) and diluted in PBS (1X). Test compound (10 μM) was added and the cells were incubated for five days at 37°C, 5% CO₂. The results were developed by calcein-AM fluorescence dye and read by microplate reader. ^c Effect of test compounds on inhibition of scrapie prion replication. ScGT1 cells were cultured in DMEM with 10% FBS, split 1:10 into Petri dishes and incubated for two days at 37°C and 5% CO₂. Test compound (10 μM), being non-cytotoxic, was added to the plated cells. After five days incubation, the protein content of the cells was extracted, quantified, digested with PK, and western blotted. ^d ND: not determined. RT: room temperature.

Table 6. Reaction conditions, yields and screening results for the DKP Series 2 and 3

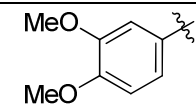
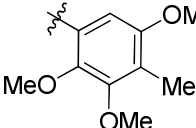
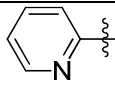
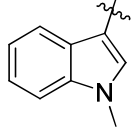
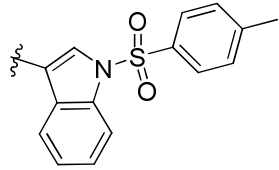
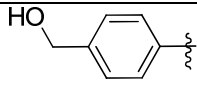
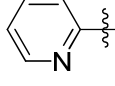


2a-d, 2j-k, 2q



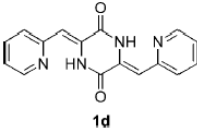
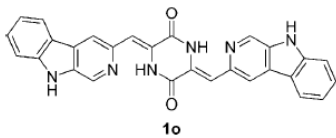
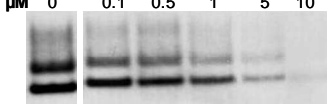
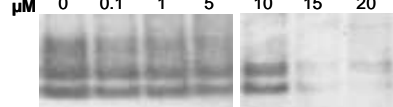
3d

Cpd	R	Conditions	Yield [%]	Viable cells [%] ^b	PrP ^{Sc} inhibition [%] ^c
2a		125 °C, 20 h	100	36.4 ± 1.2 ^a	ND ^d

2b		125 °C, 48 h	100	103.2 ± 4.2	5.9 ± 0.2 ^a
2c		125 °C, 83 h	98	96.9 ± 3.8	6.8 ± 0.3
2d		125 °C, 1 h	52	100.1 ± 4.4	18.1 ± 0.7
2j		125 °C, 48 h	76	27.5 ± 1.3	ND
2k		125 °C, 16 h	96	90.9 ± 3.6	37.7 ± 2.2
2q		125 °C, 16 h	20	110.5 ± 5.3	13.8 ± 0.4
3d		125 °C, 22 h	58	107.4 ± 4.6	12.2 ± 0.2

^a Values are mean ± the standard deviation of three experiments. ^b ScGT1 cells were cultured in DMEM with 10% FBS and plated into 96-well plates (25000 cells per each well). The compounds were dissolved in DMSO (100%) and diluted in PBS (1X). Test compound (10 μM) was added and the cells were incubated for five days at 37°C, 5% CO₂. The results were developed by calcein-AM fluorescence dye and read by microplate reader. ^c Effect of test compounds on inhibition of scrapie prion replication. ScGT1 cells were cultured in DMEM with 10% FBS, split 1:10 into Petri dishes and incubated for two days at 37°C and 5% CO₂. Test compound (10 μM), being non-cytotoxic, was added to the plated cells. After five days incubation, the protein content of the cells was extracted, quantified, digested with PK, and western blotted. ^d ND: not determined.

Table 7. Cell viability and inhibition of PrP^{Sc} accumulation in ScGT1 cells grown with **1d** and **1o**^a

Compound	 1d	 1o
EC₅₀^b (μM)	4.1 ± 0.2	15.8 ± 0.9
Viable cells^c (%)	75.2 ± 2.1	60.4 ± 4.1
Western blot		

^a Values given are the mean ± the standard deviation (SD) of three experiments. ^b The concentration of test compound required to reduce the PrP^{Sc} level in cells to 50% versus untreated cells (EC₅₀). ^c Cell viability at the EC₅₀ concentration was determined by calcein-AM cytotoxicity assay and expressed as an average percentage of viable cells versus untreated control cells.

3.3.2 Modeling Studies

To better elucidate the putative relationships between bioactivity and the planarity of tested compounds, we modeled their structural conformations. Initial structures of molecules **1d**, **1g**, **1l**, **1m**, **1n** and **1o** were drawn in Marvin version 5.0.1 from ChemAxon.²⁵⁵ 3D low-energy geometries were computed by means of density functional theory using GAUSSIAN 03 software suite.²⁵⁶ The B3LYP function was used in conjunction with a 6-31G** basis set. Bery geometry optimization procedure was applied until the interatomic forces were below 0.08 cal/Å. The planarity of the optimized geometries was measured as the value of the dihedral angle (ω) defined by the atoms C=C-C- (C/ N/ O/ S) (see Table 8). All molecules turned out to be planar, with the exception of the benzene-substituted DKP **1n**. In fact, the benzene rings are rotated by 33.6° with respect to the DKP plane in **1n** (Fig. 29). Molecular planarity may be a necessary, but not sufficient, condition for anti-prion activity. In fact, modeling results predict that compounds **1g**, **1l**, **1m** and **1o** are equally as planar as **1d** (see ω values in Table 8), but possessed lower activity.

The difference between planar (**1g**, **1l**, **1m**, **1o** and **1d**) and non-planar (**1n**) molecules is due to the presence or absence of an intramolecular hydrogen bond between the R substituents and the DKP ring. To clarify the role of the intramolecular hydrogen

bond in biological activity, the conformational analysis of molecules **1d**, **1g**, **1l**, **1m**, **1n** and **1o** was extended to conformations with the substituents rotated by 180° of ω . New geometries were optimized following the above-mentioned procedure. The corresponding flipped conformers were unable to form an intramolecular hydrogen bond. The loss of the hydrogen bond and the steric hindrance present between adjacent groups broke the planarity of the compounds, disrupting the π -electron conjugation (see Fig. 29). These flipped conformers (non-planar) were less stable than the planar ones. The energy difference between these two conformers served as a measure of the planarity strength (see Table 8). The planar geometry of **1d** was the most stable among the selected series, followed by **1g** and **1o**, which could also form a canonical intramolecular hydrogen bond. Notably, these data parallel those of activity (see Table 8). Conversely, the planarity of molecules **1l** and **1m**, which were not active, is very weak. Taken altogether, these calculations confirm that anti-prion activity of this subset of molecules is directly related to their capability to retain a planar conformation.

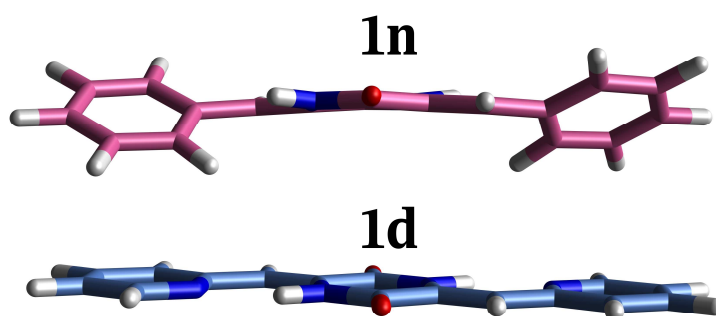
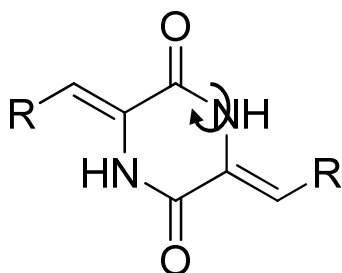


Figure 29. 3D structure of a planar (**1d**) and a non-planar (**1n**) DKP; the difference in geometry is due to the presence or absence of intramolecular hydrogen bonds.

Table 8. The putative relationships between biological activity and the planarity of tested compounds



Cpd	R	PrP ^{Sc} inhibition at 10 μ M (%)	Planarity (ω degrees)	Planar Stability ^a (ΔE kcal/mol)
1d		100.8 \pm 2.5	0.02	18.2
1g		5.1 \pm 0.1	0.01	15.6
1l		0.14 \pm 0.02	0.00	7.3
1m		1.8 \pm 0.1	0.00	1.8
1n		0.11 \pm 0.01	33.60	0.0
1o		10.4 \pm 1.2	0.07	17.2

^aA planar stability defined as the energy difference between flipped conformers

3.3.3 Mechanism of action

The biological assay performed allows us to discover compounds that are effective at any of the several steps of the misfolding pathway in the cell. Thus, compounds that block PrP^C synthesis, stabilize PrP^C, inhibit its conformational conversion and/or stimulate cellular clearance can be identified. Therefore, the mechanism of action of the active compounds must be investigated. Based on the consideration that planar aromatic molecules are reported as good inhibitors of fibril formation in several neuronal amyloidoses,²⁵⁷ we decided to study the behavior of **1d** in a PrP fibrillation assay. We used as templates recombinant mouse (recMo) full-length PrP(23-230) and truncated recMoPrP(89-230), which both form amyloid fibrils.²¹⁹ The anti-

aggregation potential of **1d** (50 μ M) was quantitatively detected by observing the increase in the mean lag phase of the fibrillation reaction, compared with control samples. Compound **1d** (50 μ M) exhibited PrP amyloid fibril formation inhibitory activity, showing a much slower kinetics than the control, in which the lag phase was 57 hours and 15 hours for recMoPrP(23-230) and recMoPrP(89-230), respectively. In particular, **1d** significantly extended the lag phase to 72 hours in recMoPrP(23-230) and 48 hours in recMoPrP(89-230) fibrillation assays. Given the potency of **1d** at inhibiting recPrP fibril formation, we suggest that the compound might interact directly with recPrP to prevent its conversion to the pathogenic PrP^{Sc}-like form.

3.4 Conclusion

In conclusion, we have identified DKP as a novel scaffold in anti-prion drug design. Compound **1d**, thanks to its planar conformation, is able to inhibit PrP amyloid fibril formation *in vitro*. Moreover, it inhibits prion replication in the low micromolar range in a cellular context. For these reasons, **1d** is a lead candidate for further optimization studies. While preliminary, these results represent a first step toward the discovery of novel DKPs with therapeutic potential against prion diseases. Clearly, proof of concept will involve *in vivo* investigation of the profile of **1d**.

A second major outcome of this work is the identification of the β -carboline derivative **1o**. Fluorescent probes that specifically target amyloid aggregates are of great relevance to advance our understanding of the molecular pathogenesis underlying cerebral amyloidoses.^{257,258} Derivative **1o** might represent a valuable starting point to design novel probes for the optical imaging of amyloid plaques in prion disease. Properly addressed studies aimed at the investigation of the fluorescent profile of **1o** and its labeling of amyloid fibrils are in progress and will be reported in due course.

4. Anti-prion activity and preliminary structure-activity relationship of benzoquinones

4.1 Introduction

Despite the numerous efforts aimed at identifying compounds useful against prion diseases, there are still no therapies on the market. Therefore, it is of continued importance to identify chemical scaffolds to be exploited for the design of novel drugs.²⁵⁹ Most of the anti-prion molecules that have been identified so far are derived from screening approaches. Structurally, diverse chemical compounds covering a broad range of the chemical space have been identified.²²⁶ Intriguingly, most of them share a common bivalent structure. This is the case of the natural product curcumin,¹³² the bis-acridine analogues,^{218,260} the diphenyl-methane derivative (GN8),²³⁹ bebeerines,⁹⁶ bisepigallocatechin digallate,⁹⁶ 2,2'-bisquinolines,¹⁴⁰ 4,5-dianilinophthalimide,²⁶¹ analogues of Congo red²³⁷ and diketopiperazines (DKP) derivatives.²⁶²

Although a structure-activity relationship is not easy to discern from such chemically unrelated compounds, we envisaged that bivalent ligands bearing lipophilic bi- or tri-(hetero)-cyclic scaffolds connected by a central core might possess anti-prion activity. Bivalency, and multivalency in general, is a well-known and efficient strategy widely used by medicinal chemists to enhance binding efficacy in molecular recognition processes.²⁶³ Multivalent chemical probes, featuring multiple copies of an amyloid binding motif connected by a spacer, have been developed with the aim to simultaneously bind to several binding sites or several amyloid peptides, thus achieving higher potency.^{232,264}

In prion research, by joining two quinacrine moieties through a piperazine spacer, May and co-workers afforded the first bivalent anti-prion ligand BiCappa (**BC**; Fig. 30), which was 10 times more potent than monomeric quinacrine.²¹⁸ Heterodimers incorporating recognition elements taken from quinacrine itself and imipramine with a piperazine unit were shown to improve the anti-prion efficacy of quinacrine up to a low nanomolar range.²⁶⁵ Furthermore, assembling multiple acridine or curcumin moieties to a cyclopeptide scaffold has emerged as a promising strategy for the development of inhibitors against amyloid formation.^{266,267}

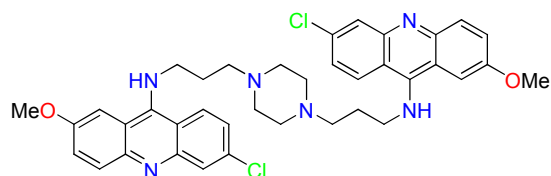


Figure 30. BiCappa (BC) structure.

Protein-protein interactions (PPIs) are crucial elements in mediating diverse cellular physiological and pathological events.²⁶⁸ They are involved in fibrillation processes and thus play a pivotal role in the pathogenesis of several neurodegenerative diseases.^{269,270} Systematic analysis of PPI interfaces reveals great heterogeneity, from large and flat to narrow and structured interactions.²⁷¹ However, the majority of PPIs deal with protein surfaces,²⁷² where a complex network of weak interactions takes place. Peptides may be good PPI blockers.^{1,273} However, they are not optimal drug candidates, due to problems with bioavailability and enzymatic degradation. To overcome this limitation, one could use combinatorial chemical libraries based on small molecules. However, the widely spaced interactions required for PPI blockers are difficult to mimic with small molecules. Despite this challenge, the strategy holds great potential for identifying novel lead compounds against PPIs.²⁷⁴ The extreme attractiveness of PPIs as drug targets has led to important progresses in this field in the last decade.^{268,275,276} In particular, Janda and co-workers have recently demonstrated the ability of what they have named “credit card” libraries to disrupt PPIs of biological relevance.²⁷⁷ The chemical structures of these libraries are built upon flat, rigid scaffolds, decorated with appended groups that span a wide range of size, aromaticity, polarity, and hydrogen-bonding capability.²⁷⁷ Their rationale was based on the concept that the ‘hot spot’ regions in protein-protein interfaces are rich in aromatic residues.

Building on the bivalent approach, we have recently reported that a 2,5-diamino-1,4-benzoquinone (BQ) linked to two phenylalanine residues displayed remarkable anti-prion activity in a cellular model of prion replication²⁷⁸ (see **part 4.2 in the thesis**). In this compound, because of a resonance effect of the BQ ring, a hydrophobic and planar system is generated, which might interfere, through hydrophobic interactions, with aromatic hydrophobic residues critical to fibril formation.²⁷⁹ This hypothesis is corroborated by the key role of planarity as a major

determinant for anti-prion activity in a recently synthesized series of bivalent DKP²⁶² (see **part 3 in the thesis**). Altogether these results allowed us to propose that the planar BQ scaffold might be considered as a privileged motif in modulating PPIs and as a promising spacer in the search for more effective bivalent anti-prion chemical probes²⁸⁰ (see **part 4.3 in the thesis**).

4.2 Synthesis and evaluation of a library of 2,5-bisdiamino-benzoquinone derivatives as probes to modulate protein-protein interactions in prions

So far, several peptides have been developed with the specific aim of blocking PPIs and reversing the aberrant conformational changes. A short synthetic peptide (iPrP13, DAPAAPAGPAVPV), designed by Soto and co-workers on the basis of sequence homology with PrP^C, acted as a β -sheet breaker, inducing unfolding of β -pleated sheet structure.¹³ More recently, Gilbert and co-workers²⁸¹ reported on a series of small peptides active at levels of 100 μ M in two prion disease models and in an *in vitro* anti-aggregation polymerization assay. Prompted by the advantages of using small molecules as PPI inhibitors as opposed to peptides, here we propose the planar 2,5-bisdiamino-benzoquinone scaffold as a privileged motif in modulating PPIs. This is based on (i) Janda's criteria for credit card libraries;²⁷⁷ (ii) the finding that a 2,5-bisdiamino-benzoquinone derivative binds to β -amyloid (A β), and interferes with the native ability of A β to self-assemble, by disrupting PPIs.²⁸² Due to a resonance effect, a hydrophobic and planar system is generated in 2,5-bisdiamino-benzoquinones. This should, in principle, perturb PPIs in the fibrillogenesis processes.²⁸³

Therefore, in our search for novel anti-prion compounds, we decided to attach seven amino acid methyl esters to two different benzoquinone cores, generating a small combinatorial library of fourteen 2,5-bisdiamino-benzoquinones (**1-7a** and **1-7b**), reported in Figure 31. The selected amino acid esters (AlaOMe (**1**), N ω -Nitro-ArgOMe (**2**), N ϵ -BOC-LysOMe (**3**), IleOMe (**4**), MetOMe (**5**), PheOMe (**6**), TrpOMe (**7**)) act as capping groups, allowing us to enlarge the library's chemical diversity by exploiting differences in size, aromaticity, polarity, and hydrogen-bonding capability. Analysis of natural amino acids involved in PPIs revealed that Trp, Phe, Tyr, and Ile are the most important in driving aggregation.²⁸⁴ Consequently, it is highly conceivable that the novel derivatives bearing these motifs might compete for binding and, therefore, efficiently disrupt the assembly of prion protein.

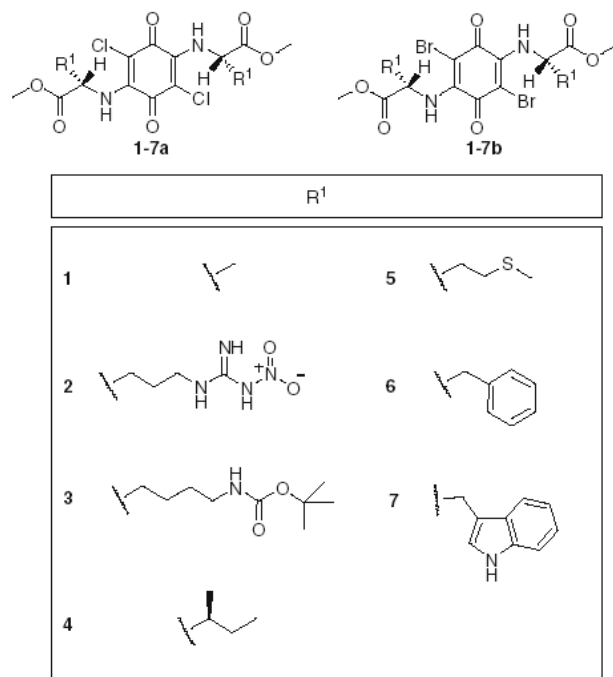
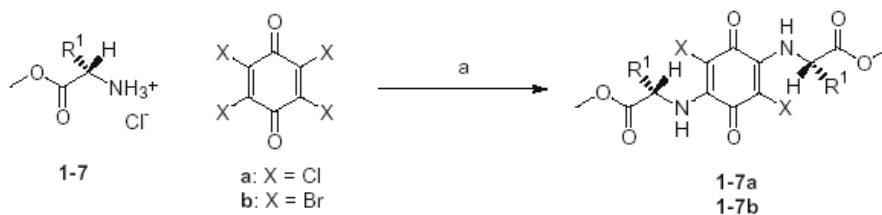


Figure 31. Chemical structures of **1-7a** and **1-7b**.

To develop an efficient parallel synthesis approach, we focused on the displacement reaction of tetrahalo-substituted quinones (chloranil, **a** and bromanil, **b**) with amino acid methyl esters (**1-7**) to afford a library of fourteen 2,5-diamino-3,6-dihalo-[1,4]benzoquinone derivatives. We carried out a one-pot reaction at room temperature that, in most cases, would achieve the quantitative conversion of the starting reactant within 3 hours (see Scheme 2). Moreover, we developed an operationally simple and versatile work-up protocol, which involved recovering high purity final products by filtration upon addition of water to the reaction mixture.



Scheme 2. Library synthesis. Reagents and conditions: (a), EtOH, NEt₃, 3 h, 30-45% yield.

A cell-screening assay was used to test anti-prion activity across the synthesized library compounds. The ability of **1-7a** and **1-7b** to reduce PrP^{Sc} concentrations in ScGT1 cells was determined by Western blotting followed by densitometry of the PK-resistant PrP^{Sc}. PrP^{Sc} levels were quantified by ELISA test. First, we determined the effects of library compounds on cell viability (Table 9). Compound toxicity is

expressed as an average percentage of viable cells when treated with a compound concentration of 1 μM , versus control cells treated with no compound. For compound **6a**, the LC_{50} value (lethal concentration, 50%) for ScGT1 cells was also identified. Anti-prion activity is expressed as the average percentage of PK-resistant PrP^{Sc} remaining after incubation with compound at the given concentration, versus control cells incubated with no compound. For entries **6a**, **6b**, and **7a**, we also calculated the EC_{50} values, which represent the effective concentrations for half-maximal inhibition.

Table 9. Cell viability and anti-prion activity on ScGT1 cells of library compounds

Cpd	% of viable cells at 1 μM^b	% of PrP^{Sc} inhibition at 1 μM^c	EC_{50}^c (μM)	LC_{50}^b (μM)
1a	71.6 \pm 5.4 ^a	0.36 \pm 0.03 ^a		
1b	91.2 \pm 6.8	0.29 \pm 0.05		
2a	81.4 \pm 8.7	0.23 \pm 0.01		
2b	74.1 \pm 4.3	0.31 \pm 0.03		
3a	40.7 \pm 5.5	ND ^d		
3b	52.3 \pm 5.9	ND		
4a	88.2 \pm 6.1	6.6 \pm 0.4		
4b	91.3 \pm 8.8	28.1 \pm 1.5		
5a	95.5 \pm 6.2	4.8 \pm 0.7		
5b	96.1 \pm 7.5	11.4 \pm 0.5		
6a	68.4 \pm 7.3	73.2 \pm 3.3	0.87 \pm 0.1	2.4 \pm 0.2
6b	80.2 \pm 5.8	18.1 \pm 0.5	3.6 \pm 0.5	
7a	96.0 \pm 7.6	0.25 \pm 0.04	7.7 \pm 1.2	
7b	65.9 \pm 3.4	0.43 \pm 0.01		

^a Values are the mean of three experiments, standard deviations are given. ^b ScGT1 cells were cultured in DMEM with 10% FBS, plated 25000 cells in each well of 96-well plates. The compounds were dissolved in DMSO (100%) and diluted in PBS (1X) before adding various concentrations (1 nM - 10 μM) and the cells were incubated for five days at 37°C and 5% CO_2 . The results were developed by calcein-AM fluorescence dye and read by microplate reader. ^c Effect of library compounds on inhibition of scrapie prion replication. ScGT1 cells were cultured in DMEM with 10% FBS, split 1:10 into Petri dishes and incubated for two days at 37°C and 5% CO_2 . Then, various compound concentrations (0.1 nM - 1 μM), being non-cytotoxic, were added to the plates. After a five-day incubation, proteins of cells were extracted, quantified, digested with PK, and western blotted. ^d ND: not determined.

Analyzing the results in Table 9, we note some interesting trends. The cytotoxic effects of **1-7a** and **1-7b** were first determined by a calcein-AM assay in the ScGT1 cell line. As reported, treating ScGT1 with the compounds (1 μM) did not significantly modify cell viability. However, treatment with the BOC-Lys derivatives **3a** and **3b** decreased cell viability by percentages of 40% and 52% respectively. Because of the toxicity profile shown, **3a** and **3b** were not screened for prion

replication, whereas the other library members were assayed at a concentration of 1 μM . Notably, despite this low concentration range, three couples of library hits were active against PrP^{Sc} accumulation. IleOMe (**4a-b**), MetOMe (**5a-b**) and PheOMe (**6a-b**) derivatives of both series at 1 μM displayed activities ranging from 4.8% to 73%. Conversely, AlaOMe (**1a-b**), N ω -Nitro-ArgOMe (**2a-b**), TrpOMe (**7a-b**) derivatives had no effect at that concentration. Due to its low cytotoxicity, **7a** could also be tested at higher concentrations, revealing a fair EC₅₀ value of 7.7 μM . For **6a**, we found a remarkable submicromolar EC₅₀ value ($0.87 \pm 0.10 \mu\text{M}$), comparable to that of quinacrine ($0.4 \pm 0.1 \mu\text{M}$), a reference anti-prion compound.^{285,286} The high activity of **6a** and **6b** was not unexpected, as it is in line with the well-known central role of pi-stacking interactions in self-assembly processes in the fields of chemistry and biochemistry.²⁸⁷

To better rationalize the obtained results, we applied a systematic procedure for identifying key fragments responsible for a given activity.²⁸⁸ We used an algorithm which breaks down a structure into fragments.²⁵⁵ Subsequently, all the obtained substructures were related to biological activities to identify hot fragments. The analysis provides a score [100 – 0] for each fragment, which gives an indication of how often a fragment occurs in the active and inactive structures (Fig. 32). From this preliminary computational study, we have identified that the 2,5-bisdiaminobenzoquinone linked with two phenyl rings by a spacer is a good anti-prion motif. In addition, our analysis suggests the relevance of the atomic size of the substituents in position 3 and 6 at benzoquinone ring (Cl being better than Br), with an inverse relationship to van der Waals radius. Both items of information can be exploited to design further series of anti-prion small molecules.

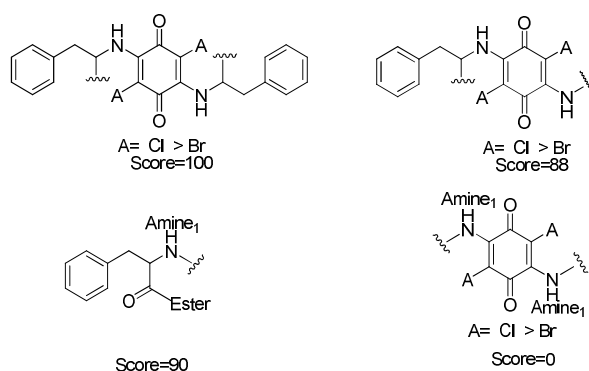


Figure 32. Substructures identified from the synthesized library.

Despite the small number of compounds synthesized, the results suggest that some are active against prion replication. Although the existing derivatives were overall quite cytotoxic toward ScGT1 cells, we identified entries **6a** and **6b** as hit compounds for further lead optimization studies. At a time when it remains challenging to design chemical entities able to target PPIs, these studies might shed light on the underlying principles governing molecular recognition and the chemical basis for the inhibition of quinone derivatives in prions.

4.3 Evaluation and preliminary structure-activity relationship of 2,5-diamino-1,4-benzoquinones as a novel class of bivalent anti-prion compound

4.3.1 Materials and methods

4.3.1.1 Design rationale

We have designed a small combinatorial library of bivalent ligands whose general structure is depicted in Figure 33. The ligands feature the BQ nucleus as central core, with two linkers in positions 2 and 5 connecting two terminal moieties. As linkers, we selected three polyamine chains (**24-26**, Scheme 3) that would allow exploring different lengths and chemical composition for the different molecules. This is of particular importance, since linker length has been shown by May and co-workers to be very critical against PrP^{Sc} formation for the bivalent acridines series.²¹⁸

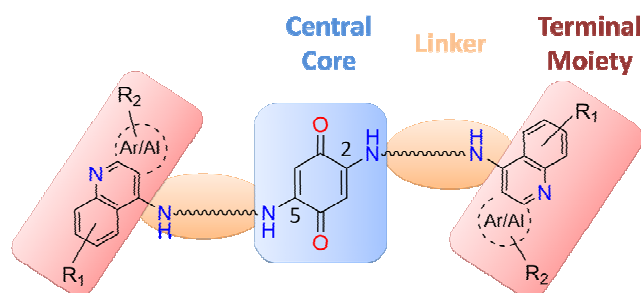


Figure 33. General structure of the designed library compounds.

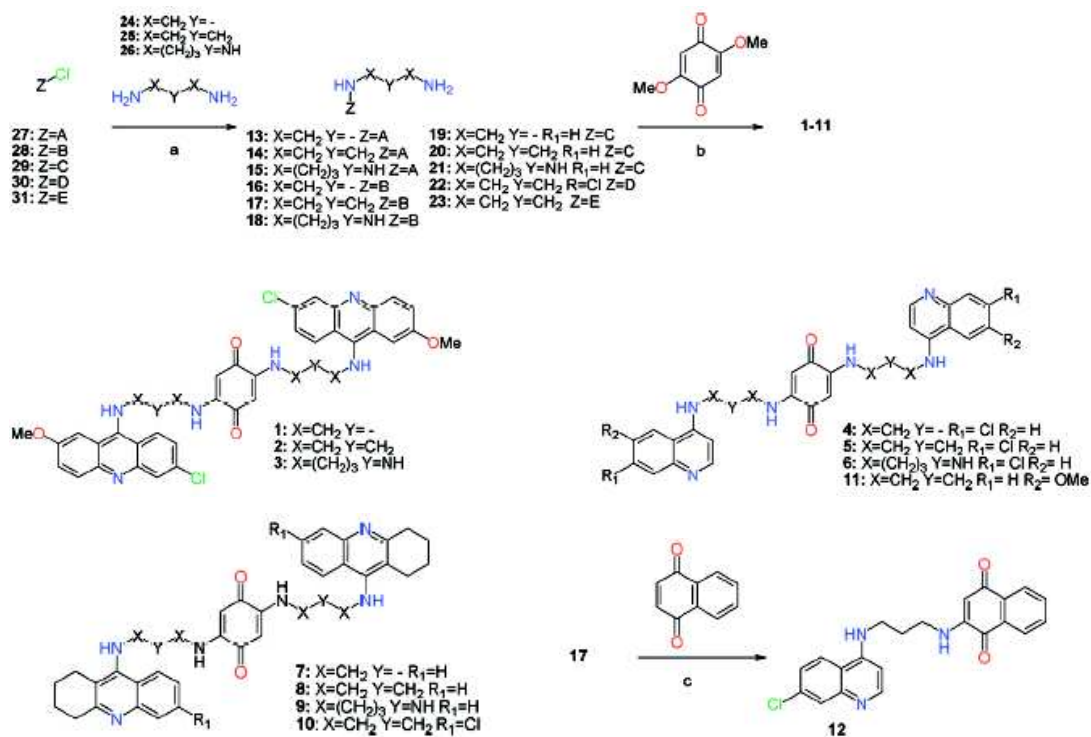
As terminal moieties, starting from the consideration that aromatic groups provided the best activity in the previous series of BQ compounds (see **part 4.2 in the thesis**), we selected several aromatic prion recognition motifs, such as 6-chloro-2-methoxyacridine (as in **1-3**, Scheme 3), 7-chloroquinoline (**4-6**), and 1,2,3,4-tetrahydroacridine (THA) (**7-9**). Several acridine and quinoline derivatives have been shown to inhibit PrP^{Sc} formation in infected cells and to bind to prion

proteins.^{140,238,289} Given that the analogous THA-9-amine is active against yeast prion,²⁹⁰ derivatives **7-9** were also designed. As a second step, on the basis of the remarkable profile shown by **5**, three other derivatives (**10-12**) were designed with the aim of further optimizing activity in the existing series of compounds. Herein, we present a solution-phase parallel synthesis of a library of bivalent BQ derivatives, which were chosen for their anti-prion activity in ScGT1 cells, together with their capability of inhibiting PrP^{Sc} aggregation and of reducing oxidative stress (OS).

4.3.1.2 Library synthesis

Disubstitution reaction of diamines with 2,5-dimethoxy-1,4-benzoquinone provides an easy access to a variety of 2,5-diamino-1,4-benzoquinones.^{283,291} Encouraged by the good yields and the straightforward work-up associated with this reaction, we decided to synthesize the designed bivalent compounds **1-11** using a solution phase parallel synthesis approach. Eleven N-substituted polyamines (**13-23**, Scheme 3) were loaded with 2,5-dimethoxy-1,4-benzoquinone into different vessels of a carousel workstation. After heating at 50°C for 5 hours, the desired products formed in moderate to good yields (38-88%). Monovalent **12** was obtained by Michael reaction starting from naftoquinone and amine **17** (40%).

The preparation of intermediates **13-23** was easily achieved treating in parallel fashion commercially available polyamines **24-26** with heteroaryl halides **27-31**. Compounds **13-23** were obtained in 25-67% yield by reacting a large excess of the polyamine with the corresponding heteroaryl halide (27:1) in phenol and using NaI as a catalyst (Scheme 3). In these conditions we were able to obtain selective mono-substitution at the terminal primary amino group of the polyamine, obviating the need for protection/deprotection of the other amino functionalities.²⁹² Furthermore, we overcame the low-yield of common S_NAr reactions and the use of costly reagents of Pd-catalyzed amination methodologies.²⁹³



Scheme 3. Library synthesis. Reagents and conditions: (a) phenol, NaI, 120°C (1 h), followed by addition of amine, 5 h, 120°C; (b) EtOH, 5 h, 60°C (38-88% yield); (c) EtOH, 80°C (1 h), followed by addition of amine, 5 h, 50°C (40%). A= 6-chloro-2-methoxyacridine; B= 7-chloroquinoline; C= 1,2,3,4-tetrahydroacridine; D= 6-chloro-1,2,3,4-tetrahydroacridine; E= 6-methoxyquinoline.

4.3.1.3 Screening methodology

A cell-screening assay was used to test anti-prion activity across the library of synthesized compounds. Prior, we determined the effects of library compounds on cell viability by calcein-AM assay, measuring viable ScGT1 cells after incubation in the drug-doped medium with various compound concentrations of 10 nM to 10 μM for five days (Table 10). Then, their ability to reduce PrP^{Sc} in ScGT1 cells was determined by Western blotting followed by densitometry of the PK-resistant PrP^{Sc}, in comparison with BiCappa (**BC**), used as a reference compound. PrP^{Sc} levels were quantified by ELISA test. For entries **BC**, **2**, **5**, **6**, and **10**, we also calculated the EC₅₀ values, which represent the effective concentrations for half-maximal inhibition. Cell viability at EC₅₀ values were expressed as an average percentage of viable cells versus untreated control (Table 10, Fig. 34, Fig. 35).

All assays for cell culture, drug treatment, cell viability, PrP^{Sc} detection and quantification were performed in accordance to the protocols described in parts **2.2.4**, **2.2.5** and **2.2.6**.

4.3.1.4 Detection of *in vitro* effect of the synthesized compounds on prion fibril formation

For compounds **BC**, **2**, **5**, **6**, and **10**, the capability of inhibiting prion fibril formation was studied *in vitro*. Fibril formation was performed in accordance to the method previously described by Colby and co-workers with a few modifications.²¹⁹ Briefly, 20 μL of the diluted compounds at indicated concentrations were added to each well containing 180 μL of reaction solution including 100 $\mu\text{g}/\text{mL}$ recombinant mouse (recMo) full-length PrP(23-230), 2 M GdnHCl and 10 μM ThT in PBS buffer (1X) in a 96-well black plate (BD Falcon). Each sample was performed in four replicates. Each well contained one 3-mm glass bead (Sigma). The plate was covered with sealing tape (Fisher Scientific), incubated at 37°C with continuous shaking and read on SpectraMax M5 fluorescence plate reader (Molecular Devices) for 72 hours by top fluorescence reading every 15 min at excitation of 444 nm and emission of 485 nm.

4.3.1.5 Detection of antioxidant activity of the compounds by lipid peroxidation assay

Lipid peroxidation is an indicator of oxidative stress. The thiobarbituric acid reactive substances (TBARS) assay measures lipid hydroperoxides and aldehydes, such as malondialdehyde (MDA), in the cell media and lysates. The assay was performed in accordance to the method previously described.²⁹⁴ Briefly, 10^6 ScGT1 cells were cultured in 1 mL of DMEM per each well of 6 well-plates for 24 hours. After 24 hours, the compounds with various concentrations were added to each well. After 3 hours, the cell media were collected and the cells were washed twice with PBS and scraped off with 1 mL of 2.5% Trichloroacetic acid (TCA). After centrifugation (13,000 \times g, 2 min), 125 μL the supernatant was added to a mixture of 100 μL 15% TCA and 200 μL 0.67% (w/v) 2-thiobarbituric acid (TBA) and heated at 95°C for 20 min. After cooling, 750 μL of 1-butanol was mixed thoroughly into the solution and centrifuged. Two hundred μL was transferred into 96-well plates. Each sample was performed in three replicates. The fluorescence in the butanol phase was measured at excitation of 521 nm and emission of 552 nm by using M5 fluorescence plate reader (Molecular Devices). A blank was performed for each sample. Standard curves specific for the assay was created using MDA.

4.3.1.6 Detection of antioxidant activity of quinone compounds by sulforaphan (4-methylsulfinylbutyl isothiocyanate, SFP) assay

The assay was performed in accordance to the method previously described.²⁹¹ Briefly, ScGT1 cells were seeded in 96-well plates at 3×10^4 cells/well in DMEM. Experiments were performed after 24 hours of incubation at 37°C in 5% CO₂ with SFP (2.5 μM), a potent inducer of cytosolic NQO1. After 24 hours, the cells were washed and treated for 24 hours with 1 μM of compounds. The antioxidant activity of compounds was evaluated after 30 minutes of incubation with 10 μM fluorescent probe (2',7'-dichlorofluorescein diacetate, DCFH-DA) in PBS. After removal of DCFH-DA, the cells were incubated with 0.1 mM tert-butyl hydroperoxide (*t*-BuOOH) in PBS for 30 min. The fluorescence values of the cells from each well were measured at excitation of 485 nm and emission of 535 nm by using M5 fluorescence plate reader (Molecular Devices). Each sample was performed in three replicates.

4.3.1.7 Docking studies

In Autodock,²⁹⁵ a Lamarckian genetic search algorithm was used to identify low energy binding sites and orientations of **10**. Binding modes were ranked by a scoring function implemented in the Autodock. A point grid with a spacing 0.386 Å and $106 \times 82 \times 66$ points were used. A point grid was centered to the center of mass of the cellular prion protein (PDBentry: 1HJM). Gasteiger atom charges were assigned to the protein atoms using AutoDock tools. Water molecules were excluded from the protein before docking. One hundred randomly seeded runs were performed. The binding poses were identified by the ACIAP 1.0 clustering procedure.²⁹⁶

4.3.2 Results and discussion

Preliminarily, the possible toxicity of **1-9** was assessed in ScGT1 cells. At 1 μM, the toxicity profiles among the library members varied from 1.5% to 114.8% (Table 10). Treatment with **1** and **3** decreased cell viability to 18.2% and 1.5%, respectively. Because of the toxicity shown, **1** and **3** were studied for their anti-prion activity at a lower concentration (0.2 μM), whereas the other library members were assayed at 1 μM. The synthesized **2**, **4-9** were found to cover a broad range of activity against PrP^{Sc} formation, with inhibition spanning from 3.4% to 89.7% (Table 10).

Table 10. Cell viability and anti-prion activity on ScGT1 cells of library compounds

Cpd	% of viable cells at 1 μM^b	% of PrP ^{Sc} inhibition at 1 μM^c	% of viable cells at 0.2 μM^b	% of PrP ^{Sc} inhibition at 0.2 μM^c	EC ₅₀ (μM) ^c	% of viable cells at EC ₅₀ ^b
BC	75.6 \pm 7.1 ^a	102.1 \pm 2.7 ^a			0.32 \pm 0.03 ^a	92.4 \pm 6.2 ^a
1	18.2 \pm 1.2	ND ^d	80.1 \pm 6.3 ^a	3.1 \pm 0.3 ^a		
2	65.5 \pm 5.6	89.7 \pm 5.1			0.68 \pm 0.05	75.2 \pm 8.4
3	1.5 \pm 0.2	ND	65.8 \pm 4.6	5.4 \pm 0.4		
4	114.8 \pm 7.9	6.2 \pm 0.6				
5	100.4 \pm 3.6	85.5 \pm 3.9			0.73 \pm 0.03	99.6 \pm 2.7
6	105.0 \pm 7.4	49.1 \pm 2.2			1.2 \pm 0.1	91.3 \pm 4.2
7	108.0 \pm 8.4	7.1 \pm 0.9				
8	104.4 \pm 5.6	3.6 \pm 0.4				
9	95.4 \pm 7.4	3.4 \pm 0.2				
10	78.6 \pm 5.2	105.3 \pm 5.5			0.17 \pm 0.01	101.5 \pm 3.6
11	87.2 \pm 5.8	4.7 \pm 0.3				
12	94.3 \pm 3.8	2.9 \pm 0.1				

^a Values are the mean of three experiments, standard deviations are given. ^b ScGT1 cells were cultured in DMEM with 10% FBS, plated 25000 cells in each well of 96-well plates. The compounds were dissolved in DMSO (100%) and diluted in PBS (1X) before adding various concentrations (10 nM - 10 μM) and the cells were incubated for five days at 37°C and 5% CO₂. The results were developed by calcein-AM fluorescence dye and read by microplate reader. ^c Effect of library compounds on inhibition of scrapie prion replication. ScGT1 cells were cultured in DMEM with 10% FBS, split 1:10 into Petri dishes and incubated for two days at 37°C and 5% CO₂. Then, various compound concentrations (10 nM - 2 μM), being non-cytotoxic, were added to the plates. After a five-day incubation, proteins of cells were extracted, quantified, digested with PK, and western blotted. ^d ND: not determined.

Compounds **1-3**, bearing an acridine moiety, displayed a general higher toxicity in the cell viability assay. **2** turned out to be the most active compound, with a submicromolar EC₅₀ (0.68 \pm 0.05 μM) and a percentage of viable cells at EC₅₀ of 75.2% (Table 10, Fig. 34 A,B). A different toxicity profile was observed for quinoline derivatives **4-6**, which were not toxic to ScGT1 cells (cell viability of > 100% at 1 μM). Intriguingly, **5** and **6** showed also remarkable submicromolar EC₅₀ values (0.73 \pm 0.03 μM , and 1.2 \pm 0.1 μM , respectively; Fig. 34A) comparable to that of **BC** (0.32 \pm 0.03 μM). To note, a series of bisquinolines with a polyamine linker have been already designed and tested in ScN2a cell line but showed a lower activity against prion infection (in the one-digit micromolar range).²³⁸ This might confirm the design rationale, indicating that the presence of a BQ core is critical for activity. The replacement of the 2,6-disubstituted acridine ring of **1-3** with the unsubstituted THA,

as in **7-9**, resulted in a complete loss of activity, pointing out to a possible role for the aromatic substituents in the recognition process. Interestingly, these latter compounds did not show toxicity. For all the three series (**1-3**, **4-6**, and **7-9**), data from the cell-screening assay suggest that a linker length of three methylenes is important for optimal activity. Intriguingly, a similar trend was observed by May and co-workers in their series of analogous bivalent ligands.²¹⁸ Altogether, these preliminary results suggest that a specific length of the linker and the presence of a chlorine substituent on the prion recognition motifs might contribute to activity against PrP^{Sc} formation. Regarding toxicity, the presence of the acridine ring seems to be a major determinant, in line with the reported DNA intercalation properties of this heterocycle.²¹⁸ Conversely, quinoline and THA moieties do not confer cytotoxicity. Building on these considerations, we decided to synthesize a second set of compounds in which the effect of the substituents on the heteroaromatic ring was investigated by synthesizing the 6-chloro-THA (**10**) and the 6-methoxyquinoline (**11**) derivatives. Furthermore, to probe the bivalent mechanism of action of **5**, its corresponding monomeric derivative **12** was designed.

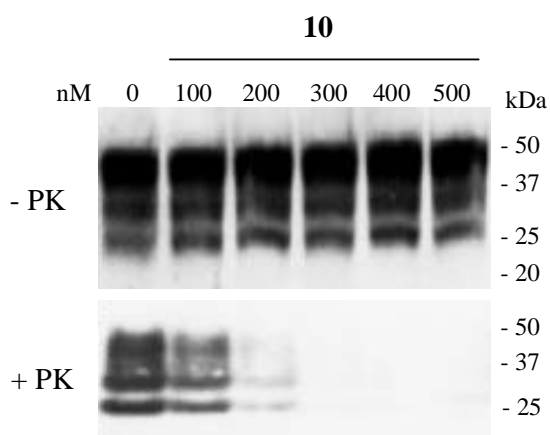
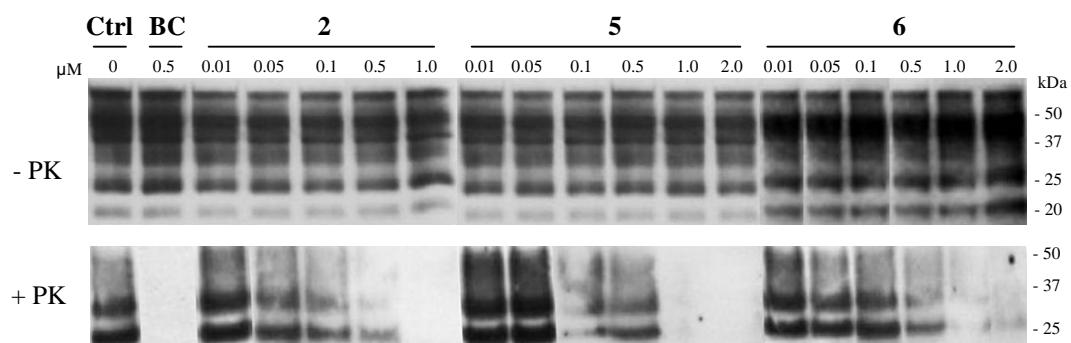
From the biological studies (Table 10), as expected, quinoline **11**, lacking the chlorine atom, was not toxic against ScGT1 cells while displaying negligible activity against prion replication (inhibition of 4.7%). These results again point out the critical role played by the chlorine substituent of the aromatic ring. This speculation was further confirmed by the outstanding activity shown by **10**. In contrast to **8**, which does not carry the chlorine atom and is devoid of anti-prion activity, **10** showed a remarkable EC₅₀ of 0.17 μ M, which is the lowest among the present series of derivatives, even better than that of **BC**. Remarkably, **10** showed a concomitant low toxicity (101.5% of viable cells at EC₅₀ value) (Fig. 34A,B).

By comparing the dramatically different profiles shown by monovalent **12** and bivalent **5** (2.9% vs 85.5% of inhibition), we were able to provide the definitive proof of principle that two proper substituted aromatic prion recognition motifs connected by a BQ spacer are critical for activity.

To study the mechanism of action of the most active compounds (**2**, **5**, **6**, and **10**) at a molecular level, a prion fibrillation assay was used. Only **5**, **10**, and **BC**, at 2 μ M, exhibited significant PrP amyloid fibril formation inhibitory activity. In fact, they extended the lag phase to \geq 53 hours, showing significantly slower kinetics than the control (45 hours, Fig. 35). These results, although preliminary, are in agreement with

the starting hypothesis that bivalent ligands might interact directly with the recPrP to prevent its conversion to the misfolded PrP^{Sc} isoform. Furthermore, the idea that hydrophobic and planar molecular features are crucial for perturbing PPIs in the prion fibrillogenesis processes seems confirmed.²⁷⁸ In addition, a key molecular determinant seems to be the presence of a chlorine substituent on the heteroaromatic terminal moieties.

A



B

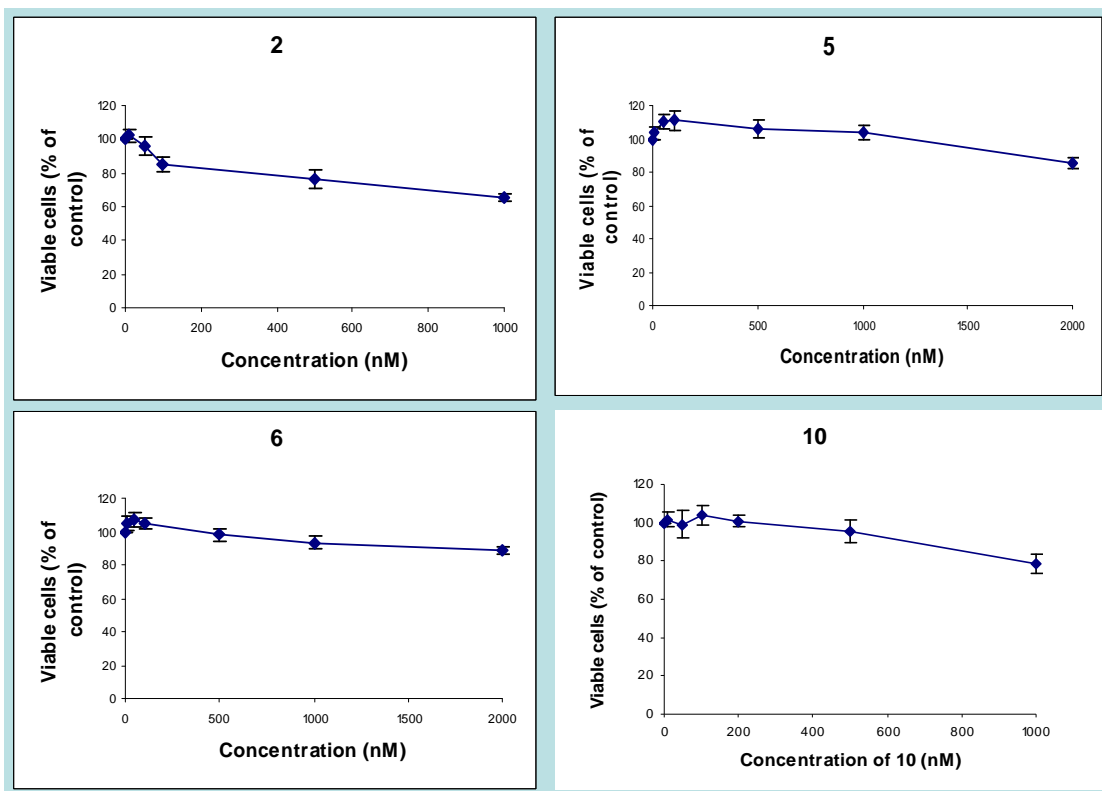


Figure 34. (A) Western blot of protease-digested ScGT1 cell lysates depicting the presence or absence of PrP^{Sc} after treatment with **2**, **5**, **6**, and **10** before (up) or after (bottom) PK; Ctrl = control. (B) Toxicity profile of compounds **2**, **5**, **6**, and **10**.

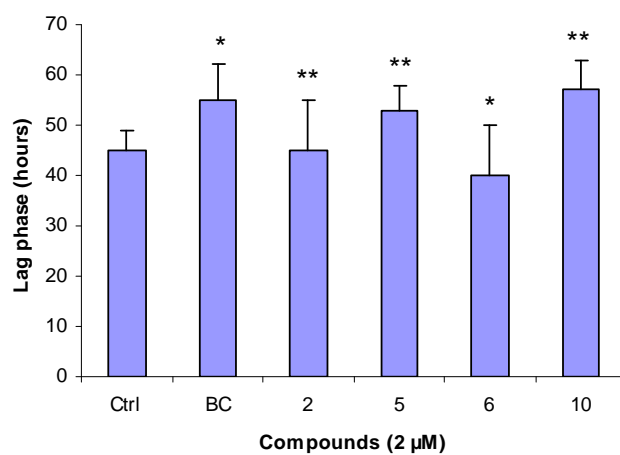


Figure 35. Prion fibril formation inhibitory activity *in vitro* for **BC**, **2**, **5**, **6**, and **10**; Ctrl = control. Statistical analysis was done by analysis of Student's t-test (n=4); (*) p ≤ 0.05, (**) p ≤ 0.01.

The PrP^{Sc} infected cells are under OS, mainly caused by mitochondrial dysfunction.^{297,298} In light of this, antioxidants might be beneficial against prion diseases.²⁹⁹ Indeed, benzoquinones, such as Coenzyme Q (CoQ), can scavenge ROS, and CoQ treatment has been proposed for prion and other neurodegenerative diseases.³⁰⁰⁻³⁰² Thus, we tested the antioxidant potential of the most active BQ derivatives (**2**, **5**, **6**, and **10**) in ScGT1 cell line by using the thiobarbituric acid reactive substances (TBARS) assay and the water-soluble derivative of vitamin E (6-hydroxy-2,5,7,8-tetramethylchroman-2-carboxylic acid, **32**) as a positive control.³⁰³ The assay measures lipid hydroperoxides and aldehydes expressed as an average percentage of TBARS of treated cells versus untreated cells. As shown in Figure 36A, **2**, **5**, and **6** displayed low antioxidant activity (83-87%) at 1 μ M while **10** behaves similarly to **32** (69% vs 71%, respectively). As expected, **BC**, which does not carry a BQ scaffold, did not show any antioxidant capacity (93%).

The antioxidant property of related BQ derivatives have been previously demonstrated^{283,291} and CoQ itself concerns mainly their reduced hydroquinone forms. NQO1, an inducible enzyme that catalyzes the reduction of quinones to hydroquinones, was shown to be responsible for the production of the CoQ-reduced antioxidant forms, as well as that of BQ derivatives.^{283,291} Therefore, since **2**, **5**, **6**, and **10** share the same BQ nucleus, their antioxidant activity was also evaluated in ScGT1, following exposure to *t*-BuOOH, and in the absence or presence of pretreatment with sulforaphane (SFP), an inducer of NQO1. Figure 36B clearly shows that **2**, **5**, **6**, and **10** (at 1 μ M) in their oxidized form show a basal antioxidant activity, but this activity was increased in cells pretreated with SFP, confirming that NQO1 is involved in the activation of BQ derivatives. As expected, the antioxidant activity of **BC** is not influenced by the overexpression of NQO1.

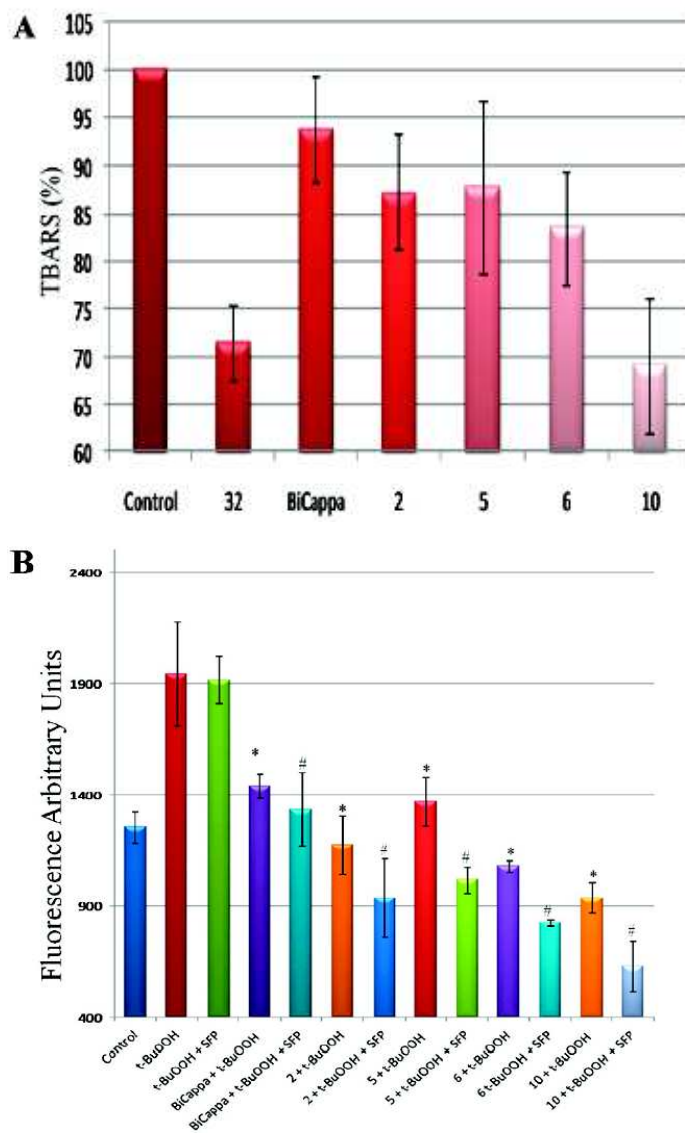


Figure 36. (A) Effect of **32**, BiCappa, **2**, **5**, **6**, and **10** (1 μ M) on ScGT1, evaluated by TBARS formation. Values are the means \pm SD (n = 3); (B) Antioxidant activity of BiCappa, **2**, **5**, **6**, and **10** in ScGT1 cells against ROS formation induced by *t*-BuOOH. Experiments were performed with ScGT1 cells treated or not with 2.5 μ M SFP; (*) $p \leq 0.05$ with respect to *t*-BuOOH treated samples, (#) $p \leq 0.05$ with respect to *t*-BuOOH + SFP treated samples.

With an aim to further unraveling the molecular mechanism whereby the present series of compounds can tackle prion-mediated infections, we carried out docking simulations by means of the AutoDock software at the putative binding region defined by the H2 helix and the loop connecting β -sheet S2 and helix H1 (Fig. 37).^{239,304,305} Such computations did not provide a unique binding mode for compound **10**, in line with our previous findings clearly demonstrating that only a combination of several different techniques would allow to propose a reasonable binding mode for the molecule GN8 at the prion protein.²⁷² Furthermore, different molecular mechanisms,

such as the simultaneous interaction with multiple prion protein, might be envisaged. For these reasons, results of the docking procedure are not shown here.

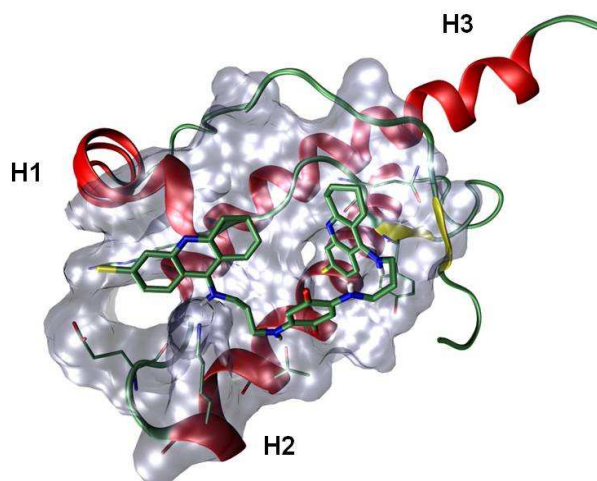


Figure 37. Predicted docking pose of compound **10** in human PrP^C (PDBentry: 1HJM).

4.3.3 Conclusion

A library of 11 symmetrical bivalent compounds was synthesized by solution phase parallel synthesis and tested against prion replication. Despite the small number of compounds, four of them (**2**, **5**, **6**, and **10**) were active against prion replication in the submicromolar range, whereas monovalent **12** showed negligible activity. These results confirmed the rationale for the design of bivalent anti-prion ligands. 7-chloroquinolines (**5** and **6**) and 6-chloro-THA (**10**) derivatives showed a concomitant encouraging low toxicity. Notably, the EC₅₀ of **10** was even lower than that displayed by BiCappa, which is a reference compound for prion diseases.²¹⁸ Furthermore, **10** showed the largest correlation between the cellular anti-prion activity and the capability of inhibiting PrP fibril formation. Interestingly, for **10** we could also find correspondence between anti-prion and antioxidant activities, in contrast to the results obtained by Miyata and co-workers in a series of very potent pyrazolone derivatives.¹⁴⁹

Although its mechanism of action is not fully disclosed (see **docking studies in part 4.3.2**), we assume that the bivalent structure of **10** favors the interaction with prion recognition domains, whereas the spacer acts simultaneously as a disrupting element

against PPIs and an effective antioxidant moiety. Remarkably, the 6-chloro-THA scaffold emerges as an effective and completely novel prion recognition motif.

In conclusion, the present series of molecules are chemical probes that may facilitate the exploration of the molecular mechanism underlying prion disease. We envisage that a better understanding of the molecular framework of bivalent ligands capable of inhibiting prion aggregation and OS would facilitate the creation of new effective anti-prion agents.

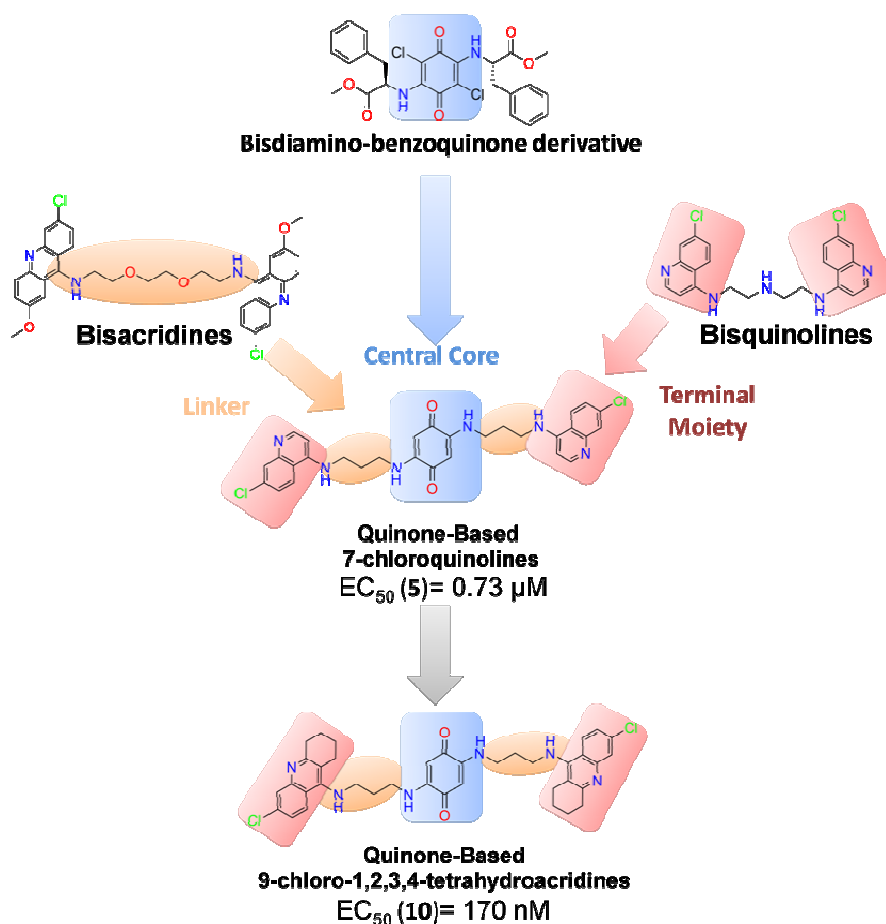


Figure 38. Summary of anti-prion potency of the designed BQ derivatives.

5. Synthesis and biological evaluation of lipoic acid hybrids as novel compounds against prion diseases

5.1 Introduction

Prion diseases pathogenesis involves a complex array of processes operating simultaneously and synergistically. These include: (i) protein aggregation,^{46,51} (ii) oxidative stress accompanied by lipid and protein oxidation,^{298,300,303,306,307} (iii) reduced levels of potent free-radical scavenger such as polyunsaturated fatty acids, α -tocopherol, and glutathione,^{299,306} (iv) unbalance of metal ions,³⁰⁸ and (v) brain inflammation with activation of astrocytes and microglia.⁴³ Thus, the failures of drug candidates developed accordingly to the traditional drug discovery paradigm “one molecule - one target” and the current challenge of discovering an efficacious therapy are likely related to such a multifactorial nature of these diseases. Against this backdrop, a polypharmacological approach, which, rather than consisting of a single compound that interacts with a single target, is a concerted pharmacological intervention of compound(s) that interact with multiple targets, offers promise for the effective treatment of prion diseases. Although this approach is still in its infancy, two different strategies have been already addressed to achieve polypharmacology: drug combination (DC) and multi-target directed ligand (MTDL) approaches. In DC approach multiple drugs (drug cocktail) are combined in the therapeutic regimen. A major drawback of DC therapy is the drug-drug interactions. Conversely, the MTDL approach, where two pharmacophores with distinct mechanism of action are chemically merged in a single structure with a single ADMET (being an acronym for absorption, distribution, metabolism, elimination, and toxicology) profile, offers advantages over DC therapy. Notably, this approach, already used in other complex diseases,³⁰⁹⁻³¹³ might be envisaged as being optimal also in prion diseases.

For prion diseases, DC strategy has been applied in numerous *in vitro* and *in vivo* approaches with the aim of exploiting synergistic effects. The several examples reported in Table 11 suggest that inhibition of prion replication can be effectively potentiated by DC treatment. As for MTDLs, the literature contains cases where the deliberate aim of creating an MTDL has not always been explicitly stated. Instead, the molecular hybridization strategy has been followed, leading to chimeric molecules capable, in principle, of modulating multiple targets.^{140,218,238,289,314} The first anti-prion chimeric ligand, Quinpramine, was designed on the basis of *in vitro* synergistic anti-

prion effects of drugs Quinacrine and Imipramine. Quinpramine, obtained by linking Quinacrine and Imipramine moieties through a piperazine ring, showed an improved anti-prion activity as much as 15-fold over quinacrine and 250-fold over imipramine.^{152,265} Recently, we have reported a new class of anti-prion compounds obtained by linking the antioxidant nucleus of 2,5-diamino-1,4-benzoquinone to several heterocyclic scaffolds potentially able to perturb protein-protein interactions in prion (6-chloro-2-methoxyacridin-9-amine, or 4-amino-7-chloroquinoline or 6-chloro-1,2,3,4-tetrahydroacridin-9-amine). These compounds displayed a multitarget profile, effectively contrasting both prion fibril formation and oxidative stress in a cell culture model of prion replication.²⁸⁰

Table 11. Drug combination strategy in anti-prion compounds

Two-drug combination	cholesterol ester modulators (everolimus, pioglitazone, progesterone, and verapamil) and an antipsychotic drug (chlorpromazine) or an antimalarial drug (quinacrine)	Ref. ³¹⁵
	anti-inflammatory drug (pentosan polysulfate) and an anticancer compound (Fe(III)meso-tetra(4-sulfonatophenyl)porphine)	Ref. ³¹⁶
	polyphenolic antioxidant (epigallocatechin-3-gallate) and 4,5-bis-(4-methoxyanilino)phthalimide	Ref. ³¹⁷
Three-drug combination	antimalarial drug (quinacrine), a tricyclic antidepressant (desipramine) and an inhibitor of cholesterol biosynthesis (simvastatin)	Ref. ¹⁵²

These encouraging results together with a solid background of MTDLs in the field of Alzheimer's disease led us to pursue in that direction. We hypothesized that the presence of a so-called prion-recognition motif (PRM), key element for anti-prion activity, along with a moiety endowed with an alternative mechanism of action against prion diseases might lead to discover more effective compounds.²⁸⁰

5.2 Materials and methods

5.2.1 Design rationale

As a first step, a 4-amino-7-chloroquinoline nucleus was linked by an alkylamino chain to diverse antioxidant moieties. The choice of a N¹-(7-chloroquinolin-4-yl)propane-1,3-diamine (**13**) as PRM was supported by our previous results²⁸⁰ and the studies of Cordeiro and co-workers that demonstrated the direct binding of **13** to

PrP.³¹⁴ As a further strength, a 4-amino-7-chloroquinoline motif recurs in a broad variety of biologically active compounds that hit different targets and pathways. Thus, it can be classified as a privileged sub-structure, with optimal pharmacokinetic properties and a high degree of drug-likeness, extremely favorable features when starting a drug discovery program.^{140,238,289}

Building on **13**, we selected different antioxidant fragments, such as caffeic acid (**9**, Scheme 4), trans-ferulic acid (**10**), and lipoic acid (**12**), for several reasons: (i) all of them are natural antioxidant; (ii) well tolerated *in vivo*; (iii) effective against fibril formation; (iv) chemically linkable to the amine group of **13** by amide bond formation. Several lines of evidence have shown that **9** and **10** act as a potent scavenger of reactive species, including ROS and reactive nitrogen species, and thereby reduce the chance of free radical attack on proteins and DNA and hence preventing their oxidative modification.³¹⁸⁻³²⁰ Furthermore, both appeared to be neuroprotective against β -amyloid-induced cytotoxicity.³²¹⁻³²³ **9** also inhibits 5-lipoxygenase (5-LOX) enzyme, which is involved in the early events of prion disease.³²⁴ **12** has been proposed as a lead structure for designing multi-target directed drugs for neurodegeneration.³²⁵ More importantly, it was administered together with other antioxidants to a patient affected by prion disease, showing moderate therapeutic effects,³²⁶ and shown to inhibit the formation of β -amyloid fibrils.^{327,328} In particular, **12** and its derivatives have been shown to have a variety of properties which interfere with several pathological events of Alzheimer's disease (AD).^{325,327,329}

As a further application of the MTDL approach, we aimed at combining **13** with the molecular features of guanidinium chloride. Guanidinium chloride causes curing of yeast prions by perturbing Hsp104, a molecular chaperone essential for both dissolving protein aggregates and inhibiting prion propagation.^{330,331} This choice was driven by previous results that guanidinium chloride and Guanabenz, a guanidine derivative, are anti-prion compounds.²⁹⁰ However, the guanidine group is nearly quantitatively protonated under physiological conditions, which might result in a lack of CNS penetration. To overcome this limitation, in **3** (Scheme 4) as guanidinium motif we selected L-arginine (**11**). The availability of a transport system for arginine in humans means that a portal of entry to the brain for circulating drugs is potentially available.

In a second round of optimization, based on the promising anti-prion profile of **4** (Scheme 4), we decided to expand the alpha-lipoic acid hybrids series. Four additional

derivatives (**5-8**) were hence designed and tested. Derivative **5** is a structural analogue of **4**, whereas in **6-8** other PRMs were selected: 6-chloro-2-methoxy-acridin-9-amine and 8-chloro-1,2,3,4-tetrahydroacridin-9-amine.

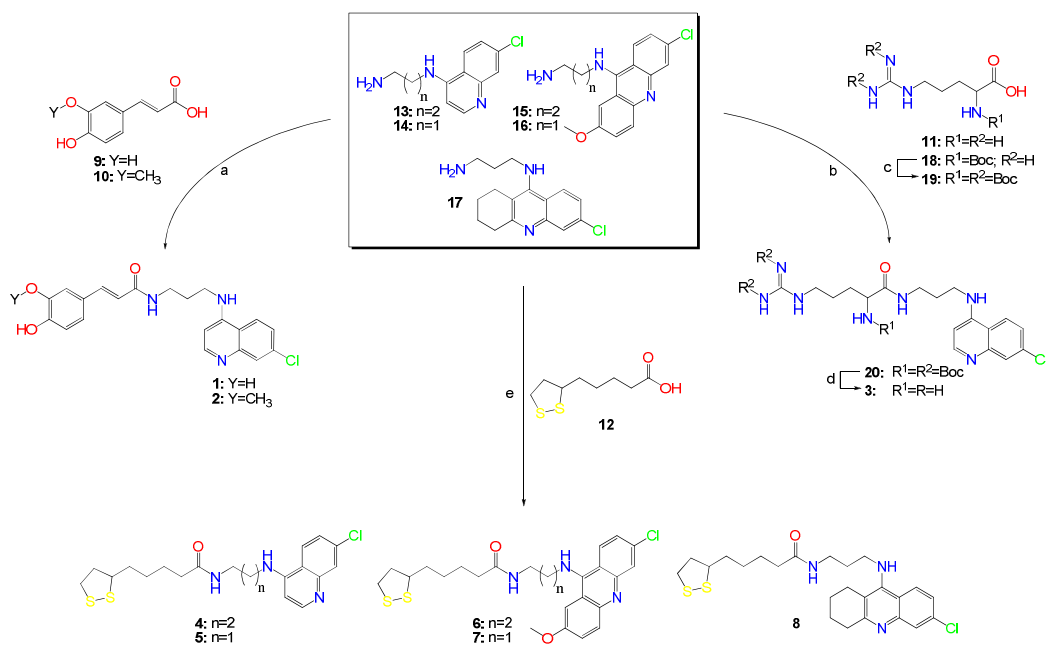
5.2.2 Library synthesis

The synthesis of **1-2** was obtained by using dicyclohexyl carbodiimide (DCC) as a coupling reagent. We have carried out the reaction of the caffeic acid (**9**) or trans-ferulic acid (**10**) with the polyamine **13** (Scheme 4) under reflux THF to give the corresponding amide products in good yield (42-53%). In these conditions we were able to obtain selective amide bond formation, obviating the need for protection/deprotection of the hydroxyl functionalities.

The synthesis of quinoline-arginine hybrid requests the protection of the guanidino and amine groups of the arginine. In our case, all groups were protected by *tert*-butoxycarbonyl groups. Using this protected arginine derivative (**19**, Scheme 4), compound **20** was prepared via standard peptide coupling procedure. Removal of the protecting groups of **20** with a solution of HCl/dioxane afforded **3** in high yield.

A reaction of diamines with lipoic acid (**12**) provides easy access to a variety of derivatives.^{291,332} Thus, we decided to synthesize the designed compounds **4-7** following the procedure described by Rosini and co-workers.³³² **12** was loaded with EDCI, HOBt and NEt₃, then N-substituted polyamine (**13-16**, Scheme 4) was added at 0°C for 2 hours. After stirring over night at room temperature, the desired product was obtained in good yields (67-96%).

The preparation of intermediate **13-16** was easily achieved by parallel synthesis as described by Bongarzone and co-workers.²⁸⁰



Scheme 4. Library synthesis. Reagents and conditions: (a) DCC, THF, reflux 3 h (53-78% yield); (b) Di-tert-butyl dicarbonate, dioxane (RT, 39 h, 76% yield); (c) EDCI, HOBt, NEt₃, DMF, 0°C (1 h), RT, overnight (47% yield); (d) HCl/dioxane (84% yield); (e) EDCI, HOBt, NEt₃, CH₂Cl₂, 0°C (0.5 h), followed by addition of amine **13-17**, RT, overnight (67-96% yield).

5.2.3 Screening methodology

A cell-screening assay was first used to test anti-prion activity across the library of synthesized compounds (**1-8**), and their corresponding fragments (**12**, **13**, and **16**). Prior, we determined the effects of all compounds on cell viability by calcein-AM assay measuring viable ScGT1 cells after incubation in the drug-doped medium with various compound concentrations of 10 nM - 10 μM for five days (Table 12). Then, their ability to reduce PrP^{Sc} concentrations in ScGT1 cells was determined by Western blotting followed by densitometry of the PK-resistant PrP^{Sc}, and PrP^{Sc} levels were quantified by ELISA test. For entries **1-8**, **12**, **13**, and **16**, we also calculated the EC₅₀ values, which represent the effective concentrations for half-maximal inhibition. Cell viability at EC₅₀ values was expressed as an average percentage of viable cells versus untreated control (Table 12, Fig. 40).

In addition, for compounds showing cellular anti-prion activity (**1-8**), the capability of inhibiting prion fibril formation was studied *in vitro* by using a previously reported PrP fibrillation assay.²¹⁹ Prion fibril formation inhibitory activity was evaluated by measuring the increase of the lag phase of PrP amyloid formation kinetics (Fig. 41). Finally, we tested the antioxidant potential of the most active hybrid derivatives (**6-8**)

in ScGT1 cell line by using the thiobarbituric acid reactive substances (TBARS) assay and the antioxidant Trolox as a positive control (Fig. 42).

All assays for cell culture, drug treatment, cell viability, PrP^{Sc} detection and quantification were performed in accordance to the protocols described in parts **2.2.4**, **2.2.5** and **2.2.6**.

Detection of *in vitro* effect of the synthesized compounds on prion fibril formation was performed in accordance to the protocol described in part **4.3.1.4**.

Detection of antioxidant activity of the compounds by lipid peroxidation assay was performed in accordance to the protocol described in part **4.3.1.5**.

5.3 Results and discussion

Preliminarily, the possible toxicity of the hybrid compounds **1-4** was assessed in ScGT1 cells. At 1 μM , the toxicity profile among quinoline-based hybrid compounds (**1-4**) was very low and therefore they were studied for their anti-prion activity at same concentration (Table 12). All hybrid derivatives **1-4** turned out to have mild anti-prion activity, with similar micromolar EC₅₀ values (2.7-9.5 μM), despite the potential different mechanism of action. However, **2** and **4**, carrying the ferulic and lipoic acids moieties respectively, were slightly more active than **1** and **3** (Table 12). To better investigate the multi-target activity of the designed compounds, we tested the anti-prion activity of their starting fragments (**9-13**). As expected, the PRM **13** showed a micromolar EC₅₀ value ($7.8 \pm 0.3 \mu\text{M}$) with no toxicity in ScGT1 cells up to 10 μM . Regarding the three antioxidant fragments (**9**, **10**, and **12**) and guanidinium derivative (**11**), only lipoic acid (**12**) possessed an interesting activity against PrP^{Sc} formation (EC₅₀ = $5.3 \pm 0.4 \mu\text{M}$), together with a suitable toxicity profile (no toxic effects up to 100 μM). To our knowledge, this is the first time that the proposed anti-prion potential of **12** has been demonstrated in a cellular model. Notably, **9-12** did not show toxicity at 10 μM (see Fig. 39). Altogether, these preliminary results suggested us to link **12** with other PRMs (6-chloro-2-methoxy-acridin-9-amine and 8-chloro-1,2,3,4-tetrahydroacridin-9-amine), already exploited by us and others in the search for anti-prion ligands and drug-likeness similar to that of **13**.^{218,265,280,289} Thus, we decided to synthesize and test a further subset of alpha-lipoic acid hybrids (**5-8**). From the biological studies (Table 12), this rational design was confirmed by the outstanding activity shown by **6** and **7**. In fact, both compounds did not show toxicity against ScGT1 cells at 1 μM , while they displayed high activity against prion

replication (107% and 102% inhibition, respectively). **6** and **7** showed a remarkable EC₅₀ of 0.18 μM and 0.15 μM respectively, which are the lowest among the synthesized derivatives and even better than the reference drug Quinacrine. We focused on **7** because preliminary results showed that it was less cytotoxic than **6** at higher concentration (Table 12). Then, we analyzed **7**'s profile in comparison to its starting fragments (**12** and **16**, Table 12). **7** showed an improved anti-prion activity as much as 35-fold over **12** and 2.3-fold over **16**. As expected, **16** did inhibit prion replication with a submicromolar activity (0.35 μM), and thus it can be truly considered a PRM. Notably, also compound **8** (Lipocrine[®]) developed as a promising drug candidate for the treatment of AD,³³² showed a submicromolar EC₅₀ value (0.85 ± 0.05 μM; Table 12 and Fig. 40) with a concomitant low toxicity.

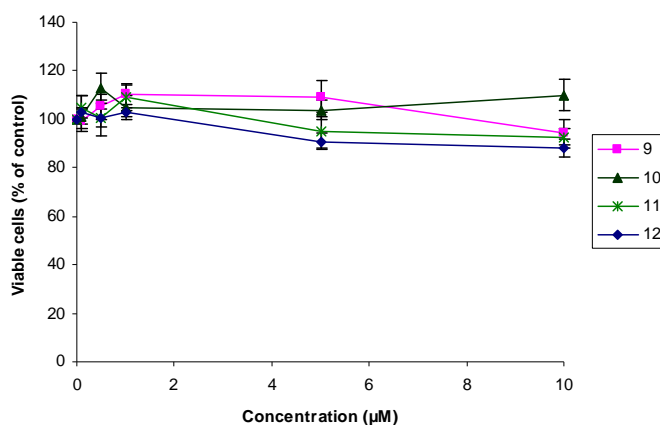


Figure 39. Toxicity profile of compounds **9-12**.

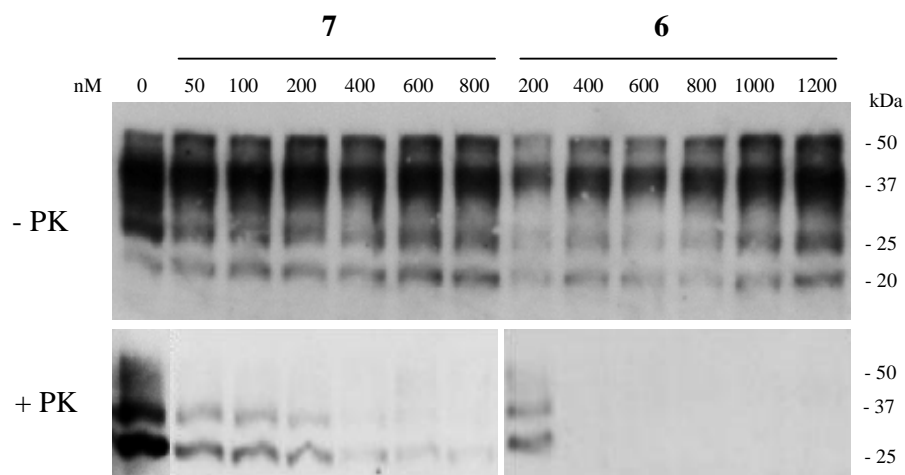
Table 12. Cell viability and anti-prion activity on ScGT1 cells of library compounds

Cpd	% of viable cells at 1 μM ^a	% of PrP ^{Sc} inhibition at 1 μM ^b	EC ₅₀ (μM) ^b	% of viable cells at EC ₅₀ ^a
Quinacrine	98.5 ± 3.9 ^c	103.8 ± 6.1 ^c	0.4 ± 0.1 ^c	100.0 ± 4.3 ^c
1	97.3 ± 6.7	9.2 ± 0.3	8.1 ± 0.3	88.4 ± 5.4
2	102.7 ± 5.8	12.8 ± 0.7	2.7 ± 0.2	105.1 ± 5.8
3	104.9 ± 5.8	4.4 ± 0.5	9.5 ± 0.5	95.7 ± 6.2
4	100.7 ± 2.2	8.7 ± 0.5	5.6 ± 0.1	95.8 ± 3.5
5	101.6 ± 4.3	13.4 ± 0.6	3.2 ± 0.2	100.8 ± 2.6

6	88.1 ± 2.3	107.1 ± 3.0	0.18 ± 0.01	101.9 ± 3.3
7	94.3 ± 5.6	102.5 ± 5.8	0.15 ± 0.01	92.1 ± 5.2
8	95.9 ± 2.1	68.3 ± 2.2	0.85 ± 0.05	94.8 ± 5.5
9	110.2 ± 3.9	Not active up to 10 μM	ND ^d	ND ^d
10	104.7 ± 5.0	Not active up to 10 μM	ND	ND
11	109.1 ± 5.7	Not active up to 10 μM	ND	ND
12	103.0 ± 1.9	2.6 ± 0.1	5.3 ± 0.4	95.4 ± 4.2
13	103.3 ± 3.7	5.8 ± 0.1	7.8 ± 0.3	90.7 ± 4.8
16	88.0 ± 5.7	98.5 ± 5.4	0.35 ± 0.02	95.4 ± 3.9

^a ScGT1 cells were cultured in DMEM with 10% FBS, plated 25000 cells in each well of 96-well plates. The compounds were dissolved in DMSO (100%) and diluted in PBS (1X) before adding various concentrations (10 nM - 10 μM) and the cells were incubated for five days at 37°C, 5% CO₂. The results were developed by calcein-AM fluorescence dye and read by microplate reader. ^b The effect of library compounds on inhibition of scrapie prion replication. ScGT1 cells were cultured in DMEM with 10% FBS, split 1:10 into Petri dishes and incubated for two days at 37°C and 5% CO₂. Then, various compound concentrations (10 nM - 2 μM), being non-cytotoxic, were added to the plates. After a five-day incubation, proteins of cells were extracted, quantified, digested with PK, and western-blotted. ^c Values are the mean of three experiments, standard deviations are given. ^d ND: not determined.

A



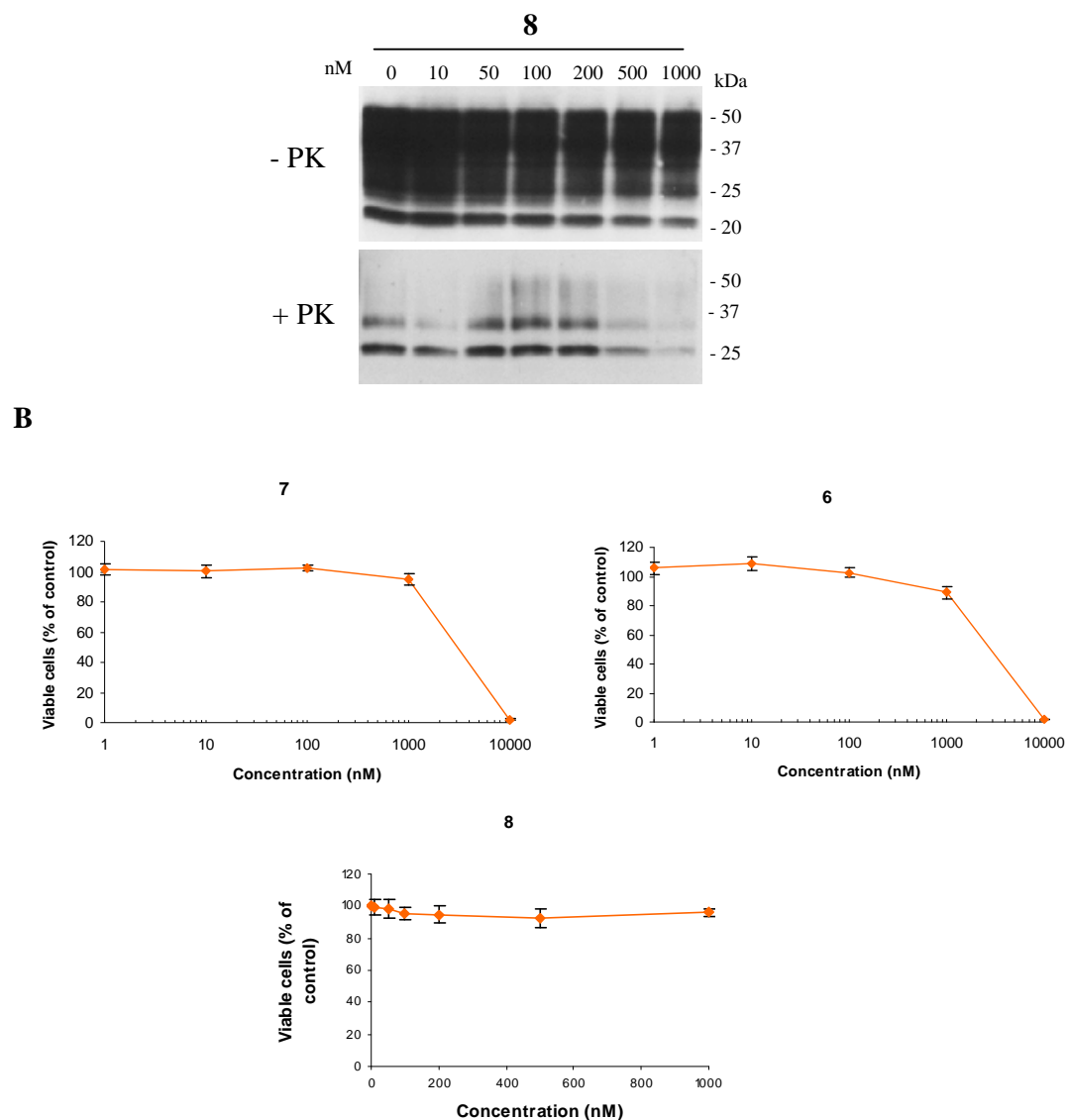


Figure 40. (A) Western blot of protease-digested ScGT1 cell lysates depicting the presence or absence of PrP^{Sc} after treatment with **6-8** before (up) or after (bottom) PK; (B) Toxicity profile of compounds **6-8**.

To study at a molecular level the mechanism of action of the active compounds (**1-8**, **12**, **13**, and **16**), a PrP amyloid fibrillation assay was used. All compounds were capable of delaying fibril formation, with lag phase spanning from 52 to 70 hours (control 49 hours, Fig. 41). Intriguingly, their *in vitro* PrP amyloid fibril formation inhibitory activity parallels the cellular anti-prion profile. In fact, **6**, **7**, and **8**, which were the most active in ScGT1 cell line, resulted in the most active also in this assay. **6** and **7** extended the lag phase to ≥ 68 hours, showing a significantly slower kinetics than the control (Fig. 41). These results, although preliminary, are in agreement with

the starting hypothesis that PRM might interact directly with PrP to prevent its conversion to the misfolded PrP^{Sc} isoform. Furthermore, the low anti-amyloid activity of **12** versus those of hybrids **4-8** suggests that marked aggregation inhibition may be achieved only when **12** and a suitable PRM are combined into the same structure, as in **6** and **7**.

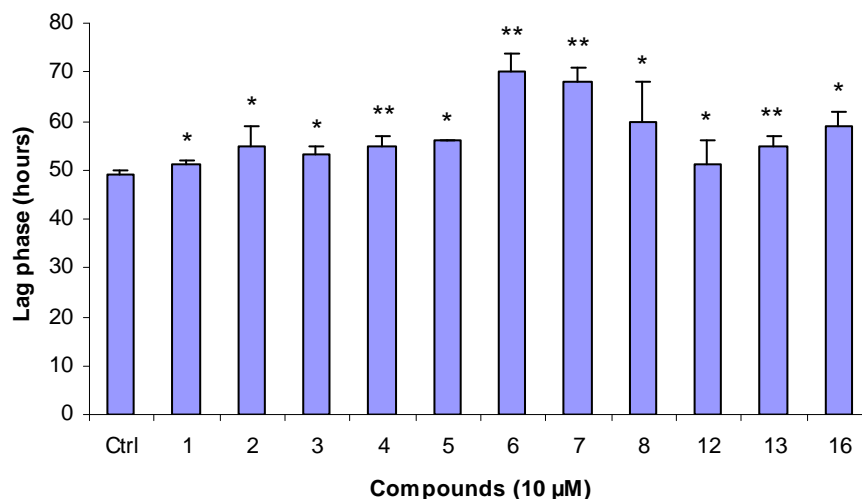


Figure 41. Prion fibril formation inhibitory activity *in vitro* for **1-8**, **12**, **13**, and **16**; Ctrl = control. Statistical analysis was done by analysis of Student's t-test (n=4); (*) p ≤ 0.05, (**) p ≤ 0.01.

The PrP^{Sc} infected cells are under OS, mainly caused by mitochondrial dysfunction.^{297,298} In light of this, antioxidant fragments might be beneficial against prion diseases.²⁹⁹ Indeed, lipoic acid hybrids scavenge ROS, and they have been proposed for the treatment of other multifactorial neurodegenerative diseases.^{300,302,312} Thus, we tested the antioxidant potential of the most active derivatives (**6-8**) in ScGT1 cell line by using TBARS assay and the antioxidant Trolox as a positive control.³⁰³ The assay measures lipid hydroperoxides and aldehydes expressed as an average percentage of TBARS of treated cells versus untreated cells. Figure 42 clearly shows that **6** and **7** displayed antioxidant activity (78-82% of control) at 1 μM, while **8** was even better than Trolox (58% vs 71%, respectively). Although a perfect match with cellular data is not evident, these results confirm the design rationale, indicating that the presence of a PRM (a lipophilic bi- or tri-(hetero)-cyclic scaffold) and an antioxidant fragment (lipoic acid) is suitable to the discovery of anti-prion hybrids.

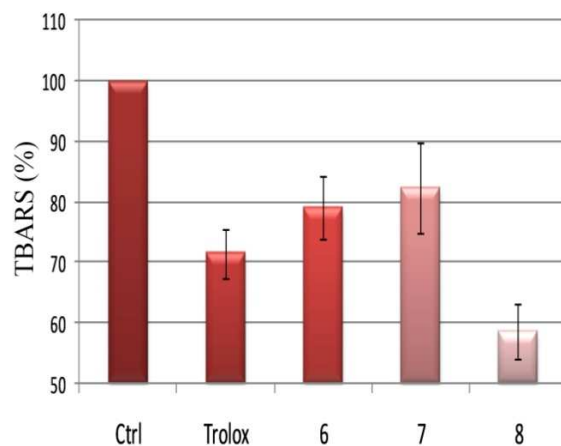


Figure 42. Effect of compounds Trolox, and **6-8** (1 μ M) on ScGT1 cells, evaluated by TBARS formation. Values are means \pm SD (n = 3); Ctrl = control.

5.4 Conclusion

The goal of this communication is to provide a starting point against the development of MTDLs for prion diseases treatment. As an example, **7**, owing to the presence of an antioxidant fragment, the lipionic acid, and a PRM, the acridine motif, is able to simultaneously interact with at least two of the multiple targets involved in prion pathology: It inhibits PrP^{Sc} accumulation, delays fibril formation and reduces oxidative stress. Altogether these *in vitro* results make **7** an effective candidate to be investigated *in vivo* for its multiple biological properties in prion diseases. Furthermore, given the promising cellular anti-prion profile of **12**, further efforts towards the design of novel lipoyl hybrids are warranted.

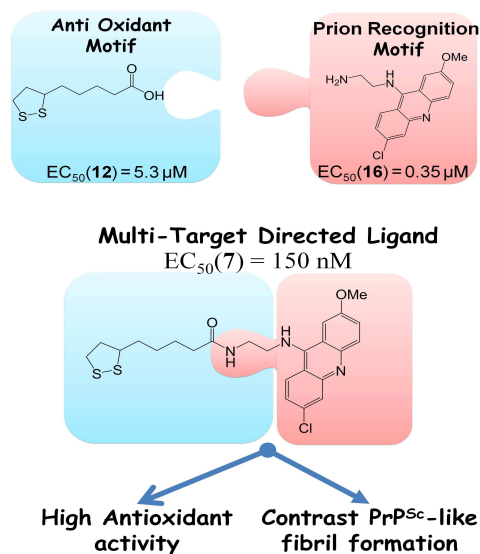


Figure 43. Summary of anti-prion potency of the designed lipionic acid hybrid **7**.

6. Concluding remarks

In the thesis, we discuss about biological evaluation of four new libraries of anti-prion compounds designed and synthesized on nanotechnology, computational study and chemistry.

Firstly, in the first library, we discovered a novel class of anti-prion compounds as polyelectrolyte multilayer-coated gold nanoparticles for their ability to interact and reduce the accumulation of the disease-causing prion protein (PrP^{Sc}) in scrapie prion-infected cell lines and mice. Gold nanoparticles coated with oppositely charged polyelectrolytes, such as polyallylamine hydrochloride and polystyrenesulfonate, were tested for potential inhibition of prion protein aggregation. Different coatings, finishing with a positive or negative layer, were tested, and different numbers of layers were investigated for their ability to interact and reduce the accumulation of PrP^{Sc} in scrapie prion-infected ScGT1 and ScN2a cells. The particles efficiently hampered the accumulation of PrP^{Sc} in ScN2a cells and showed curing effects on ScGT1 cells with a nanoparticle concentration in the picomolar range. Moreover, incubation periods of prion-infected mice treated with nanomolar concentrations of the nanoparticles were significantly longer compared to untreated controls. In addition, the coated gold nanoparticles may interact with A β and α -synuclein to inhibit β -amyloid and α -synuclein fibril formation implicated in Alzheimer's and Parkinson's diseases, respectively.

Secondly, we have also developed possible peptidomimetic fragments in inhibiting protein-protein interactions including diketopiperazines and 2,5-diamino-1,4-benzoquinones for search of bivalent anti-prion compounds. In the second library, we report the identification of a novel bifunctional diketopiperazine (DKP) derivative **1d**, which exhibited activity in the low micromolar range against prion replication in ScGT1 cells, while showing low toxicity. By properly addressed molecular modeling studies we hypothesized that a planar conformation is the major determinant for activity in this class of compounds. Moreover, studies aimed to assess the mechanism of action at a molecular level showed that **1d** might interact directly with recPrP to prevent its conversion to the pathogenic PrP^{Sc}-like form. This investigation suggests that

DKP based anti-prion compounds can serve as a promising lead scaffold in developing new drugs to combat prion diseases. In the third library, the compounds combining two different benzoquinone cores with seven (L) amino acid methyl esters (alanine, N ω -nitro-arginine, N ϵ -BOC-lysine, isoleucine, methionine, phenylalanine and tryptophan) were prepared and tested for prion replication inhibition in ScGT1 cells. The most potent hit, **6a**, displayed an EC₅₀ value of 0.87 μ M, which is very close to that of quinacrine (0.4 μ M). From this finding, a small library of twelve entries, featuring a 2,5-diamino-1,4-benzoquinone nucleus as spacer connecting two aromatic prion recognition motifs (PRMs): 6-chloro-2-methoxyacridin-9-amine, or 4-amino-7-chloroquinoline or 6-chloro-1,2,3,4-tetrahydroacridin-9-amine, was designed and evaluated against prion infection. Notably, 6-chloro-1,2,3,4-tetrahydroacridine **10** showed an EC₅₀ of 0.17 μ M, which was lower than that displayed by reference compound BiCappa. More importantly, **10** possessed the capability of inhibiting prion fibril formation and oxidative stress, together with a low cytotoxicity. This study further corroborates the bivalent strategy as a viable approach to the rational design of anti-prion chemical probes.

Finally, in the fourth library, we have designed a small library of multi-target directed ligands (MTDLs) as the alpha-lipoic acid hybrids. Hybrid compounds **6-8** are based on PRMs: 6-chloro-2-methoxyacridin-9-amine and 8-chloro-1,2,3,4-tetrahydroacridin-9-amine, possessed anti-prion activity and the capability of inhibiting prion fibril formation and oxidative stress. **7** showed a remarkable EC₅₀ of 0.15 μ M, which is the lowest among lipoic acid derivatives. **7**, owing to the presence of an antioxidant fragment, the lipoic acid, and a PRM, the acridine motif, is able to simultaneously interact with at least two of the multiple targets involved in prion disease pathology. The development of MTDLs might lead to new pharmaceutical treatments for the multifactorial pathology of prion diseases.

List of publications

1. Bongarzone S,* **Tran HN**,* Cavalli A, Roberti M, Carloni P, Legname G, Bolognesi ML. Parallel synthesis, evaluation, and preliminary structure-activity relationship of 2,5-diamino-1,4-benzoquinones as a novel class of bivalent anti-prion compound. *J Med Chem.* 2010; 53(22):8197-201. (* co-first authors)
2. **Ai Tran HN**, Sousa F, Moda F, Mandal S, Chanana M, Vimercati C, Morbin M, Krol S, Tagliavini F, Legname G. A novel class of potential prion drugs: preliminary in vitro and in vivo data for multilayer coated gold nanoparticles. *Nanoscale.* 2010; 2(12):2724-32.
3. Bolognesi ML, **Ai Tran HN**, Staderini M, Monaco A, López-Cobeñas A, Bongarzone S, Biarnés X, López-Alvarado P, Cabezas N, Caramelli M, Carloni P, Menéndez JC, Legname G. Discovery of a class of diketopiperazines as anti-prion compounds. *ChemMedChem.* 2010; 5(8):1324-34.
4. **Tran HN**, Bongarzone S, Carloni P, Legname G, Bolognesi ML. Synthesis and evaluation of a library of 2,5-bisdiamino-benzoquinone derivatives as probes to modulate protein-protein interactions in prions. *Bioorg Med Chem Lett.* 2010; 20(6):1866-8.
5. Bongarzone S,* **Tran HN**,* Cavalli A, Roberti M, Rosini M, Carloni P, Legname G, Bolognesi ML. Hybrid lipoic acid derivatives to attack prion disease on multiple fronts. *submitted.* (* co-first authors)

Acknowledgements

I would like to thank my supervisor Prof. Giuseppe Legname for giving me the opportunity to work in his group and for instructing me during my PhD study. He always helped and gave me kindly and useful advice in the research and social life.

I am grateful to my external collaborators Prof. Fabrizio Tagliavini, Dr. Silke Krol from Carlo Besta Neurological Institute (Milan, Italy) for scientific discussions and my PhD project. A special thank goes to Salvatore Bongarzone, Matteo Staderini, Dr. Fabio Moda and Dr. Fernanda Sousa who carried out experiments that supported our work, for all their discussions and friendship. Thanks go to all collaborators in the project of drug discovery, especially to Prof. Maria Laura Bolognesi, Prof. Andrea Cavalli and Prof. Marinella Roberti from University of Bologna (Italy), to Prof. Paolo Carloni from German Research School for Simulation Sciences (Aachen, Germany) and to Prof. Carlos Mennendez from University of Madrid (Spain) for giving me all fruitful discussions.

I would also like to thank all lab members of the Prion Biology Laboratory. We were always friendly in helping together as well as sharing happiness and difficulties in my lab life.

Many thanks to my husband Minh Tuan, my parents and to my brothers and sisters in Vietnam for all their love, belief and support. That was an encouragement and promotion to help me to finish my PhD.

References

- 1 Soto C. Protein misfolding and disease; protein refolding and therapy. *FEBS Lett.* 2001; **498**: 204-207.
- 2 Kelly JW. Alternative conformations of amyloidogenic proteins govern their behavior. *Curr Opin Struct Biol.* 1996; **6**: 11-17.
- 3 Carrell RW, Gooptu B. Conformational changes and disease-serpins, prions and Alzheimer's. *Curr Opin Struct Biol.* 1998; **8**: 799-809.
- 4 Johnson WG. Late-onset neurodegenerative diseases-the role of protein insolubility. *J Anat.* 2000; **196**: 609-616.
- 5 Buxbaum JN, Tagoe CE. The genetics of the amyloidoses. *Annu Rev Med.* 2000; **51**: 543-569.
- 6 Prusiner SB, Scott MR. Genetics of prions. *Annu Rev Genet.* 1997; **31**: 139-175.
- 7 Harper JD, Lansbury PT Jr. Models of amyloid seeding in Alzheimer's disease and scrapie: mechanistic truths and physiological consequences of the time-dependent solubility of amyloid proteins. *Annu Rev Biochem.* 1997; **66**: 385-407.
- 8 Cohen FE, Prusiner SB. Pathologic conformations of prion proteins. *Annu Rev Biochem.* 1998; **67**: 793-819.
- 9 Prusiner SB. Prions. *Proc Natl Acad Sci U S A.* 1998; **95**: 13363-13383.
- 10 Serpell LC *et al.* Examination of the structure of the transthyretin amyloid fibril by image reconstruction from electron micrographs. *J Mol Biol.* 1995; **254**: 113-118.
- 11 Soto C. Alzheimer's and prion disease as disorders of protein conformation: implications for the design of novel therapeutic approaches. *J Mol Med.* 1999; **77**: 412-418.
- 12 Soto C *et al.* Beta-sheet breaker peptides inhibit fibrillogenesis in a rat brain model of amyloidosis: implications for Alzheimer's therapy. *Nat Med.* 1998; **4**: 822-826.
- 13 Soto C *et al.* Reversion of prion protein conformational changes by synthetic beta-sheet breaker peptides. *Lancet.* 2000; **355**: 192-197.
- 14 Stefani M. Protein misfolding and aggregation: new examples in medicine and biology of the dark side of the protein world. *Biochim Biophys Acta.* 2004; **1739**: 5-25.

- 15 Chiti F *et al.* Rationalization of the effects of mutations on peptide and protein aggregation rates. *Nature*. 2003; **424**: 805-808.
- 16 Sitia R, Braakman I. Quality control in the endoplasmic reticulum protein factory. *Nature*. 2003; **426**: 891-894.
- 17 Goldberg AL. Protein degradation and protection against misfolded or damaged proteins. *Nature*. 2003; **426**: 895-899.
- 18 Sherman MY, Goldberg AL. Cellular defenses against unfolded proteins: a cell biologist thinks about neurodegenerative diseases. *Neuron*. 2001; **29**: 15-32.
- 19 Serpell LC *et al.* The protofilament substructure of amyloid fibrils. *J Mol Biol*. 2000; **300**: 1033-1039.
- 20 Sunde M, Blake C. The structure of amyloid fibrils by electron microscopy and X-ray diffraction. *Adv Protein Chem*. 1997; **50**: 123-159.
- 21 Lashuel HA *et al.* Neurodegenerative disease: amyloid pores from pathogenic mutations. *Nature*. 2002; **418**: 291.
- 22 Lashuel HA *et al.* Mixtures of wild-type and a pathogenic (E22G) form of Abeta40 in vitro accumulate protofibrils, including amyloid pores. *J Mol Biol*. 2003; **332**: 795-808.
- 23 Prusiner SB, DeArmond SJ. Prion diseases and neurodegeneration. *Annu Rev Neurosci*. 1994; **17**: 311-339.
- 24 Alper T, Cramp WA, Haig DA, Clarke MC. Does the agent of scrapie replicate without nucleic acid? *Nature*. 1967; **214**: 764-766.
- 25 Griffith JS. Self-replication and scrapie. *Nature*. 1967; **215**: 1043-1044.
- 26 Prusiner SB. Novel proteinaceous infectious particles cause scrapie. *Science*. 1982; **216**: 136-144.
- 27 Soto C. Prion hypothesis: the end of the controversy? *Trends Biochem Sci*. 2010; 1-8 (doi:10.1016/j.tibs.2010.1011.1001).
- 28 Simonic T *et al.* cDNA cloning of turtle prion protein. *FEBS Lett*. 2000; **469**: 33-38.
- 29 Strumbo B, Ronchi S, Bolis LC, Simonic T. Molecular cloning of the cDNA coding for *Xenopus laevis* prion protein. *FEBS Lett*. 2001; **508**: 170-174.
- 30 Rivera-Milla E, Stuermer CA, Málaga-Trillo E. An evolutionary basis for scrapie disease: identification of a fish prion mRNA. *Trends Genet*. 2003; **19**: 72-75.
- 31 Ford MJ, Burton LJ, Morris RJ, Hall SM. Selective expression of prion protein in peripheral tissues of the adult mouse. *Neuroscience*. 2002; **113**: 177-192.

- 32 Aguzzi A, Polymenidou M. Mammalian prion biology: one century of evolving concepts. *Cell*. 2004; **116**: 313-327.
- 33 Moser M, Colello RJ, Pott U, Oesch B. Developmental expression of the prion protein gene in glial cells. *Neuron*. 1995; **14**: 509-517.
- 34 Heikenwalder M, Julius C, Aguzzi A. Prions and peripheral nerves: a deadly rendezvous. *J Neurosci Res*. 2007; **85**: 2714-2725.
- 35 Riek R *et al*. NMR characterization of the full-length recombinant murine prion protein, mPrP(23-231). *FEBS Lett*. 1997; **413**: 282-288.
- 36 Riek R *et al*. NMR structure of the mouse prion protein domain PrP(121-321). *Nature*. 1996; **382**: 180-182.
- 37 Caughey B, Baron GS. Prions and their partners in crime. *Nature*. 2006; **443**: 803-810.
- 38 Aguzzi A, Baumann F, Bremer J. The prion's elusive reason for being. *Annu Rev Neurosci*. 2008; **31**: 439-477.
- 39 Hetz C, Maundrell K, Soto C. Is loss of function of the prion protein the cause of prion disorders? *Trends Mol Med*. 2003; **9**: 237-243.
- 40 Aguzzi A, O'Connor T. Protein aggregation diseases: pathogenicity and therapeutic perspectives. *Nat Rev Drug Discov*. 2010; **9**: 237-248.
- 41 Govaerts C, Wille H, Prusiner SB, Cohen FE. Evidence for assembly of prions with left-handed beta-helices into trimers. *Proc Natl Acad Sci U S A*. 2004; **101**: 8342-8347.
- 42 Budka H. Neuropathology of prion diseases. *Br Med Bull*. 2003; **66**: 121-130.
- 43 Soto C, Satani N. The intricate mechanisms of neurodegeneration in prion diseases. *Trends Mol Med*. 2011; **17**: 14-24.
- 44 Prusiner SB, Scott MR, DeArmond SJ, Cohen FE. Prion protein biology. *Cell*. 1998; **93**: 337-348.
- 45 Telling GC *et al*. Prion propagation in mice expressing human and chimeric PrP transgenes implicates the interaction of cellular PrP with another protein. *Cell*. 1995; **83**: 79-90.
- 46 Aguzzi A, Calella AM. Prions: protein aggregation and infectious diseases. *Physiol Rev*. 2009; **89**: 1105-1152.
- 47 Castilla J *et al*. Crossing the species barrier by PrP(Sc) replication in vitro generates unique infectious prions. *Cell*. 2008; **134**: 757-768.
- 48 Green KM *et al*. The elk PRNP codon 132 polymorphism controls cervid and scrapie prion propagation. *J Gen Virol*. 2008; **89**: 598-608.

- 49 Saborio GP, Permanne B, Soto C. Sensitive detection of pathological prion protein by cyclic amplification of protein misfolding. *Nature*. 2001; **411**: 810-813.
- 50 Brachmann A, Baxa U, Wickner RB. Prion generation in vitro: amyloid of Ure2p is infectious. *EMBO J*. 2005; **24**: 3082-3092.
- 51 Legname G *et al*. Synthetic mammalian prions. *Science*. 2004; **305**: 673-676.
- 52 Dobson CM. Protein folding and misfolding. *Nature*. 2003; **426**: 884-890.
- 53 Arnold JE *et al*. The abnormal isoform of the prion protein accumulates in late-endosome-like organelles in scrapie-infected mouse brain. *J Pathol*. 1995; **176**: 403-411.
- 54 Mironov A Jr *et al*. Cytosolic prion protein in neurons. *J Neurosci*. 2003; **23**: 7183-7193.
- 55 Vey M *et al*. Subcellular colocalization of the cellular and scrapie prion proteins in caveolae-like membranous domains. *Proc Natl Acad Sci U S A*. 1996; **93**: 14945-14949.
- 56 Taraboulos A, Serban D, Prusiner SB. Scrapie prion proteins accumulate in the cytoplasm of persistently infected cultured cells. *J Cell Biol*. 1990; **110**: 2117-2132.
- 57 Béranger F, Mangé A, Goud B, Lehmann S. Stimulation of PrP(C) retrograde transport toward the endoplasmic reticulum increases accumulation of PrP(Sc) in prion-infected cells. *J Biol Chem*. 2002; **277**: 38972-38977.
- 58 Kristiansen M *et al*. Disease-related prion protein forms aggresomes in neuronal cells leading to caspase activation and apoptosis. *J Biol Chem*. 2005; **280**: 38851-38861.
- 59 Lee KS *et al*. Hemin interactions and alterations of the subcellular localization of prion protein. *J Biol Chem*. 2007; **282**: 36525-36533.
- 60 Krammer C, Vorberg I, Schätzl HM, Gilch S. Therapy in prion diseases: from molecular and cellular biology to therapeutic targets. *Infect Disord Drug Targets*. 2009; **9**: 3-14.
- 61 Saborio GP *et al*. Cell-lysate conversion of prion protein into its protease-resistant isoform suggests the participation of a cellular chaperone. *Biochem Biophys Res Commun*. 1999; **258**: 470-475.
- 62 Abid K, Morales R, Soto C. Cellular factors implicated in prion replication. *FEBS Lett*. 2010; **584**: 2409-2414.
- 63 Deleault NR, Lucassen RW, Supattapone S. RNA molecules stimulate prion protein conversion. *Nature*. 2003; **425**: 717-720.

- 64 Deleault NR, Kascsak R, Geoghegan JC, Supattapone S. Species-dependent differences in cofactor utilization for formation of the protease-resistant prion protein in vitro. *Biochemistry*. 2010; **49**: 3928-3934.
- 65 Geoghegan JC *et al.* Selective incorporation of polyanionic molecules into hamster prions. *J Biol Chem*. 2007; **282**: 36341-36353.
- 66 Deleault NR *et al.* Protease-resistant prion protein amplification reconstituted with partially purified substrates and synthetic polyanions. *J Biol Chem*. 2005; **280**: 26873-26879.
- 67 Wang F, Wang X, Yuan CG, Ma J. Generating a prion with bacterially expressed recombinant prion protein. *Science*. 2010; **327**: 1132-1135.
- 68 Baron GS, Magalhães AC, Prado MA, Caughey B. Mouse-adapted scrapie infection of SN56 cells: greater efficiency with microsome-associated versus purified PrP-res. *J Virol*. 2006; **80**: 2106-2117.
- 69 Pandeya DR, Acharya NK, Hong ST. The prion and its potentiality. *Biomed Res*. 2010; **21**: 111-125.
- 70 Hill AF, Zeidler M, Ironside J, Collinge J. Diagnosis of new variant Creutzfeldt-Jakob disease by tonsil biopsy. *Lancet*. 1997; **349**: 99-100.
- 71 Kitamoto T *et al.* Abnormal isoform of prion protein accumulates in follicular dendritic cells in mice with Creutzfeldt-Jakob disease. *J Virol*. 1991; **65**: 6292-6295.
- 72 Hill AF, Collinge J. Subclinical prion infection. *Trends Microbiol*. 2003; **11**: 578-584.
- 73 Mabbott NA, MacPherson GG. Prions and their lethal journey to the brain. *Nat Rev Microbiol*. 2006; **4**: 201-211.
- 74 Gerdes HH. Prions tunnel between cells. *Nat Cell Biol*. 2009; **11**: 235-236.
- 75 Gousset K *et al.* Prions hijack tunnelling nanotubes for intercellular spread. *Nat Cell Biol*. 2009; **11**: 328-336.
- 76 Gregori L *et al.* Partitioning of TSE infectivity during ethanol fractionation of human plasma. *Biologicals*. 2004; **32**: 1-10.
- 77 Sim VL, Caughey B. Recent advances in prion chemotherapeutics. *Infect Disord Drug Targets*. 2009; **9**: 81-91.
- 78 Kimberlin RH *et al.* Disinfection studies with two strains of mouse-passaged scrapie agent. Guidelines for Creutzfeldt-Jakob and related agents. *J Neurol Sci*. 1983; **59**: 355-369.
- 79 Ehlers B, Diringer H. Dextran sulphate 500 delays and prevents mouse scrapie by impairment of agent replication in spleen. *J Gen Virol*. 1984; **65**: 1325-1330.

- 80 Diringer H, Ehlers B. Chemoprophylaxis of scrapie in mice. *J Gen Virol*. 1991; **72**: 457-460.
- 81 Priola SA, Raines A, Caughey WS. Porphyrin and phthalocyanine antiscrapie compounds. *Science*. 2000; **287**: 1503-1506.
- 82 Doh-ura K *et al*. Treatment of transmissible spongiform encephalopathy by intraventricular drug infusion in animal models. *J Virol*. 2004; **78**: 4999-5006.
- 83 Tsuboi Y, Doh-Ura K, Yamada T. Continuous intraventricular infusion of pentosan polysulfate: clinical trial against prion diseases. *Neuropathology*. 2009; **29**: 632-636.
- 84 Caughey B, Race RE. Potent inhibition of scrapie-associated PrP accumulation by congo red. *J Neurochem*. 1992; **59**: 768-771.
- 85 Meier P *et al*. Soluble dimeric prion protein binds PrP(Sc) in vivo and antagonizes prion disease. *Cell*. 2003; **113**: 49-60.
- 86 Rhie A *et al*. Characterization of 2'-fluoro-RNA aptamers that bind preferentially to disease-associated conformations of prion protein and inhibit conversion. *J Biol Chem*. 2003; **278**: 39697-39705.
- 87 Proske D *et al*. Prion protein-specific aptamer reduces PrPSc formation. *Chembiochem*. 2002; **3**: 717-725.
- 88 Peretz D *et al*. Antibodies inhibit prion propagation and clear cell cultures of prion infectivity. *Nature*. 2001; **412**: 739-743.
- 89 Horiuchi M, Baron GS, Xiong LW, Caughey B. Inhibition of interactions and interconversions of prion protein isoforms by peptide fragments from the C-terminal folded domain. *J Biol Chem*. 2001; **276**: 15489-15497.
- 90 Perrier V *et al*. Mimicking dominant negative inhibition of prion replication through structure-based drug design. *Proc Natl Acad Sci U S A*. 2000; **97**: 6073-6078.
- 91 Perrier V, Crozet C, Solassol J, Lehmann S. From chemical drug to immunotherapy: new approaches for the treatment of prion diseases. *Curr Med Chem - Immun, Endoc & Metab Agents*. 2003; **3**: 199-205.
- 92 Lorenzen S, Dunkel M, Preissner R. In silico screening of drug databases for TSE inhibitors. *Biosystems*. 2005; **80**: 117-122.
- 93 Bradley MP. An overview of the diversity represented in commercially-available databases. *Mol Divers*. 2002; **5**: 175-183.
- 94 Goede A *et al*. SuperDrug: a conformational drug database. *Bioinformatics*. 2005; **21**: 1751-1753.

- 95 Korth C, May BC, Cohen FE, Prusiner SB. Acridine and phenothiazine derivatives as pharmacotherapeutics for prion disease. *Proc Natl Acad Sci U S A*. 2001; **98**: 9836-9841.
- 96 Kocisko DA *et al.* New inhibitors of scrapie-associated prion protein formation in a library of 2000 drugs and natural products. *J Virol*. 2003; **77**: 10288-10294.
- 97 Kocisko DA, Caughey B. Searching for anti-prion compounds: cell-based high-throughput in vitro assays and animal testing strategies. *Methods Enzymol*. 2006; **412**: 223-234.
- 98 Bach S *et al.* Isolation of drugs active against mammalian prions using a yeast-based screening assay. *Nat Biotechnol*. 2003; **21**: 1075-1081.
- 99 Kiachopoulos S, Heske J, Tatzelt J, Winklhofer KF. Misfolding of the prion protein at the plasma membrane induces endocytosis, intracellular retention and degradation. *Traffic*. 2004; **5**: 426-436.
- 100 Kawatake S *et al.* Surface plasmon resonance analysis for the screening of anti-prion compounds. *Biol Pharm Bull*. 2006; **29**: 927-932.
- 101 Bertsch U *et al.* Systematic identification of antiprion drugs by high-throughput screening based on scanning for intensely fluorescent targets. *J Virol*. 2005; **79**: 7785-7791.
- 102 Breydo L, Bocharova OV, Baskakov IV. Semiautomated cell-free conversion of prion protein: applications for high-throughput screening of potential antiprion drugs. *Anal Biochem*. 2005; **339**: 165-173.
- 103 Kocisko DA *et al.* Identification of prion inhibitors by a fluorescence polarization-based competitive binding assay. *Anal Biochem*. 2007; **363**: 154-156.
- 104 Reddy TR *et al.* Library design, synthesis, and screening: pyridine dicyanides as potential prion disease therapeutics. *J Med Chem*. 2006; **49**: 607-615.
- 105 Castilla J *et al.* Protein misfolding cyclic amplification for diagnosis and prion propagation studies. *Methods Enzymol*. 2006; **412**: 3-21.
- 106 Atarashi R *et al.* Ultrasensitive detection of scrapie prion protein using seeded conversion of recombinant prion protein. *Nat Methods*. 2007; **4**: 645-650.
- 107 Saá P, Castilla J, Soto C. Ultra-efficient replication of infectious prions by automated protein misfolding cyclic amplification. *J Biol Chem*. 2006; **281**: 35245-35252.
- 108 Atarashi R *et al.* Simplified ultrasensitive prion detection by recombinant PrP conversion with shaking. *Nat Methods*. 2008; **5**: 211-212.

- 109 Kempster S, Bate C, Williams A. Simvastatin treatment prolongs the survival of scrapie-infected mice. *Neuroreport*. 2007; **18**: 479-482.
- 110 Mangé A *et al.* Amphotericin B inhibits the generation of the scrapie isoform of the prion protein in infected cultures. *J Virol*. 2000; **74**: 3135-3140.
- 111 Tilly G *et al.* Efficient and specific down-regulation of prion protein expression by RNAi. *Biochem Biophys Res Commun*. 2003; **305**: 548-551.
- 112 Leucht C *et al.* The 37 kDa/67 kDa laminin receptor is required for PrP(Sc) propagation in scrapie-infected neuronal cells. *EMBO Rep*. 2003; **4**: 290-295.
- 113 Ertmer A *et al.* The tyrosine kinase inhibitor STI571 induces cellular clearance of PrPSc in prion-infected cells. *J Biol Chem*. 2004; **279**: 41918-41927.
- 114 Yun SW *et al.* The tyrosine kinase inhibitor imatinib mesylate delays prion neuroinvasion by inhibiting prion propagation in the periphery. *J Neurovirol*. 2007; **13**: 328-337.
- 115 Supattapone S *et al.* Elimination of prions by branched polyamines and implications for therapeutics. *Proc Natl Acad Sci U S A*. 1999; **96**: 14529-14534.
- 116 Bera A, Nandi PK. Biological polyamines inhibit nucleic-acid-induced polymerisation of prion protein. *Arch Virol*. 2007; **152**: 655-668.
- 117 Winklhofer KF, Tatzelt J. Cationic lipopolyamines induce degradation of PrPSc in scrapie-infected mouse neuroblastoma cells. *Biol Chem*. 2000; **381**: 463-469.
- 118 Sigurdsson EM *et al.* Copper chelation delays the onset of prion disease. *J Biol Chem*. 2003; **278**: 46199-46202.
- 119 Pollera C, Carcassola G, Ponti W, Poli G. Development of in vitro cell cultures for the evaluation of molecules with antiprionic activity. *Vet Res Commun*. 2003; **27**: 719-721.
- 120 Tatzelt J, Prusiner SB, Welch WJ. Chemical chaperones interfere with the formation of scrapie prion protein. *EMBO J*. 1996; **15**: 6363-6373.
- 121 Furlow TW Jr, Whitley RJ, Wilmes FJ. Repeated suppression of Creutzfeldt-Jakob disease with vidarabine. *Lancet*. 1982; **2**: 564-565.
- 122 Deleault NR, Harris BT, Rees JR, Supattapone S. Formation of native prions from minimal components in vitro. *Proc Natl Acad Sci U S A*. 2007; **104**: 9741-9746.
- 123 Caughey B, Kocisko DA. Prion diseases: a nucleic-acid accomplice? *Nature*. 2003; **425**: 673-674.

- 124 Wong C *et al.* Sulfated glycans and elevated temperature stimulate PrP(Sc)-dependent cell-free formation of protease-resistant prion protein. *EMBO J.* 2001; **20**: 377-386.
- 125 Ben-Zaken O *et al.* Cellular heparan sulfate participates in the metabolism of prions. *J Biol Chem.* 2003; **278**: 40041-40049.
- 126 Doh-Ura K *et al.* Prophylactic effect of dietary seaweed Fucoidan against enteral prion infection. *Antimicrob Agents Chemother.* 2007; **51**: 2274-2277.
- 127 Kocisko DA *et al.* Potent antiscrapie activities of degenerate phosphorothioate oligonucleotides. *Antimicrob Agents Chemother.* 2006; **50**: 1034-1044.
- 128 Engelstein R, Ovadia H, Gabizon R. Copaxone interferes with the PrP Sc-GAG interaction. *Eur J Neurol.* 2007; **14**: 877-884.
- 129 Ingrosso L, Ladogana A, Pocchiari M. Congo red prolongs the incubation period in scrapie-infected hamsters. *J Virol.* 1995; **69**: 506-508.
- 130 Gilch S *et al.* Intracellular re-routing of prion protein prevents propagation of PrP(Sc) and delays onset of prion disease. *EMBO J.* 2001; **20**: 3957-3966.
- 131 Nunziante M *et al.* Charged bipolar suramin derivatives induce aggregation of the prion protein at the cell surface and inhibit PrPSc replication. *J Cell Sci.* 2005; **118**: 4959-4973.
- 132 Caughey B *et al.* Inhibition of protease-resistant prion protein accumulation in vitro by curcumin. *J Virol.* 2003; **77**: 5499-5502.
- 133 Hafner-Bratkovic I *et al.* Curcumin binds to the alpha-helical intermediate and to the amyloid form of prion protein - a new mechanism for the inhibition of PrP(Sc) accumulation. *J Neurochem.* 2008; **104**: 1553-1564.
- 134 Riemer C *et al.* Evaluation of drugs for treatment of prion infections of the central nervous system. *J Gen Virol.* 2008; **89**: 594-597.
- 135 Caughey WS, Raymond LD, Horiuchi M, Caughey B. Inhibition of protease-resistant prion protein formation by porphyrins and phthalocyanines. *Proc Natl Acad Sci U S A.* 1998; **95**: 12117-12122.
- 136 Priola SA, Raines A, Caughey WS. Prophylactic and therapeutic effects of phthalocyanine tetrasulfonate in scrapie-infected mice. *J Infect Dis.* 2003; **188**: 699-705.
- 137 Ryou C *et al.* Differential inhibition of prion propagation by enantiomers of quinacrine. *Lab Invest.* 2003; **83**: 837-843.
- 138 Collins SJ *et al.* Quinacrine does not prolong survival in a murine Creutzfeldt-Jakob disease model. *Ann Neurol.* 2002; **52**: 503-506.
- 139 Barret A *et al.* Evaluation of quinacrine treatment for prion diseases. *J Virol.* 2003; **77**: 8462-8469.

- 140 Murakami-Kubo I *et al.* Quinoline derivatives are therapeutic candidates for transmissible spongiform encephalopathies. *J Virol.* 2004; **78**: 1281-1288.
- 141 Forloni G *et al.* Tetracyclines affect prion infectivity. *Proc Natl Acad Sci U S A.* 2002; **99**: 10849-10854.
- 142 Guo YJ *et al.* Treatment of scrapie pathogen 263K with tetracycline partially abolishes protease-resistant activity in vitro and reduces infectivity in vivo. *Biomed Environ Sci.* 2007; **20**: 198-202.
- 143 Tagliavini F *et al.* Tetracycline affects abnormal properties of synthetic PrP peptides and PrP(Sc) in vitro. *J Mol Biol.* 2000; **300**: 1309-1322.
- 144 Kawasaki Y *et al.* Orally administered amyloidophilic compound is effective in prolonging the incubation periods of animals cerebrally infected with prion diseases in a prion strain-dependent manner. *J Virol.* 2007; **81**: 12889-12898.
- 145 Guo K *et al.* Synthesis and evaluation of a focused library of pyridine dicarbonitriles against prion disease. *Eur J Med Chem.* 2008; **43**: 93-106.
- 146 Gilch S, Kehler C, Schätzl HM. Peptide aptamers expressed in the secretory pathway interfere with cellular PrPSc formation. *J Mol Biol.* 2007; **371**: 362-373.
- 147 Perovic S *et al.* Effect of flupirtine on Bcl-2 and glutathione level in neuronal cells treated in vitro with the prion protein fragment (PrP106-126). *Exp Neurol.* 1997; **147**: 518-524.
- 148 Dirikoc S *et al.* Nonpsychoactive cannabidiol prevents prion accumulation and protects neurons against prion toxicity. *J Neurosci.* 2007; **27**: 9537-9544.
- 149 Kimata A *et al.* New series of antiprion compounds: pyrazolone derivatives have the potent activity of inhibiting protease-resistant prion protein accumulation. *J Med Chem.* 2007; **50**: 5053-5056.
- 150 Kishida H *et al.* Non-glycosylphosphatidylinositol (GPI)-anchored recombinant prion protein with dominant-negative mutation inhibits PrPSc replication in vitro. *Amyloid.* 2004; **11**: 14-20.
- 151 Crozet C *et al.* Inhibition of PrPSc formation by lentiviral gene transfer of PrP containing dominant negative mutations. *J Cell Sci.* 2004; **117**: 5591-5597.
- 152 Klingenstein R *et al.* Tricyclic antidepressants, quinacrine and a novel, synthetic chimera thereof clear prions by destabilizing detergent-resistant membrane compartments. *J Neurochem.* 2006; **98**: 748-759.
- 153 Perrier V *et al.* Anti-PrP antibodies block PrPSc replication in prion-infected cell cultures by accelerating PrPSc degradation. *J Neurochem.* 2004; **89**: 454-463.

- 154 Enari M, Flechsig E, Weissmann C. Scrapie prion protein accumulation by scrapie-infected neuroblastoma cells abrogated by exposure to a prion protein antibody. *Proc Natl Acad Sci U S A*. 2001; **98**: 9295-9299.
- 155 Heppner FL *et al*. Prevention of scrapie pathogenesis by transgenic expression of anti-prion protein antibodies. *Science*. 2001; **294**: 178-182.
- 156 Sen GL, Blau HM. A brief history of RNAi: the silence of the genes. *FASEB J*. 2006; **20**: 1293-1299.
- 157 Collins RE, Cheng X. Structural and biochemical advances in mammalian RNAi. *J Cell Biochem*. 2006; **99**: 1251-1266.
- 158 Kong Q. RNAi: a novel strategy for the treatment of prion diseases. *J Clin Invest*. 2006; **116**: 3101-3103.
- 159 White MD *et al*. Single treatment with RNAi against prion protein rescues early neuronal dysfunction and prolongs survival in mice with prion disease. *Proc Natl Acad Sci U S A*. 2008; **105**: 10238-10243.
- 160 Daude N, Marella M, Chabry J. Specific inhibition of pathological prion protein accumulation by small interfering RNAs. *J Cell Sci*. 2003; **116**: 2775-2779.
- 161 Golding MC *et al*. Suppression of prion protein in livestock by RNA interference. *Proc Natl Acad Sci U S A*. 2006; **103**: 5285-5290.
- 162 Pfeifer A *et al*. Lentivector-mediated RNAi efficiently suppresses prion protein and prolongs survival of scrapie-infected mice. *J Clin Invest*. 2006; **116**: 3204-3210.
- 163 White MD, Mallucci GR. Therapy for prion diseases: Insights from the use of RNA interference. *Prion*. 2009; **3**: 121-128.
- 164 Brown KL *et al*. Fetal cell grafts provide long-term protection against scrapie induced neuronal loss. *Neuroreport*. 2001; **12**: 77-82.
- 165 Hooli BV, Tanzi RE. A current view of Alzheimer's disease. *F1000 Biol Rep*. 2009; **1**: pii. 54.
- 166 Masters CL *et al*. Neuronal origin of a cerebral amyloid: neurofibrillary tangles of Alzheimer's disease contain the same protein as the amyloid of plaque cores and blood vessels. *EMBO J*. 1985; **4**: 2757-2763.
- 167 Tanzi RE, Bertram L. Twenty years of the Alzheimer's disease amyloid hypothesis: a genetic perspective. *Cell*. 2005; **120**: 545-555.
- 168 Barten DM, Albright CF. Therapeutic strategies for Alzheimer's disease. *Mol Neurobiol*. 2008; **37**: 171-186.
- 169 Gura T. Hope in Alzheimer's fight emerges from unexpected places. *Nat Med*. 2008; **14**: 894.

- 170 Dovey HF *et al.* Functional gamma-secretase inhibitors reduce beta-amyloid peptide levels in brain. *J Neurochem.* 2001; **76**: 173-181.
- 171 Siemers ER *et al.* Effects of a gamma-secretase inhibitor in a randomized study of patients with Alzheimer disease. *Neurology.* 2006; **66**: 602-604.
- 172 Imbimbo BP *et al.* In vitro and in vivo profiling of CHF5022 and CHF5074 Two beta-amyloid1-42 lowering agents. *Pharmacol Res.* 2007; **55**: 318-328.
- 173 Kukar T *et al.* Chronic administration of R-flurbiprofen attenuates learning impairments in transgenic amyloid precursor protein mice. *BMC Neurosci.* 2007; **8**: 54.
- 174 Galasko DR *et al.* Safety, tolerability, pharmacokinetics, and Aβ levels after short-term administration of R-flurbiprofen in healthy elderly individuals. *Alzheimer Dis Assoc Disord.* 2007; **21**: 292-299.
- 175 Wilcock GK *et al.* Tarenflurbil Phase II Study investigators. Efficacy and safety of tarenflurbil in mild to moderate Alzheimer's disease: a randomised phase II trial. *Lancet Neurol.* 2008; **7**: 483-493.
- 176 Vassar R *et al.* Beta-secretase cleavage of Alzheimer's amyloid precursor protein by the transmembrane aspartic protease BACE. *Science.* 1999; **286**: 735-741.
- 177 Hussain I *et al.* Identification of a novel aspartic protease (Asp 2) as beta-secretase. *Mol Cell Neurosci.* 1999; **14**: 419-427.
- 178 Lin X *et al.* Human aspartic protease memapsin 2 cleaves the beta-secretase site of beta-amyloid precursor protein. *Proc Natl Acad Sci U S A.* 2000; **97**: 1456-1460.
- 179 Sinha S *et al.* Recent advances in the understanding of the processing of APP to beta amyloid peptide. *Ann N Y Acad Sci.* 2000; **920**: 206-208.
- 180 Yan R *et al.* Membrane-anchored aspartyl protease with Alzheimer's disease beta-secretase activity. *Nature.* 1999; **402**: 533-537.
- 181 Ohno M *et al.* BACE1 deficiency rescues memory deficits and cholinergic dysfunction in a mouse model of Alzheimer's disease. *Neuron.* 2004; **41**: 27-33.
- 182 Ohno M *et al.* BACE1 gene deletion prevents neuron loss and memory deficits in 5XFAD APP/PS1 transgenic mice. *Neurobiol Dis.* 2007; **26**: 134-145.
- 183 Laird FM *et al.* BACE1, a major determinant of selective vulnerability of the brain to amyloid-beta amyloidogenesis, is essential for cognitive, emotional, and synaptic functions. *J Neurosci.* 2005; **25**: 11693-11709.
- 184 McConlogue L *et al.* Partial reduction of BACE1 has dramatic effects on Alzheimer plaque and synaptic pathology in APP transgenic mice. *J Biol Chem.* 2007; **282**: 26326-26334.

- 185 Ghosh AK, Gemma S, Tang J. Beta-secretase as a therapeutic target for Alzheimer's disease. *Neurotherapeutics*. 2008; **5**: 399-408.
- 186 Neugroschl J, Sano M. An update on treatment and prevention strategies for Alzheimer's disease. *Curr Neurol Neurosci Rep*. 2009; **9**: 368-376.
- 187 Schenk D *et al*. Immunization with amyloid-beta attenuates Alzheimer-disease-like pathology in the PDAPP mouse. *Nature*. 1999; **400**: 173-177.
- 188 Janus C, Chishti MA, Westaway D. Transgenic mouse models of Alzheimer's disease. *Biochim Biophys Acta*. 2000; **1502**: 63-75.
- 189 Sigurdsson EM *et al*. Immunization with a nontoxic/nonfibrillar amyloid-beta homologous peptide reduces Alzheimer's disease-associated pathology in transgenic mice. *Am J Pathol*. 2001; **159**: 439-447.
- 190 Bard F *et al*. Peripherally administered antibodies against amyloid beta-peptide enter the central nervous system and reduce pathology in a mouse model of Alzheimer disease. *Nat Med*. 2000; **6**: 916-919.
- 191 DeMattos RB *et al*. Peripheral anti-A beta antibody alters CNS and plasma A beta clearance and decreases brain A beta burden in a mouse model of Alzheimer's disease. *Proc Natl Acad Sci U S A*. 2001; **98**: 8850-8855.
- 192 DeMattos RB *et al*. Brain to plasma amyloid-beta efflux: a measure of brain amyloid burden in a mouse model of Alzheimer's disease. *Science*. 2002; **295**: 2264-2267.
- 193 Senior K. Dosing in phase II trial of Alzheimer's vaccine suspended. *Lancet Neurol*. 2002; **1**: 3.
- 194 Lorenzo A, Yankner BA. Beta-amyloid neurotoxicity requires fibril formation and is inhibited by congo red. *Proc Natl Acad Sci U S A*. 1994; **91**: 12243-12247.
- 195 Merlini G *et al*. Interaction of the anthracycline 4'-iodo-4'-deoxydoxorubicin with amyloid fibrils: inhibition of amyloidogenesis. *Proc Natl Acad Sci U S A*. 1995; **92**: 2959-2963.
- 196 Tomiyama T *et al*. Inhibition of amyloid beta protein aggregation and neurotoxicity by rifampicin. Its possible function as a hydroxyl radical scavenger. *J Biol Chem*. 1996; **271**: 6839-6844.
- 197 Kisilevsky R *et al*. Arresting amyloidosis in vivo using small-molecule anionic sulphonates or sulphates: implications for Alzheimer's disease. *Nat Med*. 1995; **1**: 143-148.
- 198 Pappolla M *et al*. Inhibition of Alzheimer beta-fibrillogenesis by melatonin. *J Biol Chem*. 1998; **273**: 7185-7188.

- 199 Soto C, Kindy MS, Baumann M, Frangione B. Inhibition of Alzheimer's amyloidosis by peptides that prevent beta-sheet conformation. *Biochem Biophys Res Commun*. 1996; **226**: 672-680.
- 200 Ruipérez V, Darios F, Davletov B. Alpha-synuclein, lipids and Parkinson's disease. *Prog Lipid Res*. 2010; **49**: 420-428.
- 201 Goedert M. Alpha-synuclein and neurodegenerative diseases. *Nat Rev Neurosci*. 2001; **2**: 492-501.
- 202 Schulz-Schaeffer WJ. The synaptic pathology of alpha-synuclein aggregation in dementia with Lewy bodies, Parkinson's disease and Parkinson's disease dementia. *Acta Neuropathol*. 2010; **120**: 131-143.
- 203 Bar-On P *et al*. Statins reduce neuronal alpha-synuclein aggregation in in vitro models of Parkinson's disease. *J Neurochem*. 2008; **105**: 1656-1667.
- 204 Recchia A *et al*. Alpha-synuclein and Parkinson's disease. *FASEB J*. 2004; **18**: 617-626.
- 205 Leegwater-Kim J, Bortan E. The role of rasagiline in the treatment of Parkinson's disease. *Clin Interv Aging*. 2010; **5**: 149-156.
- 206 Meyer AK *et al*. Restorative approaches in Parkinson's Disease: which cell type wins the race? *J Neurol Sci*. 2010; **289**: 93-103.
- 207 Li HT *et al*. Inhibition of alpha-synuclein fibrillization by dopamine analogs via reaction with the amino groups of alpha-synuclein. Implication for dopaminergic neurodegeneration. *FEBS J*. 2005; **272**: 3661-3672.
- 208 Latawiec D *et al*. Modulation of alpha-synuclein aggregation by dopamine analogs. *PLoS One*. 2010; **5**: e9234.
- 209 May BC, Govaerts C, Cohen FE. Developing therapeutics for the diseases of protein misfolding. *Neurology*. 2006; **66**: S118-122.
- 210 Cisse M, Mucke L. Alzheimer's disease: A prion protein connection. *Nature*. 2009; **457**: 1090-1091.
- 211 Laurén J *et al*. Cellular prion protein mediates impairment of synaptic plasticity by amyloid-beta oligomers. *Nature*. 2009; **457**: 1128-1132.
- 212 Sahoo SK, Labhasetwar V. Nanotech approaches to drug delivery and imaging. *Drug Discov Today*. 2003; **8**: 1112-1120.
- 213 Turkevich J, Stevenson PC, Hillier J. A study of the nucleation and growth processes in the synthesis of colloidal gold. *Disc Farad Soc*. 1951; **11**: 55-75.
- 214 Schneider G, Decher G. Functional core/shell nanoparticles via layer-by-layer assembly. Investigation of the experimental parameters for controlling particle aggregation and for enhancing dispersion stability. *Langmuir*. 2008; **24**: 1778-1789.

- 215 Chanana M *et al.* Interaction of polyelectrolytes and their composites with living cells. *NanoLetters*. 2005; **5**: 2605-2612.
- 216 Schneider G, Decher G. From functional core/shell nanoparticles prepared via layer-by-layer deposition to empty nanospheres. *NanoLetters*. 2004; **4**: 1833-1839.
- 217 Liu X, Atwater M, Wang J, Huo Q. Extinction coefficients of gold nanoparticles with different sizes and different capping ligands. *Coll Surf B: Biointerfaces*. 2007; **58**: 3-7.
- 218 May BC *et al.* Potent inhibition of scrapie prion replication in cultured cells by bis-acridines. *Proc Natl Acad Sci U S A*. 2003; **100**: 3416-3421.
- 219 Colby DW *et al.* Prion detection by an amyloid seeding assay. *Proc Natl Acad Sci U S A*. 2007; **104**: 20914-20919.
- 220 Guenther K, Deacon RJ, Perry VH, Rawlins JN. Early behavioral changes in scrapie-affected mice and the influence of dapsone. *Eur J Neurosci*. 2001; **14**: 401-409.
- 221 Dell'Olmo G *et al.* Early behavioural changes in mice infected with BSE and scrapie: automated home cage monitoring reveals prion strain differences. *Eur J Neurosci*. 2002; **16**: 735-742.
- 222 Giaccone G *et al.* Creutzfeldt-Jakob disease: Carnoy's fixative improves the immunohistochemistry of the proteinase K-resistant prion protein. *Brain Pathol*. 2000; **10**: 31-37.
- 223 Fraser H, Dickinson AG. The sequential development of the brain lesions of scrapie in three strains of mice. *J Comp Path*. 1968; **78**: 301-311.
- 224 Decher G. Polyelectrolyte multilayers, an Overview. In Multilayer thin films, edited by G. Decher, J. Schlenoff. *Wiley-VCH, Weinheim*. 2003: pp. 1-17.
- 225 Supattapone S *et al.* Branched polyamines cure prion-infected neuroblastoma cells. *J Virol*. 2001; **75**: 3453-3461.
- 226 Trevitt CR, Collinge J. A systematic review of prion therapeutics in experimental models. *Brain*. 2006; **129**: 2241-2265.
- 227 De Jong WH *et al.* Particle size-dependent organ distribution of gold nanoparticles after intravenous administration. *Biomaterials*. 2008; **29**: 1912-1919.
- 228 Sonavane G, Tomoda K, Makino K. Biodistribution of colloidal gold nanoparticles after intravenous administration: Effect of particle size. *Coll Surf B: Biointerfaces*. 2008; **66**: 274-280.
- 229 Sousa F *et al.* Functionalized gold nanoparticles: a detailed in vivo multimodal microscopic brain distribution study. *Nanoscale*. 2010; **2**: 2826-2834.

- 230 Soto C, Martin Z. Therapeutic strategies against protein misfolding in neurodegenerative diseases. *Expert Opin Drug Discov.* 2009; **4**: 71-84.
- 231 Beekes M. Prions and prion diseases. *FEBS J.* 2007; **274**: 575.
- 232 Carrell RW, Lomas DA. Conformational disease. *Lancet.* 1997; **350**: 134-138.
- 233 Baxa U. Structural basis of infectious and non-infectious amyloids. *Curr Alzheimer Res.* 2008; **5**: 308-318.
- 234 Zahn R *et al.* NMR solution structure of the human prion protein. *Curr Pharm Design.* 2000; **97**: 145-150.
- 235 DeMarco ML, Daggett V. From conversion to aggregation: protofibril formation of the prion protein. *Proc Natl Acad Sci U S A.* 2004; **101**: 2293-2298.
- 236 King DJ, Safar JG, Legname G, Prusiner SB. Thioaptamer interactions with prion proteins: sequence-specific and non-specific binding sites. *J Mol Biol.* 2007; **369**: 1001-1014.
- 237 Sellarajah S *et al.* Synthesis of analogues of Congo red and evaluation of their anti-prion activity. *J Med Chem.* 2004; **47**: 5515-5534.
- 238 Klingenstein R *et al.* Similar structure-activity relationships of quinoline derivatives for antiprion and antimalarial effects. *J Med Chem.* 2006; **49**: 5300-5308.
- 239 Kuwata K *et al.* Hot spots in prion protein for pathogenic conversion. *Proc Natl Acad Sci U S A.* 2007; **104**: 11921-11926.
- 240 Reinke AA, Gestwicki JE. Structure-activity relationships of amyloid beta-aggregation inhibitors based on curcumin: influence of linker length and flexibility. *Chem Biol Drug Des.* 2007; **70**: 206-215.
- 241 Mammen M, Choi SK, Whitesides GM. Polyvalent interactions in biological systems: Implications for design and use of multivalent ligands and inhibitors. *Ang Chem Int Ed.* 1998; **37**: 2755-2794.
- 242 Nieddu E, Pasa S. Interfering with protein-protein contact: molecular interaction maps and peptide modulators. *Curr Top Med Chem.* 2007; **7**: 21-32.
- 243 De Vega MJ, Martin-Martinez M, Gonzalez-Muniz R. Modulation of protein-protein interactions by stabilizing/mimicking protein secondary structure elements. *Curr Top Med Chem.* 2007; **7**: 33-62.
- 244 Niida A *et al.* Stereoselective synthesis of 3,6-disubstituted-3,6-dihydropyridin-2-ones as potential diketopiperazine mimetics using organocopper-mediated anti-SN2' reactions and their use in the preparation of low-molecule CXCR4 antagonists. *J Org Chem.* 2006; **71**: 3942-3951.

- 245 Faden AI, Knoblach SM, Movsesyan VA, Cernak I. Novel small peptides with neuroprotective and nootropic properties. *J Alzheimers Dis.* 2004; **6**: S93-97.
- 246 Teixido M *et al.* Diketopiperazines as a tool for the study of transport across the blood-brain barrier (BBB) and their potential use as BBB-shuttles. *J Am Chem Soc.* 2007; **129**: 11802-11813.
- 247 O'Neill JC, Blackwell HE. Solid-phase and microwave-assisted syntheses of 2,5-diketopiperazines: small molecules with great potential. *Comb Chem High Throughput Screen.* 2007; **10**: 857-876.
- 248 Frydman-Marom A *et al.* Cognitive-performance recovery of Alzheimer's disease model mice by modulation of early soluble amyloidal assemblies. *Ang Chem Int Ed Engl.* 2009; **48**: 1981-1986.
- 249 Martin L, Olives AI, del Castillo B, Martin MA. Fluorescence quenching of beta-carboline alkaloids in micellar media. A study to select the adequate surfactant to use in analytical techniques. *Luminescence.* 2005; **20**: 152-161.
- 250 Garcia-Zubiri IX *et al.* A spectroscopic study of the interaction of the fluorescent beta-carboline-3-carboxylic acid N-methylamide with DNA constituents: nucleobases, nucleosides and nucleotides. *J Fluoresc.* 2008; **18**: 961-972.
- 251 Tejedor D, Garcia-Tellado F. Chemo-differentiating ABB' multicomponent reactions. Privileged building blocks. *Chem Soc Rev.* 2007; **36**: 484-491.
- 252 Katritzky AR *et al.* Conjugated systems derived from piperazine-2,5-dione. *J Het Chem.* 1988; **25**: 591-597.
- 253 Marcuccio JM, Elix JA. Pyrazine chemistry. II. Reduction of 3,6-dibenzylidenepiperazine-2,5-diones. *Austr J Chem.* 1984; **37**: 1791-1794.
- 254 Ghaemmaghani S, May BC, Renslo AR, Prusiner SB. Discovery of 2-aminothiazoles as potent antiprion compounds. *J Virol.* 2010; **84**: 3408-3412.
- 255 Chemaxon Marvin 5.0.1. 2008. (<http://www.chemaxon.com>).
- 256 Frisch MJ *et al.* Gaussian 03, Revision B.01. *Gaussian, Inc., Wallingford CT.* 2008.
- 257 Nesterov EE *et al.* In vivo optical imaging of amyloid aggregates in brain: Design of fluorescent markers. *Ang Chem Int Ed.* 2005; **44**: 5452-5456.
- 258 Aslund A *et al.* Novel pentameric thiophene derivatives for in vitro and in vivo optical imaging of a plethora of protein aggregates in cerebral amyloidoses. *ACS Chem Biol.* 2009; **4**: 673-684.
- 259 Cashman NR, Caughey B. Prion diseases-close to effective therapy? *Nat Rev Drug Discov.* 2004; **3**: 874-884.

- 260 Csuk R *et al.* Synthesis of monomeric and dimeric acridine compounds as potential therapeutics in Alzheimer and prion diseases. *Arch Pharm.* 2009; **342**: 699-709.
- 261 Wang H *et al.* Direct and selective elimination of specific prions and amyloids by 4,5-dianilinophthalimide and analogs. *Proc Natl Acad Sci U S A.* 2008; **105**: 7159-7164.
- 262 Bolognesi ML *et al.* Discovery of a class of diketopiperazines as antiprion compounds. *ChemMedChem.* 2010; **5**: 1324-1334.
- 263 Corson TW, Aberle N, Crews CM. Design and applications of bifunctional small molecules: why two heads are better than one. *ACS Chem Biol.* 2008; **3**: 677-692.
- 264 Kim YS, Lee JH, Ryu J, Kim DJ. Multivalent & multifunctional ligands to beta-amyloid. *Curr Pharm Des.* 2009; **15**: 637-658.
- 265 Dollinger S *et al.* A chimeric ligand approach leading to potent antiprion active acridine derivatives: design, synthesis, and biological investigations. *J Med Chem.* 2006; **49**: 6591-6595.
- 266 Dolphin GT *et al.* A multimeric quinacrine conjugate as a potential inhibitor of Alzheimer's beta-amyloid fibril formation. *Chembiochem.* 2008; **9**: 952-963.
- 267 Ouberai M, Dumy P, Chierici S, Garcia J. Synthesis and biological evaluation of clicked curcumin and clicked KLVFFA Conjugates as inhibitors beta-amyloid fibril formation. *Bioconjugate Chem.* 2009; **20**: 2123-2132.
- 268 Arkin MR, Wells JA. Small-molecule inhibitors of protein-protein interactions: progressing towards the dream. *Nat Rev Drug Discov.* 2004; **3**: 301-317.
- 269 Forman MS, Trojanowski JQ, Lee VM. Neurodegenerative diseases: a decade of discoveries paves the way for therapeutic breakthroughs. *Nat Med.* 2004; **10**: 1055-1063.
- 270 Trojanowski JQ, Lee VM. "Fatal attractions" of proteins. A comprehensive hypothetical mechanism underlying Alzheimer's disease and other neurodegenerative disorders. *Ann N Y Acad Sci.* 2000; **924**: 62-67.
- 271 Nooren IM, Thornton JM. Diversity of protein-protein interactions. *EMBO J.* 2003; **22**: 3486-3492.
- 272 Kranjc A *et al.* Docking ligands on protein surfaces: The case study of prion protein. *J Chem Theory Comput.* 2009; **5**: 2565-2573.
- 273 Soto C. Unfolding the role of protein misfolding in neurodegenerative diseases. *Nat Rev Neurosci.* 2003; **4**: 49-60.

- 274 Gestwicki JE, Marinec PS. Chemical control over protein-protein interactions: beyond inhibitors. *Comb Chem High Throughput Screen.* 2007; **10**: 667-675.
- 275 Haydar SN, Yun HE, Staal RG, Hirst WD. Small-Molecule Protein-Protein interaction inhibitors as therapeutic agents for neurodegenerative diseases: Recent progress and future directions. In annual reports in medicinal chemistry. *Elsevier Academic: San Diego.* 2009; **44**: 51.
- 276 Blazer LL, Neubig RR. Small molecule protein-protein interaction inhibitors as CNS therapeutic agents: current progress and future hurdles. *Neuropsychopharmacology.* 2009; **34**: 126-141.
- 277 Xu Y *et al.* A credit-card library approach for disrupting protein-protein interactions. *Bioorg Med Chem.* 2006; **14**: 2660-2673.
- 278 Tran HN *et al.* Synthesis and evaluation of a library of 2,5-bisdiamino-benzoquinone derivatives as probes to modulate protein-protein interactions in prions. *Bioorg Med Chem Lett.* 2010; **20**: 1866-1868.
- 279 Talaga P. Beta-amyloid aggregation inhibitors for the treatment of Alzheimer disease: Dream or reality? *Mini Rev Med Chem.* 2001; **1**: 175-186.
- 280 Bongarzone S *et al.* Parallel synthesis, evaluation, and preliminary structure activity relationship of 2,5-diamino-1,4-benzoquinones as a novel class of bivalent anti-prion compound. *J Med Chem.* 2010; **53**: 8197-8201.
- 281 Sellarajah S *et al.* Synthesis and testing of peptides for anti-prion activity. *Eur J Med Chem.* 2008; **43**: 2418-2427.
- 282 Bartolini M *et al.* Insight into the kinetic of amyloid beta (1-42) peptide self-aggregation: elucidation of inhibitors' mechanism of action. *Chembiochem.* 2007; **8**: 2152-2161.
- 283 Bolognesi ML *et al.* Novel class of quinone-bearing polyamines as multi-target-directed ligands to combat Alzheimer's disease. *J Med Chem.* 2007; **50**: 4882-4897.
- 284 Pawar AP *et al.* Prediction of "aggregation-prone" and "aggregation-susceptible" regions in proteins associated with neurodegenerative diseases. *J Mol Biol.* 2005; **350**: 379-392.
- 285 Yung L *et al.* Pharmacokinetics of quinacrine in the treatment of prion disease. *BMC Infect Dis.* 2004; **4**: 53.
- 286 Ghaemmaghami S *et al.* Continuous quinacrine treatment results in the formation of drug-resistant prions. *PLoS Pathog.* 2009; **5**: e1000673.
- 287 Gazit E. A possible role for pi-stacking in the self-assembly of amyloid fibrils. *FASEB J.* 2002; **16**: 77-83.
- 288 Lewell XQ, Judd DB, Watson SP, Hann MM. RECAP--retrosynthetic combinatorial analysis procedure: a powerful new technique for identifying

- privileged molecular fragments with useful applications in combinatorial chemistry. *J Chem Inf Comput Sci.* 1998; **38**: 511-522.
- 289 Cope H *et al.* Synthesis and SAR study of acridine, 2-methylquinoline and 2-phenylquinazoline analogues as anti-prion agents. *Eur J Med Chem.* 2006; **41**: 1124-1143.
- 290 Tribouillard-Tanvier D *et al.* Antihypertensive drug Guanabenz is active in vivo against both yeast and mammalian prions. *Plos One.* 2008; **3**: e1981.
- 291 Bolognesi ML *et al.* Toward a rational design of multitarget-directed antioxidants: Merging memoquin and lipoic acid molecular frameworks. *J Med Chem.* 2009; **52**: 7883-7886.
- 292 Mamos P *et al.* Simple total syntheses of N-substituted polyamine derivatives using N-tritylamino acids. *Tetrahedron Lett.* 1995; **36**: 5187-5190.
- 293 Margolis BJ *et al.* Assembly of 4-aminoquinolines via palladium catalysis: A mild and convenient alternative to SNAr methodology. *J Org Chem.* 2007; **72**: 2232-2235.
- 294 Dubuisson ML *et al.* Antioxidative properties of natural coelenterazine and synthetic methyl coelenterazine in rat hepatocytes subjected to tert-butyl hydroperoxide-induced oxidative stress. *Biochem Pharmacol.* 2000; **60**: 471-478.
- 295 Morris GM *et al.* Automated docking using a Lamarckian genetic algorithm and an empirical binding free energy function. *J Comput Chem.* 1998; **19**: 1639-1662.
- 296 Bottegoni G, Rocchia W, Recanatini M, Cavalli A. ACIAP, autonomous hierarchical agglomerative cluster analysis based protocol to partition conformational datasets. *Bioinformatics.* 2006; **22**: E58-E65.
- 297 Choi SI *et al.* Mitochondrial dysfunction induced by oxidative stress in the brains of hamsters infected with the 263 K scrapie agent. *Acta Neuropathol.* 1998; **96**: 279-286.
- 298 Milhavel O *et al.* Prion infection impairs the cellular response to oxidative stress. *Proc Nat Acad Sci U S A.* 2000; **97**: 13937-13942.
- 299 Singh N, Singh A, Das D, Mohan ML. Redox control of prion and disease pathogenesis. *Antiox Redox Signal.* 2010; **12**: 1271-1294.
- 300 Pamplona R *et al.* Increased oxidation, glycoxidation, and lipoxidation of brain proteins in prion disease. *Free Radical Biol Med.* 2008; **45**: 1159-1166.
- 301 Martin SF *et al.* Coenzyme Q and protein/lipid oxidation in a BSE-infected transgenic mouse model. *Free Radical Biol Med.* 2007; **42**: 1723-1729.

- 302 Bolognesi ML, Cavalli A, Melchiorre C. Memoquin: A multi-target-directed ligand as an innovative therapeutic opportunity for Alzheimer's disease. *Neurotherapeutics*. 2009; **6**: 152-162.
- 303 Klamt F *et al.* Imbalance of antioxidant defense in mice lacking cellular prion protein. *Free Radical Biol Med*. 2001; **30**: 1137-1144.
- 304 Yamamoto N, Kuwata K. Regulating the conformation of prion protein through ligand binding. *J Phys Chem B*. 2009; **113**: 12853-12856.
- 305 Ji HF, Zhang HY. Beta-sheet constitution of prion proteins. *Trends Biochem Sci*. 2010; **35**: 129-134.
- 306 Arlt S *et al.* Increased lipid peroxidation in cerebrospinal fluid and plasma from patients with Creutzfeldt-Jakob disease. *Neurobiol Dis*. 2002; **10**: 150-156.
- 307 Freixes M, Rodríguez A, Dalfó E, Ferrer I. Oxidation, glycooxidation, lipoxidation, nitration, and responses to oxidative stress in the cerebral cortex in Creutzfeldt-Jakob disease. *Neurobiol Aging*. 2006; **27**: 1807-1815.
- 308 Lehmann S. Metal ions and prion diseases. *Curr Opin Chem Biol*. 2002; **6**: 187-192.
- 309 Vramovich-Tirosh Y *et al.* Therapeutic targets and potential of the novel brain-permeable multifunctional iron chelator-monoamine oxidase inhibitor drug, M-30, for the treatment of Alzheimer's disease. *J Neurochem*. 2007; **100**: 490-502.
- 310 Zhan P, Liu XY. Designed multiple ligands: An emerging anti-HIV drug discovery paradigm. *Curr Pharm Design*. 2009; **15**: 1893-1917.
- 311 Pokrovskaya V, Baasov T. Dual-acting hybrid antibiotics: a promising strategy to combat bacterial resistance. *Expert Opin Drug Discov*. 2010; **5**: 883-902.
- 312 Cavalli A, Bolognesi ML. Neglected tropical diseases: Multi-target-directed ligands in the search for novel lead candidates against Trypanosoma and Leishmania. *J Med Chem*. 2009; **52**: 7339-7359.
- 313 Petrelli A, Giordano S. From single- to multi-target drugs in cancer therapy: When aspecificity becomes an advantage. *Curr Med Chem*. 2008; **15**: 422-432.
- 314 Macedo B *et al.* Synthesis and anti-prion activity evaluation of aminoquinoline analogues. *Eur J Med Chem*. 2010; **45**: 5468-5473.
- 315 Orru CD *et al.* In vitro synergistic anti-prion effect of cholesterol ester modulators in combination with chlorpromazine and quinacrine. *Central Eur J Biol*. 2010; **5**: 151-165.

- 316 Kocisko DA, Caughey B, Morrey JD, Race RE. Enhanced antiscrapie effect using combination drug treatment. *Antimicrob Agents Chemother.* 2006; **50**: 3447-3449.
- 317 Roberts BE *et al.* A synergistic small-molecule combination directly eradicates diverse prion strain structures. *Nat Chem Biol.* 2009; **5**: 936-946.
- 318 Gulcin I. Antioxidant activity of caffeic acid (3,4-dihydroxycinnamic acid). *Toxicology.* 2006; **217**: 213-220.
- 319 Kikuzaki H *et al.* Antioxidant properties of ferulic acid and its related compounds. *J Agri Food Chem.* 2002; **50**: 2161-2168.
- 320 Srinivasan M, Sudheer AR, Menon VP. Ferulic acid: therapeutic potential through its antioxidant property. *J Clin Biochem Nutr.* 2007; **40**: 92-100.
- 321 Kim YC. Neuroprotective phenolics in medicinal plants. *Arch Pharm Res.* 2010; **33**: 1611-1632.
- 322 Sul D *et al.* Protective effect of caffeic acid against beta-amyloid-induced neurotoxicity by the inhibition of calcium influx and tau phosphorylation. *Life Sci.* 2009; **84**: 257-262.
- 323 Kim HS *et al.* Inhibitory effects of long-term administration of ferulic acid on microglial activation induced by intracerebroventricular injection of beta-amyloid peptide (1-42) in mice. *Biol Pharm Bull.* 2004; **27**: 120-121.
- 324 Stewart LR *et al.* Involvement of the 5-lipoxygenase pathway in the neurotoxicity of the prion peptide PrP106-126. *J Neurosci Res.* 2001; **65**: 565-572.
- 325 Bolognesi ML, Minarini A, Tumiatti V, Melchiorre C. Lipoic acid, a lead structure for multi-target-directed drugs for neurodegeneration. *Mini Rev Med Chem.* 2006; **6**: 1269-1274.
- 326 Drisko JA. The use of antioxidants in transmissible spongiform encephalopathies: A case report. *J Am Coll Nutr.* 2002; **21**: 22-25.
- 327 Ono K, Hirohata M, Yamada M. Alpha-lipoic acid exhibits anti-amyloidogenicity for beta-amyloid fibrils in vitro. *Biochem Biophys Res Commun.* 2006; **341**: 1046-1052.
- 328 Packer L, Witt EH, Tritschler HJ. Alpha-lipoic acid as a biological antioxidant. *Free Radical Biol Med.* 1995; **19**: 227-250.
- 329 Holmquist L *et al.* Lipoic acid as a novel treatment for Alzheimer's disease and related dementias. *Pharmacol Ther.* 2007; **113**: 154-164.
- 330 White CR *et al.* L-Arginine inhibits xanthine oxidase-dependent endothelial dysfunction in hypercholesterolemia. *FEBS Lett.* 2004; **561**: 94-98.

- 331 Dasgupta T, Hebbel RP, Kaul DK. Protective effect of arginine on oxidative stress in transgenic sickle mouse models. *Free Radical Biol Med.* 2006; **41**: 1771-1780.
- 332 Rosini M *et al.* Rational approach to discover multipotent anti-Alzheimer drugs. *J Med Chem.* 2005; **48**: 360-363.